ABSTRACT

Title of Dissertation: EXPERIMENTAL AND THEORETICAL

INVESTIGATION OF OIL RETENTION IN

VAPOR COMPRESSION SYSTEMS

Lorenzo Cremaschi, Ph.D., 2004

Dissertation Directed By: Professor R. Radermacher,
Department of Mechanical Engineering

   The design of any system needs to consider a number of parameters according

different needs. In heating, ventilation and air conditioning systems the overall

efficiency, the reliability of the components, the cost and volume, and the

refrigerant/oil charge are only some examples of variables that can be optimized. An

important aspect is the selection of lubricants that provide the same or improved

characteristics relative to traditional mineral oils. In HVAC systems, the oil exists

only because the compressor requires it for lubrication and sealing. Proper oil

management is necessary in order to improve the compressor reliability, increase the

overall efficiency of the system, and minimize the system cost by avoiding

redundancy.

   Several literature sources focused on oil/refrigerant properties (Thome, 1995), oil

return characteristics (Biancardi et al., 1996) and oil transport phenomena

(Mehendale, 1998). An analytical and experimental study of the oil retention has been

developed for automotive air conditioning systems using carbon dioxide (Jun-Pyo Lee, 2002). However, a general comprehensive model for oil retention and oil distribution in heat pump systems using other refrigerant/oil mixtures does not exist and is of importance to future design considerations.

The purpose of this thesis is to experimentally and theoretically investigate the physics of oil retention and oil transport in different components of the system. Condenser, evaporator, suction and liquid lines are studied using different pairs of refrigerant-oil mixtures. Oil retention is measured directly using an experimental apparatus, and oil film thickness is estimated. At oil mass fractions of 8 wt.%, the pressure drops increase up to 40% in the suction line, 20% in the evaporator and 30% in the condenser as compared to oil-free operating conditions. New pressure drop correlations need to include this penalty factor due to oil retention. An analytical model for vapor and two-phase refrigerant flows utilizing minimal empirical data is developed. The model is able to estimate the oil distribution in the entire system providing good design guidelines for the selection of the proper refrigerant/oil mixture, the optimization of the component geometries, and the management of the oil/refrigerant charge.

EXPERIMENTAL AND THEORETICAL INVESTIGATION OF

OIL RETENTION IN VAPOR COMPRESSION SYSTEMS

By

Lorenzo Cremaschi

Dissertation submitted to the Faculty of the Graduate School of the
University of Maryland, College Park, in partial fulfillment
of the requirements for the degree of
Doctor of Philosophy
2004

Advisory Committee:
Professor Reinhard Radermacher, Chair
Associate Professor Jungho Kim
Associate Professor Gregory Jackson
Associate Professor Kenneth Kiger
Associate Professor Gary A. Pertmer

Dedication

Dedicated to my parents

Acknowledgements

I would first like to thank my advisor, Dr. Reinhard Radermacher, for having given me the opportunity and support to conduct research and gain an advanced education at the University of Maryland, College Park. His encouragement was much- needed and cherished; his dedication, inspiring; his faith in my ability, priceless. I am also grateful to the other members of my committee—Dr. Jungho Kim, Dr. Gregory Jackson, Dr. Kenneth Kiger, and Dr. Gary A. Pertmer—all of whom reviewed my dissertation with interest and great care. A warm thank you also goes to my immediate supervisor, Dr. Yunho Hwang, for his guidance at crucial moments throughout the research process.

For their continuous cooperation and friendship, I thank my colleagues Arm Gado, Hans-Joachim Huff, Jun-Pyo Lee, Layla Monajemi, Robert Andrew Schwentker, John Linde, and James Kalinger. Each helped make the hours I spent in the office more enjoyable.

Special thanks is extended to the many companies whose support of the Center for Environmental Energy Engineering at the University of Maryland made the research presented in this thesis possible.

Finally, I take this opportunity to express a whole-hearted thank you to my parents, my brothers and sisters, and my fiancée. Your love and support have always motivated me to do my best. Please accept this completed work, and the accompanying degree, as a return on your immeasurable investment in me. Although separated by great distance, you were always there for me throughout this process—and you will each be close to my heart always.

TABLE OF CONTENTS

LIST OF FIGURES

LIST OF TABLE

NOMENCLATURE

A	Area [m^2]
A, a	Semi-empirical Parameters
AB	Alkybenzene
ASHRAE	American Society of heating, Refrigerating and Air Conditioning
B, b	Semi-empirical Parameters
BWMO	Blendedn White Mineral Oil
C	Capacitance [pF]
c_p	Specific Heat [$J/(kgK)$]
CFC	Chlorofluorocarbon
COP	Coefficient of Performance
D	Pipe Inside Diameter [m]
d	Diameter, characteristic length
DAS	Data Acquisition System
EES	Engineering Equation Solver
F	Force [N]
f	Friction Factor, generic function
g	Gravitational Acceleration [m/s^2]
G	Mass Flux [$kg/(m^2s)$]
h	Enthalpy, dimensionless height, convective heat transfer coefficient [$W/(m^2K)$]

HCFC	Hydrochlorofluorocarbon
HFC	Hydrofluorocarbon
I.D.	Inner Diameter [m]
j	Superficial Velocity [m/s]
j*	Dimensionless Superficial Velocity
K	Dielectric Constant [pF/m]
k	Conductivity [$W/(mK)$]
L	Characteristic Length [m]
m	Mass [kg]
$\dot{m}$	Mass Flow Rate [kg/s]
m''	Mass Flux [$kg/(m^2s)$]
MFR	Mass Flow Rate [kg/s]
MO	Mineral Oil
Nu	Nusselt Number
O.D.	Outer Diameter [m]
OMF	Oil Mass Fraction [weight $\%$]
OR	Oil Retention Mass [g], Oil Retention Volume [ml]
ORM	Oil Retention Mass [g]
ORV	Oil Retention Volume per Unit Length [ml/m]
p	Pressure [kPa]
PAG	Polyalkylene Glycole

PDPF	Pressure Drop Penalty Factor
Pr	Prandtl Number
POE	Polyol Ester
Q	Cooling capacity [W], Volume Flow Rate [m^3/s]
$\tilde{q}$	Volume Flow Rate Ratio
r	Radial Coordinate
R	Pipe Inner Radius [m], Resistance [K/W]
Re	Reynolds Number
s	Solubility [weight %]
S	Slip Ratio
s_g	Specific Gravity [N/m^3]
T	Temperature [K or ^oC]
t	Time [s]
Tr	Transport Number
u	Velocity [m/s], uncertainty
U	Overall Heat Transfer Coefficient [$W/(m^2K)$]
V	Volume [m^3]
v	Velocity [m/s]
vfr	Viscosity Ratio Factor
VG	Viscosity Grade
We	Weber Number

X	Martinelli Parameter
x	Vapor Quality
X	Corrected Mass Flux Ratio
Y	Corrected Mass Flux

Greek Symbols

α	Void Fraction
β	Volume Flow Ratio
δ	Liquid Film Thickness [m]
ε	Dimensionless liquid film thickness, extractor efficiency, average relative error
ϕ	Two-Phase Pressure Drop Multiplier
γ_{misc}	Semi-empirical Constant of Miscibility between Refrigerant and Oil
η	Efficiency
λ	Density Correction Factor
μ	Dynamic viscosity [$Pa{\cdot}s$]
$\tilde{\mu}$	Dynamic viscosity Ratio
ν	Kinetic viscosity [cSt]
$\tilde{\nu}$	Kinetic Viscosity Ratio
θ	Wetted Surface Angle

ρ	Density [kg/m^3]			
$\tilde{\rho}$	Density Ratio			
σ	Surface tension [N/m]			
ψ	Mole Fraction, surface-viscosity-density correction factor			
τ	Shear Stress [Pa]			
ω	Weight Concentration			
ξ	Dimensionless Radial Coordinate, modified mole fraction			

Subscripts

bub	Bubble Point		misc	Miscibility
c	Core, Condenser		mix	Mixture
dew	Dew Point		o	Oil
e	Evaporator		out	Outlet, outer
exp	Experimental		pred	Predicted
ext	Extracted		r	Refrigerant, radial
f	Film (Liquid Film)		ref	refrigerant
g	Gas		ret	Retained
h	Horizontal, hydraulic		s	Suction
i	Interfacial, inner		Sat	Saturation

in	Inlet, Inner	segm	Segment
inj	Injected	θ	Angular
L	Liquid	tot	Total
l	Liquid Line	TP	Two-Phase
liq	Liquid	tt	Turbulent
LV	Latent Heat of Vaporization	v	Vertical
m	Mixture	w	Wall
max	Maximum	wet	Wetted
min	Minimum	z	Axial

LIST OF FINDINGS

- Oil Retention amount in all major components of A/C systems with R22/MO, R410A/MO, R410A/POE, R134a/POE and R134/PAG mixtures was experimentally measured.

- The physics of oil retention in the system components was studied both experimentally and theoretically.

- Models to predict oil retention in the suction line were verified and new semi-empirical correlations were developed.

- A semi-empirical model to estimate oil retention in the evaporator and condenser was developed and various void fraction models were verified for actual operating conditions of air conditioning systems.

- The oil influence on the evaporation and condensation processes was analyzed and various heat transfer and pressure drop correlations for oil-refrigerant mixtures were verified with experimental results.

- Guidelines for optimizing the major components of A/C systems and recommendations for selecting the proper refrigerant-oil mixture were made.

Chapter 1: Introduction

1.1 Overview

The purpose of this research is to identify the physics of the two-component two-phase flows of refrigerant and oil mixtures in vapor compression systems.

In a refrigeration cycle, a small portion of the oil circulates with the refrigerant flow through the cycle components, while most of the oil stays in the compressor. The compressor in a refrigeration system needs oil for the following reasons: to prevent surface-to-surface contact, to remove heat, to provide sealing, to keep out contaminants, to prevent corrosion, and to dispose of debris created by wear (Vaughn, 1971 [112]). Most of the compressor mechanical failures are due to improper oil management that leads to a lack of proper lubrication inside the compressor. Oil return behavior is a complex function of fluid properties as well as system components and configuration aspects. The circulating oil, which is missing from the compressor, can form a fairly homogeneous mixture with the liquid refrigerant or it can exist as an oil film on the tube wall, the thickness of which is affected by the system conditions (Mehendale, 1998 [78]). Each cycle component has different amounts of oil retention. Large amounts of oil retention cause a decrease in heat transfer and an increase of pressure drop. As a result, the performance of the air conditioning systems and the reliability of compressors depend on how much oil is circulated (Hwang *et al.*, 2003 [50]) and retained (Lee, 2002 [68]) in each component of the system. The current research will focus on three different types of oils: mineral oil (MO), polyol ester (POE), and polyalkylene glycole (PAG) synthetic

lubricants. Three different refrigerants have been selected to investigate the effects of different refrigerant mass fluxes, solubility, and miscibility of the carrier fluid. The selected refrigerants are R22, R410A, and R134a.

1.2 Motivation

Oil exists in the refrigeration system only because the compressor requires it for lubrication and sealing. Oil is required in the compressor crankcase, but refrigerant present in the compressor (except in the motor compartment, suction plenum, cylinders, and heads) might be considered a contaminant. Liquid refrigerant is always a contaminant in the compressor because it usually dissolves in the oil, thereby changing its viscosity and interfering with lubrication. During the off period of the compressor, both liquid refrigerant and oil are in the crankcase of the compressor. A stratified level of liquid stands below or above a consistent layer of oil depending upon the density ratio between the two fluids. Immediately after the compressor start up, liquid refrigerant boils and the oil-refrigerant mixture is flung onto the cylinder walls and possibly into the cylinder. Then, there is a significant rise in the rate at which the oil is pumped from the compressor. The lubricant may accumulate in bends and pockets of the system components such as the condenser, evaporator, accumulator, and suction line. Therefore, the oil level in the crankcase of the compressor can decrease to a level that is not sufficient to guarantee proper lubrication. In 1976 Jacobs *et al.* proposed one of the earliest correlations for transport of mineral oil by the R12 and R22 refrigerant vapors

2

[54]. This correlation recommends a simple equation for the refrigerant mass flow rate to ensure oil return in a vertical pipe. It does not include the effect of lubricant concentration, nor does it account for viscosity changes of the oil.

As global warming and ozone depletion receive more attention, not only have the refrigerants CFC 11 and CFC 12 been phased out in new machines but further restrictions have been applied to HCFC 22. New refrigerants such as R410A, R407C, and R502 are alternative refrigerants for R22. This change led to research and development of compatible synthetic lubricants such as polyolesters (POEs) and polyalkylene glycols (PAGs). For example, Sundaresan and Radermacher studied the oil return characteristics in residential heat pump systems (1996 [105]). By comparing R22/MO with R410A/POE and R407C/POE, they identified good oil return when POE oil is used but poor oil return if MO is adopted in combination with R410A. When mineral oil is used with the new HFC blends, the refrigerants are immiscible in the liquid phase. Poor miscibility leads to high oil film viscosity in the heat exchangers (evaporator and condenser) and the suction line. If the refrigerant mass flux cannot return the oil back to the compressor, then the oil level inside the crankcase can decrease below the lowest acceptable limit, preventing proper lubrication. Once the geometry of the suction line is fixed, the minimum refrigerant flow rates or minimum cooling capacities of the system can be computed, ensuring safe compressor lubrication.

In order to have a satisfactory theory for oil charge management, it is necessary to consider the oil distribution in the entire system with conditions similar to those of the real applications. The oil charged into the compressor, the number of the components in a

3

vapor compression cycle, the geometry and configuration of each component, and the interaction between refrigerant and oil are only some of the variables upon which the oil retention amount depends. Lee developed a semi-empirical model to estimate the oil retention volume in air conditioning systems using carbon dioxide (2002, [68]). The model was not verified for vapor compression systems that use conventional refrigerants, like R22 and the new HFC blends combined with different types of oil. When considering HCFC and HFC refrigerants, properties and refrigerant mass fluxes are significantly different from those of CO_2 air conditioning systems. A consistent model should take into account different levels of solubility and miscibility that change the oil film proprieties. Also, the pressure drop correlations need to include the oil film. Empirical correlations have been developed from CO_2 air conditioning systems with microchannel heat exchangers. For heat pump systems with conventional fin-and-tube heat exchangers, there are no pressure drop correlations that consider the presence of oil in the tube. While in automotive systems an oil separator is usually adopted, in stationary applications, the manufacturers usually avoid using oil separators because they are relatively expensive components. Thus, a proper oil charge needs to consider that there is a certain amount of oil circulating outside the compressor crankcase. The volume of oil that resides outside the compressor is referred to as the oil retention volume. Based upon system geometries, cycle pressures and temperatures, and refrigerant and oil flow rates, the amount of oil in each component changes.

1.3 Objectives

The objective of the current research work is to conduct a comprehensive study of oil distribution in vapor compression systems for stationary applications. The oil injection/extraction experimental methodology is used to estimate the amount of oil retained in the evaporator, and condenser, and suction and liquid lines. A parametric analysis of the oil retention volume is performed while considering different oil mass fractions, refrigerant mass flow rates, and oil film viscosities. The latter depends on the degree of mutual miscibility and solubility between oil and refrigerant. A second objective is to develop an analytical model that can predict oil retention volume and serve as a design tool for air conditioning systems. The oil that needs to be charged initially in the compressor can be estimated ensuring reliable compressor lubrication. Optimized geometries of heat exchangers have to account for pockets and oil traps that lead to potential oil accumulation phenomena. If proper oil management exists, oil separators can be avoided without compromising compressor reliability and system performance significantly. One aim is to create a visualization section in the suction line and before each heat exchanger. In order to select the proper void fraction model, the flow patterns inside the pipes need to be determined and verified. The specific experimental and modeling objectives are listed below:

Experimental Objectives

- Design and construct a test facility for oil retention tests.

- Measure the oil retention volume in the suction line, evaporator, liquid line, and condenser of a vapor compression system using the following refrigerant and oil mixtures:

  - R22 – Blended White Mineral Oil (BWMO);

  - R410A – BWMO;

  - R410A – POE;

  - R134a – POE;

  - R134a – PAG;

  The above pairs of refrigerants and oils are only a sample of fluids selected so that the effects of fluid density, viscosity, and surface tension variations over a wide range can be studied.

- Visualize the refrigerant-oil mixture flow pattern in the smooth tubes of the heat exchangers and in the suction line. Changes in pressures, temperatures, vapor qualities, and refrigerant or oil mass fluxes produce different flow regimes and flow types.

- Measure the increase of pressure drops in the suction line, evaporator, and condenser due to the existing oil accumulated in the test section.

- Study the effect of the following parameters on oil retention volume for each of the above mentioned system components:

- Refrigerant mass flow rate;

- Refrigerant evaporation and condensation temperature, pressure and vapor quality (two-phase flow, sub-cooled liquid, superheated vapor);

- Oil Mass Fraction (OMF);

- oil film viscosity, which depends on the refrigerant-lubricant affinity such as mutual solubility and miscibility.

Modeling Objectives

- Check the validity of the existing correlations (Mehendale [78], Fukuta [35], Wongwise [116], Bai [5], and Lee [68]) for the experimental data obtained.

- Develop an analytical/semi-empirical model to predict the oil retention volume in each component of the system.

- Examine various void fraction models to be used to calculate oil retention in all system components.

- Quantify the effects of various parameters on oil retention by using the model developed at the suction line and for the heat exchangers.

- Provide new pressure drop correlations for fin-and-tube heat exchangers and suction lines that include oil penalty effects on the refrigerant flow.

- Develop design guidelines for geometries, configurations, and orientations of the system components, which can help minimize oil retention volume without decreasing the system performance.

Chapter 2: Background

2.1   Literature Review for Steady State Conditions

The now banned refrigerant CFC-12 and its standard lubricant, mineral oil (MO), formed a highly miscible combination (i.e., they dissolved in each other in all proportions). It was found early on that the approved replacement HFC refrigerants and the old MO lubricant were not highly miscible. There was concern that the reduced miscibility would inhibit oil return to the compressor and would affect heat transfer. The literature pertinent to oil-refrigerant interactions can be divided into two main types: studies in steady state conditions and works that focus on transient mode operating conditions. Figure 2.1 shows the percentage of these two main areas, which are 88% for steady state conditions and only 12% for transient mode operating conditions. In the first category, the oil return, oil retention, and the influence of the oil on the system performances have been investigated while the vapor compression systems run in steady state conditions. In contrast, in the second type of works, the transient period of the system was the main object of investigation.

Oil transport by refrigerant poses quite a number of thermodynamic and hydrodynamic problems. When a two-component multi-phase flow is investigated, several different aspects need to be considered such as flow regime, fluid property change, heat transfer reduction, and pressure drop increase. The available research works in literature did not consider all the oil effects using a satisfactory general comprehensive theory. They rather focused on specific aspects while neglecting others. From this point of view, this thesis

provides a theoretical insight about oil retention physics and oil influence on fluid flow, evaporation and condensation processes in the major components of air conditioning systems. It also investigate oil retention characteristic for the widest possible range of transport properties of refrigerant-oil mixtures.

Among steady state works, the scenario can be summarized as shown in Figure 2.2. About 6% of the available research in literature focused on oil retention in heat exchangers, and only 3% estimated oil retention in suction line. There aren't any experimental results that measured directly oil retention for suction line and tube-and-fin heat exchangers for the wide range of transport proprieties in air conditioning applications. The experimental work and the simulations of this thesis are quite innovative and pioneering because they measure and predict oil retention of refrigerant-oil mixtures typically used in industry, and conditions of the system.

2.1.1   Oil Property Literature Database

An important aspect to consider when dealing with two-component two-phase flows is the property variation of each phase. Viscosity, density, and surface tension of the liquid oil rich mixture film depend on the dissolved fraction of the refrigerant. The amount of refrigerant dissolved into the oil depends on the temperature of the film and the pressure of the gas phase, which has to be equal to the vapor pressure of the mixture. Oil properties literature database is of fundamental importance to study any other oil-related research area. In particular, the local properties of the oil rich mixture phase need

to be computed accurately to estimate oil retention. About 15% of the literature (10% in the suction line and 5% in the evaporator and condenser) investigated oil properties variations in air conditioning systems. Mineral oils are soluble and miscible with R22 but they have very poor miscibility with R407C, R410A, and R134a (Kramer, [66]). Sunami *et al.* (1994, [102]) pointed out the poor miscibility and solubility of alkybenzene oils (AB) compared to POE when used in combination with R134a. Consequently, high viscosities were observed in AB/R134a mixtures. Solubility and viscosity data of R134a with AB, POE, and MO oils were published by Sunami *et. al* in 1994 [103]. Their investigation provided a comprehensive table of miscibility at different temperatures. Additives can used with AB oils to improve their miscibility with R134a. They showed that additives can improve the oil return characteristic of AB/R134a mixtures.

Very few researchers have investigated the surface tension changes in oil-refrigerant solutions. The surface tension of a mixture, especially for one with low refrigerant concentration, is far lower than an interpolating procedure would predict (Riedle *et al.* 1972, [93]). A refrigerant concentration of 20% by weight brings the oil film surface tension fairly close to the value of pure refrigerant.

Short and Cavestri (1992, [99]) investigated the effect of high viscosity ester lubricants for alternative refrigerants. The viscosity of oil-refrigerant solutions with ISO 68 modified ester oil and R134a were presented to help to identify the proper lubricant for hydrodynamic lubrication and sealing of compression areas. Cavestri *et al.* (1994, [22]) studied the solubility, viscosity, and density of R134a/PAG mixtures. The charts were given for 32 ISO VG PAG and 80 cSt PAG oil combined with R134a. For given

10

pressure and temperature, the corresponding solubility, density, and viscosity of the solution were evaluated. *ASHRAE Handbook 2002* [2] shows more charts of solubility, density, and viscosity of oil-refrigerant mixtures. In particular, the 32 ISO VG and 68 ISO VG POE with R410A mixture properties are given in a wide range of pressures and temperatures. Pavel *et al.* (2003, [87]) estimated the proprieties of CO_2/PAG oil by use of the pulse heating method, which allows researchers to measure experimentally gas solubility at different temperatures, short time thermostability, and thermal conductivity.

2.1.2   Oil Flow Characteristic Studies

Abundant literature can be found on flow pattern characteristics inside simple geometries. Oil retention characteristic is affected by the flow pattern of the refrigerant-oil mixture because the magnitude of the forces exerted on the fluid element depends on the type of motion of the fluid, relative interfacial surface area between the two phases, and velocity slip ratio between gas and liquid phases. Few research investigated flow patterns for refrigerant-oil mixtures used in air conditioning industry while many researchers studied the flow characteristics for mixture of air/water or air/pure oil. They correlated their data using dimensionless numbers and applied their correlations to the flows for refrigerant-oil mixtures used in air conditioning systems during actual operating conditions.

If a gas and a liquid flow together in a duct, several flow patterns can be observed. Based on flow pattern characteristics, the mixture flow exerts different effects on the

11

hydrodynamics in the pipe and produces various frictional pressure drops. The generally accepted flow patterns, in order of increasing vapor quality, are bubbly flow, slug flow, churn flow, annular flow, and annular-mist flow. Stratified flow and wavy flow are addition patterns which occur only in horizontal orientations. Based on data for air-water mixtures and from natural gas pipelines, Riedle *et al.* indicated which type of flow patterns are expected for given gas and liquid flow rates (1972, [93]). The fluid properties are taken into account in their maps by using two parameters that were developed for flooding correlations in distillation columns. Moriyama *et al.* (1992, [79]) proposed an analytical model to solve the frictional pressure drops and heat transfer of boiling two-phase flows. The theoretical approach focused on R113 boiling two-phase flows in narrow channels. Flow patterns and void fraction models play a key role not only in determining the frictional pressure drops, but also in estimating the oil transport capability of the refrigerant flow [43]. The vertical suction line is considered to be a weak place for oil return because the refrigerant has to overcome gravity to carry the oil vertically upward. Moreover, the low pressure and relatively high temperature lower the amount of refrigerant dissolved into the oil film. Thus, the oil film viscosity is higher, increasing the resistance of the oil carried along the line.

Hwang *et al.* (2000, [52]) investigated the flow characteristics of refrigerant-oil mixtures in vertical upward flows. Their experiment compared R134a combined with MO oil and AB oil. Using an extensive visualization work, annular and churn flows were observed and the mean film thickness was estimated for different Reynolds numbers. The Re number ranged from 3×10^3 to 22×10^3 and the mean oil film thickness ratio (δ/R)

was from 0.14 to 0.40 for MO oil and from 0.06 to 0.30 for 10 ISO VG AB oil. The lowest values occurred at the highest refrigerant Re numbers, and MO oil showed higher values of oil film thickness than those of the AB oils tested. Their study investigated oil accumulation characteristics, too. At high refrigerant Reynolds numbers (Re=13,000 and Re=16,000), the flow pattern was observed to be an annular flow that continuously forced oil upward, regardless of the oil flow rate. On the other hand, churn flow was observed at low refrigerant Reynolds numbers (Re=4,000), which yielded an unstable flow with oscillations. The oil film on the wall flowed downward, accumulated, and eventually formed plugs, that is, a complete blockage. The MO and high viscosity AB oil caused a larger oil amount to accumulate in the test section and about 2 to 17% of the oil initially charged in the compressor was found in the suction line.

Fukuta *et al*. (2000, [35]) studied the flow characteristics of oil films in suction lines of refrigeration cycles, in which the refrigerant mass flow rates are usually lower compared to those of the air conditioning systems. Air with 20 and 56 VG MO oil have been used as working fluids in their experiments. They proposed the refrigerant gas core Reynolds number to be the main parameter upon which flow pattern depends. By experimental results, they correlated the oil film thickness, pressure gradient, and oil film average velocity to the Reynolds number of the core region. The average oil film thickness was shown to decrease with an increase of the air velocity and pressure. If the oil viscosity increased, the average oil film thickness increased as well. The proposed correlation between gas Reynolds number (Re_g) and liquid film Reynolds number (Re_f) was the following:

$$\mathrm{Re}_f = 10^{-7.2025}\,\mathrm{Re}_g^{3.6494}\left(\frac{d}{d'}\right)^{-2.2656}\left(\frac{\rho_g}{\rho_f}\right)^{-1.8098}\left(\frac{\mu_g}{\mu_f}\right)^{3.2745}$$

where $d' = \left(v_l^2/g\right)^{1/3}$ is a representative length of the shear stress on the liquid film and d is the inner pipe diameter. By the above correlation, the oil film thickness was estimated and then experimentally verified, using measurements with a capacitance sensor. Their correlations were used for Re_g numbers ranging from 5,000 to 30,000. However, in order to derive a design criterion for the suction line of the upward flow in the refrigeration cycle, they concluded that it is necessary to extend the above correlation with the data over a wider range including oil-refrigerant two-phase flow. Analytical models of two-phase laminar annular flows in a pipe are often verified using air-water, air-oil, and oil-water mixtures. For stratified two-phase pipe flows, a numerical solution of Navier-Stokes equations using bipolar coordinates is possible, as described by Issa (1988, [53]).

The simple theory provides a starting point for further developments. It offers approximate predictions, which provide preliminary estimates. It is often simpler and cheaper to perform a suitable experiment in order to complete the theory such that it will be useful in practice. Hall and Hewitt (1993, [42]) presented approximate models that solve quite well the gas-water and oil-water mixture flows between flat plates and in circular pipes. The characteristic parameter that determined the oil film thickness was the Martinelli parameter, which is defined as:

$$X^2 = \frac{u_{liq}}{u_{core}}\cdot\frac{\mu_{liq}}{\mu_{core}} = \frac{1}{\widetilde{Q}\cdot\widetilde{\mu}}$$

where

u_{liq} = liquid film average velocity; u_{core} = core average velocity;

μ_{liq} = liquid film dynamic viscosity; μ_{core} = core dynamic viscosity;

$\widetilde{Q} = \dfrac{u_{core}}{u_{liq}}$ = velocity ratio; $\widetilde{\mu} = \dfrac{\mu_{core}}{\mu_{liq}}$ = viscosity ratio.

Hall and Hewitt's approach showed an increase of the liquid film height if the Martinelli parameter increased. For all physical realistic gas-liquid flows, the agreement between the two-fluid model and the exact solution in both 2-D and 3-D geometries was very close. For oil-water flows, where the viscosity ratio can vary from approximately one upwards, there was a significant deviation in holdup predictions for lower viscosity ratios. Taitel *et al.* [108] solved the structure of three-layer stratified flow and published their work in 1995. In their study, the gas/oil/water holdups for stratified phase flows were calculated. The levels of the two liquids in the pipe for any given set flow rates were estimated and the results were presented using a dimensionless height variable versus average liquid velocity with average gas velocity as parameter. They concluded that, by analogy to the two-phase flow case, the thinnest layer solution was the only one that can physically occur when gas velocities are above a certain threshold value.

2.1.3   Oil Return Studies

Introducing hydrofluorocarbon (HFC) refrigerants as alternative refrigerants for CFCs and HCFCs has raised a refrigerant and oil miscibility issue. *ASHRAE Handbook* (Refrigeration System and Application [2],[4]), which includes most of the experimental

information collected in the refrigeration and HVAC industry, contains tables that give minimum refrigeration capacities for oil "entrainment" up suction risers. The word entrainment, as used here, means film and droplets transport. Several research results on the oil return characteristics of miscible and immiscible refrigerant-oil mixtures have been published and are summarized below.

Fung and Sundaresan (1994, [36]) studied oil return characteristics in display cases using R404A and R502 with polyol ester (POE) and naphthenic mineral oil (NMO). They measured the oil level in the compressor crankcase to determine the oil return characteristics. The new refrigerant blends showed significantly better oil return characteristics when combined with POE oil rather than using NMO oil. Sundaresan *et at*. (1996, [105]) worked on oil return characteristics in residential heat pump systems using R22, R407C, and R410A with MO and POE oils. From their experiments, they recommended the use of synthetic poly ester oils with the new refrigerant blends. Indeed the MO showed poor oil return characteristics as a consequence of poor miscibility with R407C and R410A. Jacobs *et al.* (1976, [54]) conducted an experimental study to verify the ASHRAE data about minimum capacities for oil transport. Oil was injected into the test section and the critical refrigerant mass fluxes needed to transport oil upward were obtained using sight glasses. The refrigerant was always in the vapor phase at the test section. Typical compressor suction and discharge conditions were simulated and the working fluids were combinations of R12 and R22 with 150 and 300 SUS naphthenic oil. (NMO). As a conservative boundary to guarantee oil transport within the range of data studied, the authors suggested the equation

$$\sqrt{\mathrm{j}_g^{\dot{*}}} = 0.85$$

where

$$j_g^* = j_g \frac{\sqrt{\rho_g}}{\sqrt{gD(\rho_l - \rho_g)}} = \text{dimensionless refrigerant core mass flux}$$

j_g = core refrigerant velocity; g = gravity; D = hydraulic diameter;

ρ_g = core refrigerant density; ρ_l = liquid film mixture density

The dimensionless grouping for j_g^* relates the ratio between inertia force of the core and buoyant force due to difference in density (Mehendale, 1998, [78]):

$$J_c^{\dot{*}2} = \frac{[F_{inertia}]}{[F_{buoyancy}]} \approx \frac{\rho_c L^2 u_c^2}{g L \Delta\rho}$$

Biancardi *et al.* (1996, [15]) conducted experimental and analytical efforts to determine the lubricant circulation characteristics of HFC/POE and HFC/MO pairs in a residential heat pump system and compared the behavior with a R22/MO solution. The minimum flow rate for "the worst-case," in which the velocities occurred in the vertical vapor line, were determined by visual observations. They reported that minimum flow velocities ranging from 1.8 to 1.9 m/s were required in the cooling mode, and R407C/POE mixtures presented similar oil return characteristics as R22/MO pairs.

Oil return performance comparisons between MO and POE have been evaluated by Reyes-Gavilan *et al.* (1996, [91]). They experimentally investigated the oil return and lubricant flow characteristics for R134a with POE and MO at different evaporator temperatures in domestic refrigeration systems. Their study showed that gas velocities

played an important role in proper oil return to the compressor, and lubricant flow characteristics were similar for both refrigerant-oil pairs for similar suction conditions.

Sunami *et al.* (1998, [104]) conducted oil return tests and durability tests with HFC refrigerants and AB oils in split air conditioners. They observed exceptional oil return for ABs and reported no significant difference among the different oil viscosities. In addition, immiscible refrigerant pairs, such as R407C/AB, showed superior anti-wear properties in the compressor compared to miscible refrigerant-oil mixtures, such as R22/MO and R407C/POE.

Oil return characteristics in vertical upward flows were experimentally and theoretically investigated by Mehendale (1998, [78]) and Mehendale and Radermacher (2000, [77]). The critical mass flow rates for preventing oil film reversal in a vertical pipe were estimated. Vapor refrigerant of R22, R407C, and R410A with MO and POE oils were compared with the results obtained by Jacobs *et al.* [54]. When the refrigerant mass flow rates were reduced below the critical values, the stable upward moving oil film became unstable, started oscillating, and reversed its direction of motion. The critical refrigerant mass flow rates for oil transport by superheated vapor in vertical pipes were found to be slightly higher than that predicted from the correlation of Jacobs *et al*. At the onset of flow reversal, corresponding to $j_c^* = 0.9661$, the velocity gradient at the pipe inner wall became zero, but the oil film velocity was still positive, i.e. all the film was moving upward. When the refrigerant mass flow rate was reduced to a value below the onset of flow reversal, $j_g^* = 0.9$, the liquid next to the wall started flowing downward. The experimental data were bounded up to 4% higher and 7% lower by the analytical

18

predictions of the onset of flow reversal. Using R22/MO mixture, for evaporation temperature of 7.2ºC and with 10 degrees of superheat, the average film density was 942 kg/m³, the pipe ID was 8 mm, and the average film viscosity was 10 cSt. The mineral oil density and viscosity at the same temperature are about 885 kg/m³ and 110 cSt, respectively. At 0.5 wt.% of oil mass fraction, the critical mass flow rate ranged from 1.5 to 2.1 g/s for refrigerant vapor density of 10 kg/m³ to 30 kg/m³, respectively. For R410A/POE mixture, the average film density was about 988 kg/m³ and the average film viscosity was 30 cSt. At similar oil mass fraction (equal to about 0.5 wt.%) and using the same pipe inner diameter, the critical refrigerant mass flow rate slightly increased to about 2.5 g/s due to heavier and more viscous liquid film. With the same evaporating temperatures, an increase of pipe inner diameter from 8 to 25 mm caused a significant increase of the critical refrigerant mass flow rate from 2.5 to 45 g/s. It should be noted that the critical mass flow rate depends inversely upon the vapor quality, as reported in Mehendale's results.

2.1.4 Oil Mass Fraction (OMF) and System Performance Investigations

The amount of oil carried over with the refrigerant in a vapor compression system is referred to as the oil mass fraction (OMF):

$$OMF \: [wt.\%] = \frac{\dot{m}_{oil}}{\dot{m}_{ref} + \dot{m}_{oil}} \times 100 \tag{2.1}$$

where

19

$\dot{m}_{oil}$ = mass flow rate of oil; $\dot{m}_{ref}$ = mass flow rate of refrigerant.

Some investigators refer to OMF as "oil concentration" or "oil circulation ratio" (in mass%). OMF and oil concentration are used interchangeably throughout this thesis and they are both defined by Equation (2.1). The pressure drops in the connecting lines and in the heat exchangers, such as the condenser, evaporator, and suction line heat exchanger (SLHX), depend on the refrigerant flow rate and on the amount of oil that exists in each component.

Scheideman *et al.* (1975, [94]) investigated the pressure drop increases of refrigerant-oil mixtures in suction and discharge lines. The tested fluids were R12 and R22 in combination with 150 SUS Naphthenic Mineral Oil (NMO) and 300 SUS AB oils. Correlations between pressure drops and OMFs are given for different temperatures. Alofs and Hassan (1990, [1]) published pressure drop correlations in suction lines for R12 and R502 combined with 150 SUS NMO. Their results confirmed that an increase of oil mass fraction always caused an increase of pressure drops.

Baustian *et al.* (1998, [8]) conducted OMF measurements using a U-tube vibrating densimeter. The tested fluids were R12/NMO, R22/NMO and R502/AB mixtures and the measurements were taken in a simulated liquid line. The oil mass fraction was changed from 0 to 30 weight percent and the uncertainty was about ± 2 weight percent. Then, they compared the results with those obtained by an acoustic velocity sensor presented in a different paper (Baustian *et al.* 1988, [11]). For the same mixtures and similar oil mass fractions, the OMF uncertainty was reduced to about ± 1 weight percent using the acoustic velocity sensor. Biancardi *et al.* (1996, [15]) proposed a new type of optical

20

sensor to measure the OMF in systems using R22 and R407C in combination with MO and POE oils. The JASCO ultraviolet oil concentration meter allowed measuring the oil content by determining the amount of ultraviolet (UV) light that a refrigerant-oil mixture absorbs. The concentration ranged from 0 to 10 wt.%. because a loss of signal occurred at higher concentrations. Moreover, they concluded that the UV measurements were not reliable to measure the oil mass fraction for immiscible solutions.

A different method to measure the oil mass fraction is presented by Hwang *et al.* (2002, [51]). In their study, they focused on carbon dioxide (R744) and PAG oil, which are partially miscible with each other. A capacitance sensor read the value of the dielectric constant of the mixture flowing between flat plate electrodes. Thus, a variation in the mixture density can be detected by measuring the change in the dielectric constant. During the calibration, the OMF was changed from 0 to 10 wt.%. Results showed that the uncertainty was about ± 0.5 wt.%, and the relative average error was about 13%.

Several researchers investigated the effect of oil on overall system performance. When oil is either retained or circulated in system components, the pressure drop increases and the heat transfer generally decreases. Green (1971, [40]) investigated the effects of oil on the heat transfer coefficient and pressure drops in the evaporator for R12 and R22 vapor compression systems. His results showed that if the oil content was less that 10 wt. %, there was no significant effect on the heat transfer coefficient. On the other hand, oil caused the pressure drop to double in the evaporator compared to a similar oil-free system. Eckels and Pate (1991, [29]) studied the effects of oil on two-phase heat transfers. Their results showed disagreement between evaporator and condenser heat

transfer behaviors: while up to 3% oil mass fraction, heat transfer in the evaporator tended to increase, the presence of oil always degrades the heat transfer in the condenser at any concentration. Reduction in condenser performance indirectly penalizes system performance. System performance degradation due to oil accumulation was observed by Grebner and Crawford (1993, [39]). In particular, they focused on R12 and R134a capacity reductions if mineral and ester oils are used. Assuming standard operating conditions and neglecting pressure drops in the evaporator, significant reductions of the evaporator capacity were predicted due to an increase in saturation temperatures resulting from the presence of oil. R12/MO mixtures showed the most sensible capacity reduction due to their higher oil solubility, compared to R134a/POE and R134a/PAG mixtures, for which the capacity reduction was less marked. Popovic (1999, [89]) experimentally measured the system performance degradation in systems that use R134a with MO and POE and he found that a small amount of circulating oil could significantly alter the evaporator heat transfer. The overall coefficient of performance could be improved by as much as 5% by selecting miscible oils over immiscible ones. The oil effects on the evaporation heat transfer in microchannel heat exchangers were experimentally investigated by Zhao *et al.* (2001, [124]). CO_2 mass fluxes, saturation temperatures, and vapor qualities were taken as parameters upon which the heat transfer coefficient depends. The average evaporation heat transfer coefficient was measured under various oil mass fractions, ranging from 0 to 7wt.% and using polyalkylene-glycol (PAG) oil. When oil is present, it decreased vapor quality and degraded the heat transfer coefficient because oil acted as thermal resistance on the wall at high vapor quality. Moreover,

pressure drop increased with an increase of the oil mass fraction because of higher CO_2/oil mixture viscosity. Hwang *et. al.* (2002, [50]) confirmed these results by investigating the overall evaporator and condenser performances and pressure drop variations with OMF. The coefficient of performance (COP) of the air conditioning system was measured experimentally and the oil mass fraction was measured on line by using a capacitance sensor. If the OMF increased from 0.5 wt.% to 7wt.%, it was observed that the COP degraded about 8% and 11% in idling and driving conditions, respectively.

2.1.5 Oil Retention and Oil Distribution Literature Review

While the oil is of primary importance for the compressor, in all other components it represents an undesired effect. The influence of thermophysical proprieties of oil on lubrication must satisfied different needs. For example, the compressor needs high viscosity for hydrodynamic lubrications while the system needs low viscosity for proper oil return and minimized oil retention (Kruse 1984, [67]).

In 1972, Ridle, Macken, and Gouse [93] were among of the first researchers to characterize systematically the flow of oil-refrigerant mixtures. Their analytical model, based on minimum gas velocities, introduced the concepts of void fraction, oil entrainment, and liquid film thickness for oil-refrigerant mixtures. Schlager *et al.* (1990, [95]) conducted experiments in order to determine the quantity of oil in smooth and micro-fin tubes during evaporation and condensation of refrigerant-oil mixtures. They

showed that the parameters that affect the oil retention were mass flux, oil mass fraction, viscosity, evaporator exit conditions (i.e vapor quality at the evaporator outlet), and evaporation pressure. They used R22 in combination with 150 to 300 SUS mineral oil. The main parameter that affected the oil retention was the oil mass fraction, which was changed from 1 to 5 wt. %, and the degree of superheat at the evaporator outlet. Significant increase of the oil mass quantity in the evaporator was observed if the evaporator exit temperature was above the pure refrigerant saturation temperature. Variations of mass flux and saturation pressure did not have a significant effect on the quantity of oil retained. Using the most viscous oil, they observed about 25% more oil retention compared to the case when the least viscous oil was adopted. Shedd and Newell (1998, [97]) proposed a non-intrusive, automated, optical film thickness measurement technique to be used with a wide range of fluids and flow configurations. In their method, light was reflected from the surface of a liquid film flowing over a transparent wall and it generated an image on the outside wall, which was captured and eventually digitalized. Static liquid optical measurements agreed to within 2.2% of average relative error with measurements made using the needle-contact method. Their results showed the liquid film thickness for both round and square test sections operating under annular two-phase flow conditions of air and water. Bai and Newell (2002, [5]) took a similar approach to describe the characteristics of two-phase, viscous flow of air and 300 SUS AB oil. Using an extensive experimental flow visualization in horizontal and vertical pipes, the oil film thickness versus oil mass flow rate was plotted, with vapor velocity and pipe diameter as parameters. Shear stress correlations were proposed and verified with experimental data.

The oil viscosity was 66 cSt and the density was 875 kg/m^3 while the air Reynolds number ranged from 6,000 to 30,000.

In 2002, Lee [68] proposed a model for oil retention and oil distribution in CO_2 air conditioning systems. The lubricant used was PAG oil, which is partially miscible with CO_2. The solubility of CO_2 in PAG oil was about from 10 wt.% to 40 wt.%. The oil film viscosity ranged from 9.2 cSt to 43 cSt. The author proposed interfacial shear stress correlations that were experimentally verified for refrigerant vapor core Reynolds numbers ranging from 16×10^4 to 32×10^4. Using these semi-empirical correlations, the set of equations formed a close system and the oil retention volumes were computed in both suction line and microchannel heat exchangers. The simulations and the experimental data were in agreement within ± 15%. The oil retention volume in the systems was from 10 to 98 ml, which represented about 4% and 39% of the oil charged initially in the compressor, respectively. Lee also showed the effect of the oil retention on pressure drops in the suction line, evaporator, and gas cooler. Pressure drops can easily double when the oil mass fraction increases up to 5 wt.%. Thus, design pressure drop correlations need to consider this penalty factor due to oil accumulation in each component.

2.2   Literature review for Transient Mode Conditions

Few research has been performed in transient mode operating conditions as shown in Figure 2.1. When a system under transient operating conditions is studied, the effect of

the oil during compressor start up, shut off, and cycling modes is the main object of the investigation. Among the transient studies on oil management, the state of the available public literature can be summarized as shown in Figure 2.3. Yokizeki (2002, [120]) studied the time-dependent absorption behavior of ISO 68 POE oil in different refrigerants such as R134a, R125, R32, and R22. By extrapolation, they obtained solubility limits and diffusion constants for the above mixtures. Biancardi *et al.* (1996, [15]) made great efforts to study oil return and oil mass fraction characteristics in heat pump systems that operate in cooling and heating modes. Using R22 and R407C with MO and POE oils, they reported the behavior of the oil mass fraction during transient mode conditions, such as cycling from cooling to heating mode and from cooling to defrosting mode. Depending upon the oil mass fraction, viscosity, and miscibility of the oil-refrigerant mixtures, they identified opportunities for oil trapping and pooling in both the indoor and outdoor sections of the heat pump, especially near the manifolds, distributors, and valves of the system. Their observations have been converted into flow velocities for good or poor oil return. From their point of view, the industry recommendations appeared to provide appropriate but conservative guidelines for the minimum mass fluxes (and hence flow velocities) required for good oil management practice. Hwang *et. al.* (2003, [50]) investigated the effect of the oil mass fraction on the system performance of a CO_2 control climate system. During their tests, a capacitance sensor was used to measure the oil mass fraction on line during steady state and transient operating conditions. Thus, the OMF was measured during compressor start up, shut off, and compressor cycling from idling (RPM=1000) to driving (RPM=1800) conditions. An

open type compressor for automotive applications was used in their tests and they compared two different systems with and without discharge oil separator. Immediately after the compressor start up, the OMF increased higher than 10 wt.% if the system did not have the discharge oil separator but with an oil separator, the OMF was maintained at 0.5 wt.% and 1.1 wt.% for idling and driving conditions, respectively.

OIL MANAGEMENT

Steady State 88%

Transient Mode 12%
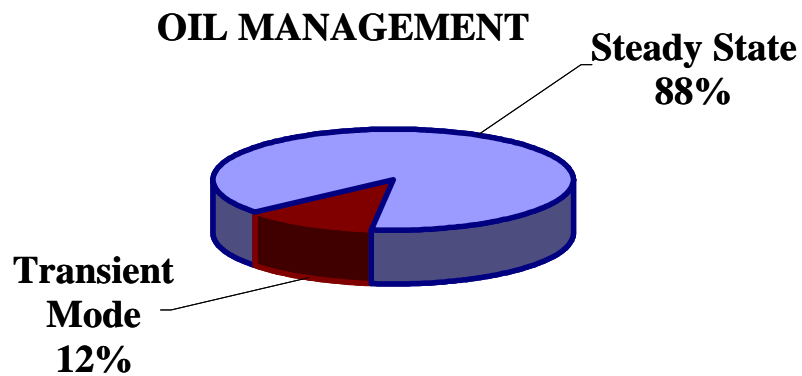
Figure 2.1: Literature Review for Oil-Refrigerant Studies
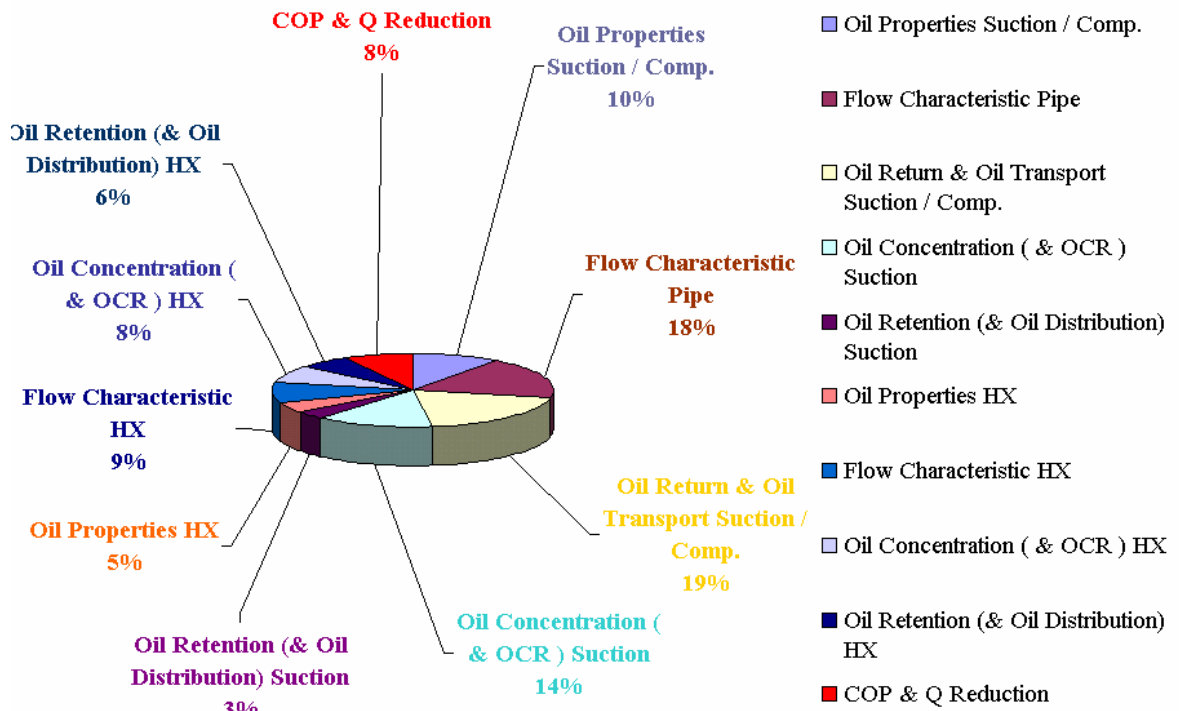
Figure 2.2: Literature Review for Steady State Operating Conditions
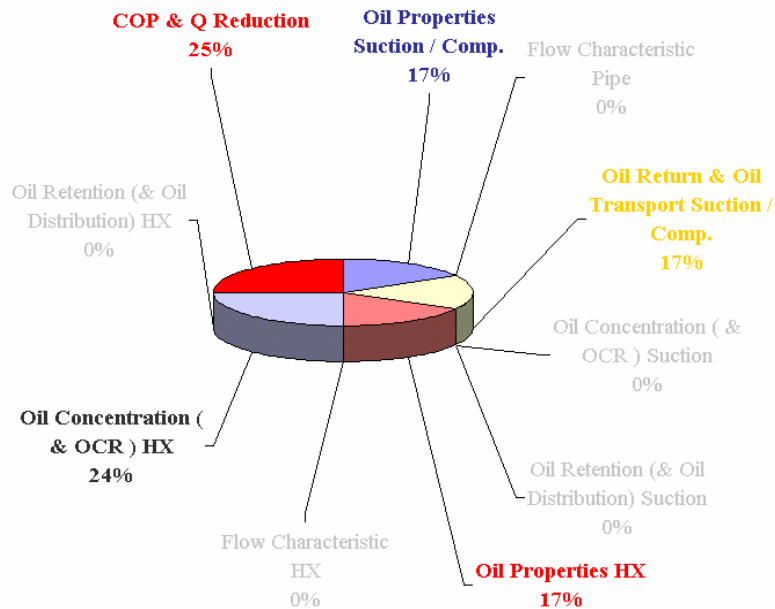
Figure 2.3: Literature Review for Transient Operating Conditions

Chapter 3: Working Fluids

In an air-conditioning or refrigeration system, a small amount of oil migrates from the compressor into the refrigerant. Thus the working fluid is not only the refrigerant but the refrigerant-oil mixture. While some oil leaves by forming an equilibrium mixture with refrigerant, some is simply dragged as a result of very high refrigerant vapor velocity at the compressor discharge. As a minor difficulty, the oil clogs and in time forms a layer on all surfaces - an undesirable action because it creates additional resistance. When a system runs with a refrigerant-oil mixture that has low degree of solubility, using a simple device called an oil separator at the compressor discharge line may solve the above problem quite easily. However, oil separators are not effective for many popular refrigerant-oil mixtures, including most organics or halocarbons. For heat pump systems, separators are seldom used because they are relatively expensive components and they add pressure drops in the system. Rather, the various system components are designed to assure proper oil flow and satisfactory oil return to the compressor.

In order to investigate the effect of density, viscosity, and mass flux variations over the widest possible range, the refrigerant-oil mixtures that will be experimentally tested need to be selected properly. It is important to understand the oil entrainment phenomena and identify the key parameters that affect oil retention volume. From the literature review, it appears that one of the main parameters for oil entrainment is the refrigerant mass flux. However, some authors prefer to use either the refrigerant velocity or the refrigerant core Reynolds numbers. Only a few publications proposed a correction factor

due to the surface tension of the liquid film. If only refrigerant mass fluxes or refrigerant core Re numbers are considered, the property variations of the liquid film cannot be linked to the oil retention volume change. Solubility and miscibility between refrigerant and oil affect the density and viscosity of the liquid film in the oil rich area. Thus, a more consistent model should take into account viscosity and density of both the phases. In the next chapters, the properties of refrigerants and oils have been calculated by assuming evaporation and condensation temperatures typical of vapor compression systems. The procedure for selecting the refrigerant-oil mixtures to be used in the experimental tests is explained next. The purpose of the following analysis is to reduce the experimental test matrix without losing significant information about the oil entrainment phenomena. The main task performed was to search for valid parameters that impact oil film thickness.

3.1 Refrigerants

In order to generate an oil retention model that will cover the widest possible range of refrigerant-oil solutions commonly used in vapor compression systems, several properties of the mixtures need to be considered. This study focuses mainly on those properties that impact oil entrainment, such as refrigerant and oil mass fluxes, Reynolds numbers, film density, and film viscosity. Various flow patterns occur in different sections of the vapor compression system. The actual flow is single phase only in the liquid line and oil and liquid refrigerant can be more or less homogeneously mixed. In the evaporator, condenser, and suction line the flow is two-phase separated flow with

refrigerant vapor and oil and liquid refrigerant mixture flowing in the pipe. The flow pattern depends on many variables but usually annular flow occurs in air conditioning applications. It is also the simplest flow that can be analytically studied among separated two-phase flows patterns. Generally, the dynamics of annular flow are governed by the interplay between various forces. These forces result from at least seven causes, as described by Wallis (1970, [115]):

- The pressure gradient;   - Buoyancy

- Surface tension   - Inertia of the gas

- Inertia of the liquid   - Viscosity of the gas

- Viscosity of the liquid.

The object of this section is to present an approach for annular flow that is sufficiently simple to be useful and, at the same time, is based on the major physical phenomena that occur. The driving force for oil entrainment is the interfacial shear stress between two phases: the refrigerant core and the more viscous film region at the pipe wall. The interface between them depends on the flow pattern characteristic. For annular flow usually appears wavy, and much of the interfacial shear stress, τ_i, is due to formation of drag on these waves (Wallis, [115]). The surface tension of the lubricant influences the foaming of the refrigerant oil solution and affects the shape of the wave along the interfacial boundary surface. Foaming in the oil reservoir of a refrigerating compressor is unfavorable for hydrodynamics lubrication, because the oil pump in that case is not able to pump a necessary amount of oil to the sliding part of the compressor. However, the surface tension force plays a secondary role in oil retention and its effect is rather small

31

compared to the viscous and inertia forces. Consequently, at first approximation, the surface tension force is neglected during the procedure of selecting the refrigerant-oil mixtures.

R22 is widely adopted in vapor compression systems in many applications. For this reason, it has been chosen as a base refrigerant to which all alternative refrigerants have been compared. Figure 3.1 shows the characteristic mass flux range for different refrigerants. For given air side conditions, R22 has a maximum mass flux of about 376 kg/(m^{2}s). The normalized mass flux showed on the x-axis of Figure 3.1 is defined as:

$$\widetilde{m}_i^* = \frac{\dot{m}_i''}{\dot{m}_{max,R-22}''}$$

where

$\widetilde{m}_i^*$ = normalized mass flux of the refrigerant i

$\dot{m}_i''$ = mass flux of the refrigerant i

$\dot{m}_{max,R-22}''$ = maximum mass flux of R22.

It should be noted that, in contrast to the mass flow rate, the mass flux is not constant among a vapor compression system because of the change in the cross section area of each component. The experimental apparatus, which will be described in detail in the next chapter, consists of an R22 residential split system heat pump with given suitable dimensions, i.e., inside-pipe inside diameter (ID), compressor displacement volume (V) and RPM. The compressor volumetric efficiency depends on the pressure ratio and it affects the refrigerant mass flow rate while the isentropic efficiency has been assumed constant and equal to about 0.7, which represents the average computed value from

preliminary R22/MO tests. If the geometries of the system are invariant, the expected refrigerant mass fluxes can be computed by volume flow rates and density estimations. A simple model to compute mass flow rates, densities, and refrigerant velocities has been developed using the assumptions of similar system geometries, equal compressor displacement volume, RPM, and isentropic efficiency. The same temperature approaches at the heat exchangers were used to estimate evaporation and condensation pressures. The simulated pressures, temperatures, and mass flow rates of the vapor compression cycles have been checked by comparing their order of magnitude with R22, R410A, R134a, and R290 experimental data available at the CEEE heat pump laboratory (University of Maryland). Using the same experimental test facility, if R22/MO is replaced with any refrigerant-oil pair, the potential changes in mass fluxes, density, and viscosity were predicted. CO_2 mass fluxes have been computed from previous experimental work (Lee 2002, [68]). Figure 3.1 shows the trend of expected refrigerant mass fluxes for the most common R22 alternative refrigerants. Minimum mass fluxes are expected by using R152a, R290 (propane), or R134a. Maximum refrigerant mass fluxes belong to R744 (Carbon Dioxide), R125, and R410A. Figure 3.2 shows the viscosity range for different refrigerants and Figure 3.3 summarizes the Reynolds (Re_{core}) numbers. These figures suggest that R134a (or R152a) and R410A (or R502) are the main candidates for an experimental investigation because the widest range of refrigerant mass flux (or Reynolds number) can be observed. If R134a and R410 are selected, the next step is to estimate the oil film density and viscosity when different oils are used. In the next paragraph, the procedure for selecting the proper oil to be tested is explained.

33

3.2   Lubricants

A lubricant that satisfies any possible need in the system does not exist, and a compromise must be made to balance the requirements. A high viscosity lubricant seals the gas pressure, but may offer more frictional resistance. Slight foaming can reduce noise, but excessive foaming can carry too much lubricant into the cylinder and cause structural damage. Lubricants that are most chemically stable are not necessarily good lubricants. The lubricant should not be considered alone, because it functions as a lubricant-refrigerant mixture.

The best method for calculating the entrainment rate is still an open question since the entrainment rate is proportional to the film thickness, (Luninski *et. al.* 1983 [73]). From literature review, the oil mass fraction (OMF), or oil concentration, is the main variable that affects oil retention. Thus, a parametric study will be experimentally performed while changing the OMF, independent of the type of refrigerant and oil selected. The task that is addressed in this chapter is to predict the oil-refrigerant mixtures that will have minimum or maximum oil retention volume at given OMFs. It is necessary to have some insights into the basic physics of the oil entrainment phenomena. A simple analytical model considers both refrigerant and oil properties and how the two phases interact with each other.

The first step is to analyze a vapor compression system from a transport proprieties perspective. Figure 3.4 shows the refrigerant proprieties in a vapor compression system.

Minimum refrigerant mass fluxes occur usually at the suction line while minimum refrigerant velocities are at the condenser outlet. Usually homogeneous flow models better describe liquid-liquid flows while separated flow models work well for gas-liquid flows. All gases are soluble to some extent in lubricants, and many refrigerant gases are highly soluble. The amount dissolved depends on the pressure of the gas and the temperature of the lubricant, as well as the nature of the gas and the nature of the lubricant. Because refrigerants are much less viscous than lubricants, any appreciable amount in solution causes a marked reduction in viscosity. The highest viscosity usually does not occur at the lowest temperature, because the lubricant contains a large amount of dissolved refrigerant. As temperature increases, the lubricant loses some of the refrigerant and the viscosity reaches a maximum at a point away from the cold spot in the system. On the other hand, dissolving lubricant in liquid refrigerant affects the thermo dynamic proprieties of the working fluid. The vapor pressures of refrigerant-lubricant solutions at given temperatures are always less than the vapor pressures of pure refrigerant at the same temperature. Therefore, dissolved lubricant in an evaporator leads to lower suction pressures and higher evaporator temperatures than those expected from pure refrigerant tables (ASHRAE 2002, [2]). From R22 preliminary test results, the maximum liquid film viscosity was about 22 mPa·s, while the minimum viscosity was about 12 mPa·s as shown in Figure 3.5. Other estimated oil-refrigerant viscosities are shown in Figure 3.6 and they have been normalized with respect to the maximum oil film viscosity found for MO/R22 pair.

3.3 Understanding the Oil Entrainment Phenomena

In the annular flow pattern, a continuous liquid film flows along the wall of a pipe while the gas flows in a central "core." If the core contains a significant number of entrained droplets, the flow is described as annular mist, which could be regarded as a transition between ideal annular flow and a fully dispersed drop flow pattern. Annular flow is the predominant flow pattern in evaporators, natural gas pipelines, and steam heating systems (Wallis [113]). The method of analysis can be applied to either the gas or the liquid and numerous combinations are possible. Jacob et al. in 1975 [54], and later Mehendale in 1998 [78], proposed the characteristic dimensionless mass flux as the oil entrainment key parameter in gas and liquid two-phase flows for vertical upward suction lines. For each oil-refrigerant solution, the dimensionless mass flux was computed as

$$j_c^* = j_c \frac{\sqrt{\rho_c}}{\sqrt{gD(\rho_l - \rho_c)}}$$

where

j_c = core refrigerant velocity; g = gravity; D = hydraulic diameter;

ρ_c = core refrigerant density; ρ_l = liquid film density.

The dimensionless grouping for j_c^* relates the ratio between inertia force of the core and hydrostatic buoyant force due to difference in density (Mehendale [78]):

$$j_c^{*2} = \frac{[F_{inertia}]}{[F_{buoyancy}]} \approx \frac{\rho_c u_c^2}{\Delta\rho\, g\, D}$$

36

The plot of the dimensionless mass fluxes for different oil-refrigerant mixtures is given in Figure 3.7. Experimental data showed that, at about $j_c^* \approx 0.9$, oil flow reversal eventually occurs because the inertia forces (i.e., the refrigerant core velocities) cannot carry the oil-refrigerant liquid up the suction line. With the proposed experimental Air Conditioning system, diameter and refrigerant velocities are such that proper oil return is always guaranteed. Figure 3.7 shows that CO_2 has the highest dimensionless mass flux, followed by R502 and R410A. Low dimensionless mass fluxes have been predicted for R134a. However, if only the ratio between inertia and buoyancy force is considered, the effect of solubility and miscibility on the viscosity of the oil film cannot be determined. Looking only at Figure 3.7, it is difficult to understand why miscible oil-refrigerant pairs, like R410A/POE, tend to behave differently with respect to the immiscible ones, such as R410A/MO. The effect of the solubility and miscibility is generally more marked on oil film viscosity reduction than on oil film density change. In this section, a different approach will be describe since the viscous shear stresses of the liquid film cannot be neglected. Alternative parameters might be the ratio between the oil film viscous force and the core refrigerant inertia force or the ratio between viscous and buoyancy forces. A more detailed procedure for describing the characteristics of annular laminar flow will be presented in Chapter 7. A simplified approach can be summarized here in order to estimate the order of magnitude of the forces responsible for oil transport. One usually finds that more complex analysis provides a method for predicting empirical factors in simpler models, or for evaluating correction factors that increase the level of accuracy. Consider the two-phase separated annular laminar pipe flow shown in Figure 3.8.

Following Feng and Klausner (1997, [31]), a force balance on a cylindrical element of the liquid film in which acceleration is ignored leads to,

$$\tau = \tau_i \left(\frac{R-\delta}{r} \right) + \frac{1}{2} \left(\frac{dp}{dz} + \rho_l g_z \right) \cdot \left(\frac{(R-\delta)^2 - r^2}{r} \right) \tag{3.1}$$

By replacing the radial coordinate (r) with the distance from the wall (y), the following equation is obtained:

$$\tau = \mu_l \frac{du}{dy} = \tau_i \left(\frac{R-\delta}{R-y} \right) + \frac{1}{2} \left(\frac{dp}{dz} + \rho_l g_z \right) \cdot (R-y) \cdot \left[\left(\frac{R-\delta}{R-y} \right)^2 - 1 \right] \tag{3.2}$$

where τ = shear stress at the distance y from the pipe wall;

τ_i = interfacial shear stress on the liquid film by the core;

δ = liquid film thickness; R = Inner Pipe Radius ($=D/2$)

μ_l = liquid film dynamic viscosity; ρ_l = liquid film density;

$\dfrac{dp}{dz}$ = pressure gradient in the pipe; g_z = z-component of the gravity.

As it will be derived in Chapter 7.3, a steady state force balance on the core refrigerant leads to the following equation:

$$\frac{dp}{dz} = -\frac{4\,\tau_i}{D-2\delta} - \rho_g g_z = -\frac{2\,\tau_i}{R-\delta} - \rho_g g_z \tag{3.3}$$

Thus, the combination of equations (3.2) and (3.3) yields to:

$$\tau = \mu_l \frac{du}{dy} = \tau_i \left(\frac{R-y}{R-\delta} \right) + \frac{1}{2} (\rho_l - \rho_g) \cdot g_z \cdot (R-y) \cdot \left[\left(\frac{R-\delta}{R-y} \right)^2 - 1 \right] \tag{3.4}$$

38

In equation (3.4), the three forces acting on the liquid film control volume are the viscous, inertia and buoyancy forces. From an oil transport point of view, the physical meaning and order of magnitude for each term can be summarized as follows:

- Viscous shear stress (τ) represents some sort of resistance that the oil film exerts to get carried along with the refrigerant and it has an order of magnitude

$$\tau \approx \mu_l \frac{\Delta u}{\Delta y} \approx \mu_l \frac{\left(u_{l,y=\delta} - u_{l,y=0}\right)}{\delta} = \mu_l \frac{u_c}{\delta} \; .$$

- Inertia force represents the driving force for oil transport due to the refrigerant mass flux and viscosity and it can be expressed as

$$F_{inertia} \approx R^2 \cdot \tau_i \approx R^2 \cdot \frac{1}{2} \rho_c f_i \left(u_c - u_l\right)^2 \approx R^2 \cdot \frac{1}{2} \rho_c f_i u_c^2 \; .$$

- Buoyancy force takes into account the gravitation effects and it is of the form

$$F_g \approx \left(\rho_l - \rho_g\right) g_z R^3 \; .$$

Moreover, as shown in Chapter 7.4, the friction factor f_i can usually be expressed by empirical correlations of the form:

$$f_i = A \cdot \frac{1}{Re_g^n} \cdot \left(\frac{D}{\delta}\right)^m$$

where A, n, and m are constant coefficients and usually $0<|n|<1$ and $0<m<1$.

Core and liquid film proprieties, pipe geometry, oil film thickness, and average velocities of both phases contribute to each single force. If the gravitational term is small compared to the other two terms, like for example in horizontal pipes ($g_z = 0$) or for core and film phases with approximately the same density ($\rho_l \cong \rho_g$), then the ratio between inertia force and viscous force represents the transport capability of the refrigerant and oil

39

mixture. The higher the inertia force will be, with respect to the viscous force, the greater the oil will be stretched and eventually the easier it will be carried over. In other words, higher core inertia forces should lead to less oil in the pipe and lower oil film thickness δ per unit length of pipe. Several authors confirmed this observation. Schlager *et al.* (1990, [95]) showed that higher values of R22 mass fluxes lead to less quantity of mineral oil in smooth and micro-fin tubes. Lee (2002, [68]) investigated the oil retention for CO_2 air conditioning systems using PAG oil, which is partially miscible with the refrigerant. For fixed OMF, his results showed a significant decrease in oil retention volume if the refrigerant mass flux increased. Hall and Hewitt (1993, [42]) proposed an approximate analytical model to solve stratified two-phase flow between horizontal flat plates and inside pipes. Their solutions showed an increase of liquid height when the Martinelli parameter (X^2) increased. The numerical solution they derived for stratified flow suggests that if the velocity or viscosity of the gas increased, then the liquid height decreased. When the gravitational force is neglected, equation (3.4) becomes:

$$\tau = \tau_i \left(\frac{R-y}{R-\delta} \right)$$

To estimate each terms order of magnitude, consider the shear stress at the wall ($\tau_w = \tau|_{y=0}$). Then, the balance between the two forces yields to:

$$\mu_l \frac{u_c}{\delta} \approx \frac{\rho_c}{Re_g^n} \left(\frac{D}{\delta} \right)^m u_c^2 \left(\frac{R-0}{R-\delta} \right) \tag{3.5}$$

Multiply equation (3.5) by the characteristic radius $R=D/2$ and grouping as follows:

$$\mu_l \frac{u_c}{\frac{\delta}{R}} \approx \frac{\mu_c}{Re_g^n} \left(\frac{\rho_c u_c D}{\mu_c} \right) \left(\frac{1}{\frac{\delta}{R}} \right)^m u_c \left(\frac{1}{1 - \frac{\delta}{R}} \right)$$

It is useful to define the dimensionless oil film thickness as

$$\varepsilon = \frac{\delta}{R} \qquad\qquad 0 < \varepsilon < 1 \qquad\qquad (3.6)$$

so the force balance becomes

$$\mu_l \frac{1}{\varepsilon} \approx \frac{\mu_c}{Re_g^n} \left(Re_g \right) \left(\frac{1}{\varepsilon} \right)^m \left(\frac{1}{1 - \varepsilon} \right)$$

Consequently, when taking the ratio of viscous force over inertia force, the result is:

$$1 \approx \frac{[\tau_{viscous}]}{[\tau_{inertia}]} = \frac{\mu_l \dfrac{1}{\varepsilon}}{\mu_c \, Re_g^{1-n} \left(\dfrac{1}{\varepsilon} \right)^m \left(\dfrac{1}{1 - \varepsilon} \right)} \qquad\qquad (3.7)$$

Grouping all terms in ε on the left side of equation (3.7), the result is

$$f(\varepsilon) = \frac{\varepsilon^{1-m}}{1 - \varepsilon} \approx \frac{\mu_l}{\mu_c} \frac{1}{Re_g^{1-n}} \qquad\qquad (3.8)$$

Observe that usually $0<m<1$, and if ε is small, $\varepsilon<<1$ (i.e., $1-\varepsilon \approx 1$), then the dimensionless function

$$f(\varepsilon) = \frac{\varepsilon^{1-m}}{1 - \varepsilon} \approx \varepsilon^{1-m} \qquad\qquad (3.9)$$

increases like ε^{1-m}. On the right side of the equation (3.8), a dimensionless group appears, which still represents qualitatively the ratio of the viscous force in the oil liquid film at

the pipe wall and the drag force due to the inertia of the refrigerant core mass flux. A dimensionless characteristic transport number (Tr) associated with the refrigerant-oil mixture can be defined as a combination of the refrigerant vapor Reynolds number and the mixture viscosity ratio:

$$\frac{1}{Tr} = \frac{\left[\tau_{viscous,film}\right]}{\left[\tau_{inertia,core}\right]} = \frac{\mu_l}{\mu_c} \frac{1}{Re_g^{1-n}} \tag{3.10}$$

Shen and Groll (2003, [98]) referred to the mixture Reynolds number (Re_m), which was defined in their work as

$$Re_m = \frac{G_{tot} \cdot D}{\mu_l} ; \qquad\qquad G_{tot} = \frac{\dot{m}_{tot}}{A}$$

Re_m is equivalent to Tr to describe the transport characteristics of the refrigerant and oil mixtures. Indeed if $n=0$ in the expression (3.10), Tr becomes exactly Re_m. The physical meaning of the transport number (Tr) or of the mixture Reynolds number (Re_m) is the ratio of the driving force for oil transport over the resistance force the oil exerts to be carried over at a given oil mass fraction (OMF) of the refrigerant-oil mixture:

$$Tr = \frac{\left[Inertia\ transport\ force\ of\ the\ core\right]}{\left[Viscous\ resis\tan ce\ in\ the\ oil\ film\right]} = \frac{\left(\mu_c Re_g^{1-n}\right)}{\left(\mu_l\right)} \tag{3.11}$$

High Tr numbers mean good transport capability of the refrigerant-oil mixture. The dimensionless oil film thickness ε should be inversely proportional to the transport number Tr:

$$\varepsilon \propto \frac{1}{Tr} = \frac{\mu_l}{\mu_c} \frac{1}{Re_g^{1-n}} \tag{3.12}$$

This simple and approximate analysis provides an intuitive physical framework that rests on the same main parameters that determine oil film thickness. Consider the miscible mixture R410A/POE and the immiscible mixture R410A/MO with the same OMFs. With the same system configuration, they will have approximately the same gas core mass flux or Reynolds number (Re_g) at the suction line location. However, they will have different transport numbers (Tr) because the immiscible pair will have higher liquid film viscosity. Equation (3.11) predicts lower Tr numbers for R410A/MO than R410A/POE, and according to equation (3.12), higher oil film thickness is expected for R410A/MO. From the literature review, the experimental results showed that immiscible oil-refrigerant mixtures, such as R410A/MO, caused oil return problems (Sundaresan, 1996, [105]). The oil leaving the compressor accumulated in the suction line and in the evaporator tubes. Schlager *et al.* (1990, [95]) compared the oil retention in smooth and micro-fin tubes using R22 and 150 or 300 SUS oil. Pure oil viscosity itself has minor effects on the amount of oil retained because what determines the oil film thickness in equation (3.12) is the liquid film viscosity μ_l in the pipe, which depends on the solubility and miscibility of the refrigerant in the oil. Nevertheless, in their experimental results, there was from 20% to 25% more oil present with the most viscous 300 SUS oil compared to the least viscous 150 SUS oil.

Equation (3.12) does not include density variations of the liquid film since the hydrostatic buoyancy force was neglected. In the next section, the gravitational force is taken into consideration. Consider again the equation (3.4), but now assume a vertical pipe. Falling film flow is a simple case of vertical annular flow. Assume the hydrostatic

buoyancy force and the inertia forces are much larger than the viscous force in the oil film. In other words, compute the ratio of the inertia force over the buoyancy force for zero wall shear stress. The force balance (3.2) can be rewritten as,

$$0 = \tau_i \left(\frac{R-y}{R-\delta} \right) + \frac{1}{2} \left(\rho_l - \rho_g \right) \cdot g_z \cdot (R-y) \cdot \left[\left(\frac{R-\delta}{R-y} \right)^2 - 1 \right]$$

When $y=0$, the above equation leads to

$$\tau_i \left(\frac{R}{R-\delta} \right) \approx -\frac{1}{2} \left(\rho_l - \rho_g \right) \cdot g_z \cdot R \cdot \left[\left(\frac{R-\delta}{R} \right)^2 - 1 \right]$$

(3.13)

After some algebra and specifying τ_i, the following equation is obtained

$$\frac{\rho_c u_c^2}{Re_g^n} \left(\frac{1}{\varepsilon} \right)^m \left(\frac{1}{1-\varepsilon} \right) \approx \left(\rho_l - \rho_g \right) \cdot g_z \cdot R \cdot \varepsilon \cdot (2-\varepsilon)$$

(3.14)

The ratio between the left and right sides of the above equation represents the ratio between the inertia force due to the core mass flux and the buoyancy force due to gravitation and density difference. At zero wall shear stress, these two forces are on the same order of magnitude, so the ratio is approximately one.

$$\frac{\left[F_{inertia,core} \right]}{\left[F_{buoyancy} \right]} = \frac{\dfrac{\rho_c u_c^2}{Re_g^n} \left(\dfrac{1}{\varepsilon} \right)^m \left(\dfrac{1}{1-\varepsilon} \right)}{\left(\rho_l - \rho_g \right) \cdot g_z \cdot R \cdot \varepsilon \cdot (2-\varepsilon)} \approx 1$$

(3.15)

By grouping all the ε terms together, the following relation is drawn:

$$g(\varepsilon) = \varepsilon^{1+m} (2-\varepsilon)(1-\varepsilon) = \frac{\rho_c u_c^2}{\left(\rho_l - \rho_g \right) g_z R} \cdot \frac{1}{Re_g^n}$$

$$= j_c^{*2} \cdot \frac{1}{Re_g^n}$$

(3.16)

where $\overset{*\,2}{j_c}$ is the critical mass flux in vertical upward flow (Mehendale, [78]). Thus, the

final result is summarized qualitatively by the following equation:

$$\frac{\left[F_{inertia,core}\right]}{\left[F_{buoyancy}\right]} \approx \overset{*\,2}{j_c} \cdot \frac{1}{Re_g^n} \cdot \frac{1}{g(\varepsilon)} \tag{3.17}$$

This simple analysis allows one to derive the same parameter that described the oil flow

reversal onset in Mehendale's analysis [78]. In his investigation, the friction factor was

independent from the gas core Reynolds number. The equation (3.17) collapses to

Mehendale's parameter if the dependence of the interfacial friction factor f_i from the core

Reynolds Re_g number can be neglected.

Figure 3.9 is meant to clarify the behavior of different pairs of oil-refrigerant

solutions at the evaporator inlet and at the suction line based on estimated mass fluxes

and fluid proprieties. At the evaporator inlet, the flow pattern depends on vapor quality,

and the previous separated annular flow model should not be used. Martinelli's two-

phase flow model needs to be applied in the evaporator and condenser to achieve more

accurate conclusions. Assuming $n=0.768$ as suggested by Wongwises and

Kongkiatwanitch (2001, [116]), the viscosity ratio change becomes the most significant

influences on dimensionless liquid thickness in the equation (3.12). The separate cylinder

model, which resembles Martinelli's original formulation, still has the virtue of allowing

one to pursue a qualitative conclusion. For given refrigerant-oil mixture A_1/A_2 (example

R22/MO), the estimated oil film thickness can be computed using the relation (3.12),

yielding to a certain oil film thickness $\delta_{A,min}$ and $\delta_{A,max}$. For a different refrigerant-oil

mixture B_1/B_2, the minimum and maximum film thickness $\delta_{B,min}$ and $\delta_{B,max}$ will be

different from $\delta_{A,min}$ and $\delta_{A,max}$. Similarly, C_1/C_2 mixture will also exhibit different behavior. An oil film thickness range can be established because the minimum oil retention volume occurs at the liquid line, while the maximum film thickness is expected at the suction line. Figure 3.10 summarized qualitatively oil film thickness estimations for different refrigerant-oil mixtures. It highlights situations of poor oil return and high oil retention volume, which usually occurs for those oil-refrigerant pairs with high film over low refrigerant vapor viscosity ratio. The viscosity is a consequence of miscibility, so immiscible pairs, such as R410A/MO and R407C/MO, are the most critical mixtures from oil transports perspective. The expected oil film thicknesses have been normalized with respect to that of R22/MO mixture.

Finally, the following refrigerant and oil mixtures should cover the widest range of dimensionless mass flux j_g^*, core Reynolds numbers Re_g, and viscosity ratios $\mu^* = \mu_l/\mu_c$:

- R22/MO;
- R410/MO and R410/POE;
- R134a/POE and R134a/PAG;

The oil retention experimental data about CO_2/PAG oil (Lee, 2002 [68]) will be included as well to complete the framework. The effect of miscibility and solubility between oil and refrigerant can be investigated while changing only one fluid at a time during the experiments. Since the air conditioning system is designed for R22/MO, a certain number of tests will be carried out for mixtures with the following variables as parameters:

- OMF from 0 to 8 wt.%

46

- Refrigerant flow rate from 42 to 60 g/s

This approach should produce a consistent set of experimental data for the development of a semi-empirical oil retention model. Once the model is established, enough experimental points will be taken for all other refrigerant-oil mixtures to confirm that they behave as the simulations do.

Table 3.1 Environmental Effects of Refrigerants (Hwang, 1997)

Refrigerants		Ozone Depletion Potential (ODP)	Global Warming Potential (GWP, 100 yr)
CFC	R12	1	7100
HCFC	R22	0.055	1500
HFCs	R134a	0	1200
	R407C	0	1600
	R410A	0	2200
Natural Refrigerants	R744 (Carbon dioxide)	0	1
	R717 (Ammonia)	0	0
	R290 (Propane)	0	3
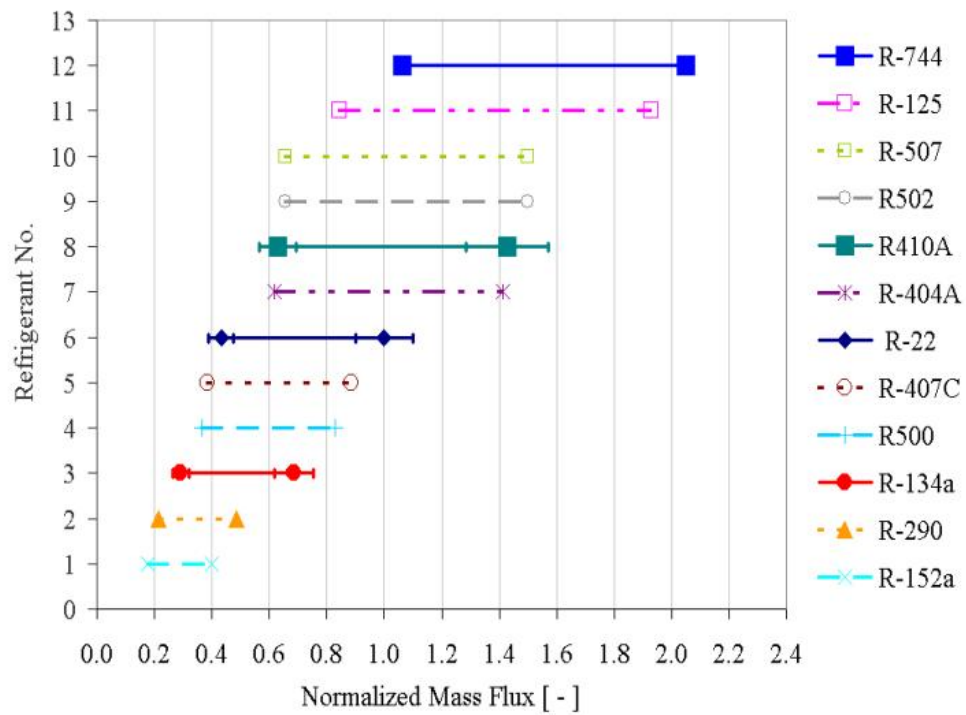
Figure 3.1: Mass Flux Range for Different Refrigerants
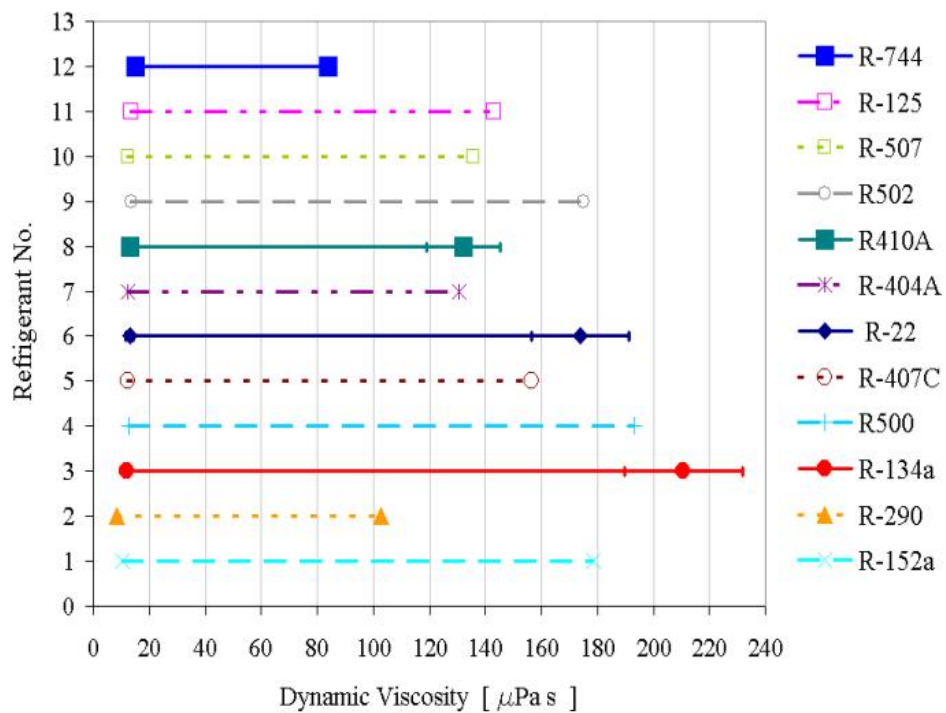
Figure 3.2: Viscosity (μ_c) Range for Different Refrigerants

49
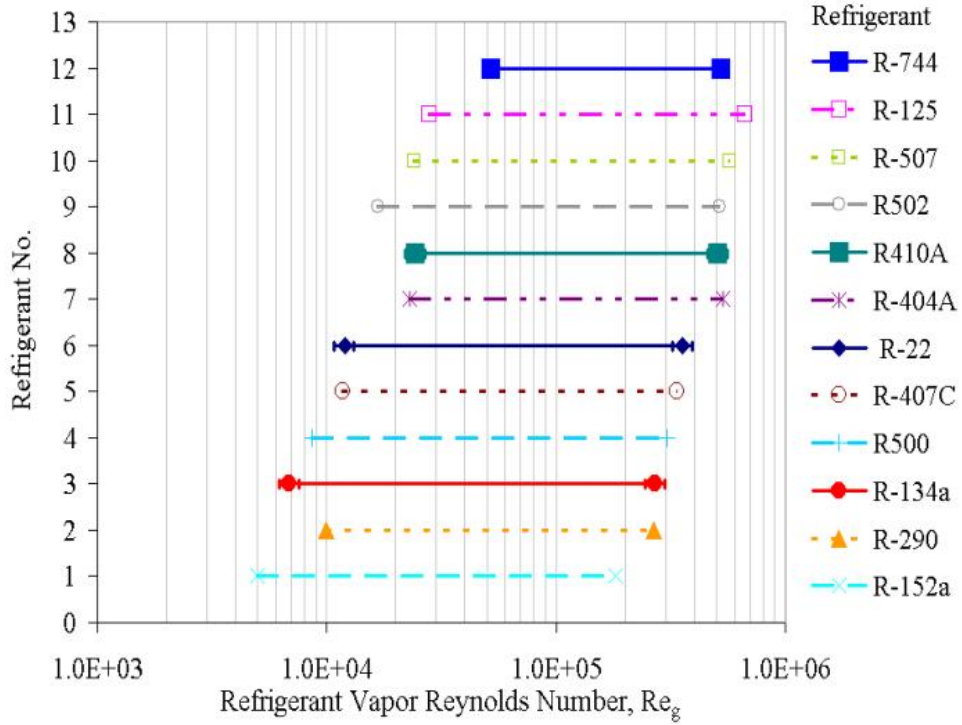
Figure 3.3: Reynolds Number Range (at the Suction Line) for Different Refrigerants
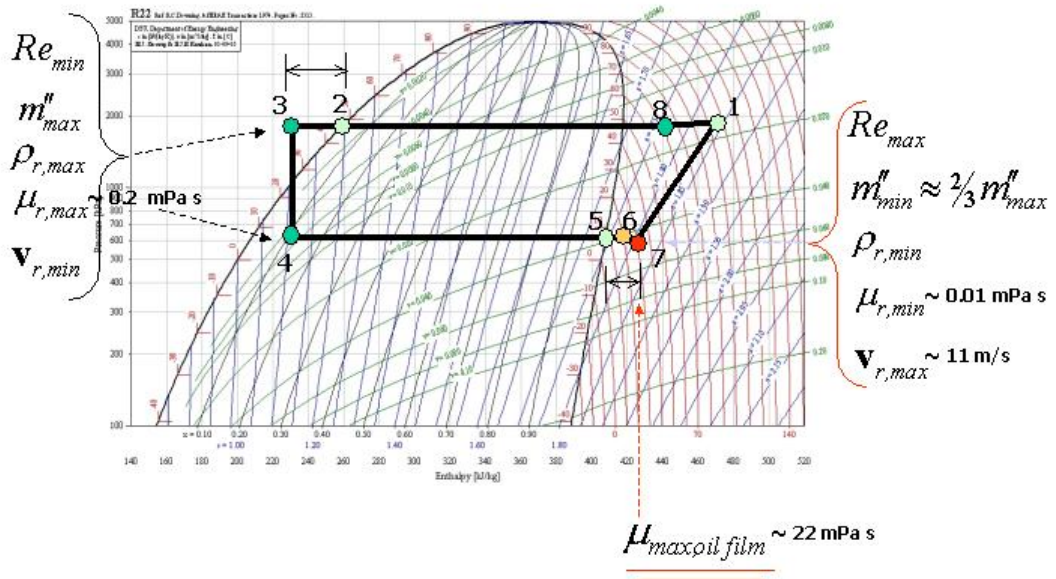
Figure 3.4: Refrigerant and Oil Film Properties in R22 Vapor Compression Cycle
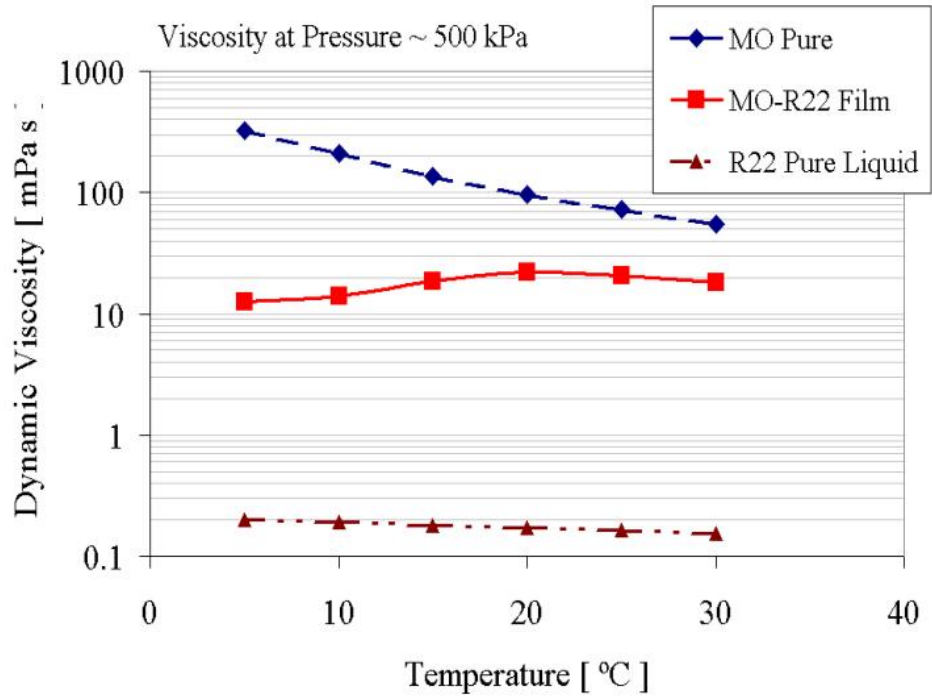
Figure 3.5: Viscosity Variations For BWMO/R22 Oil Film
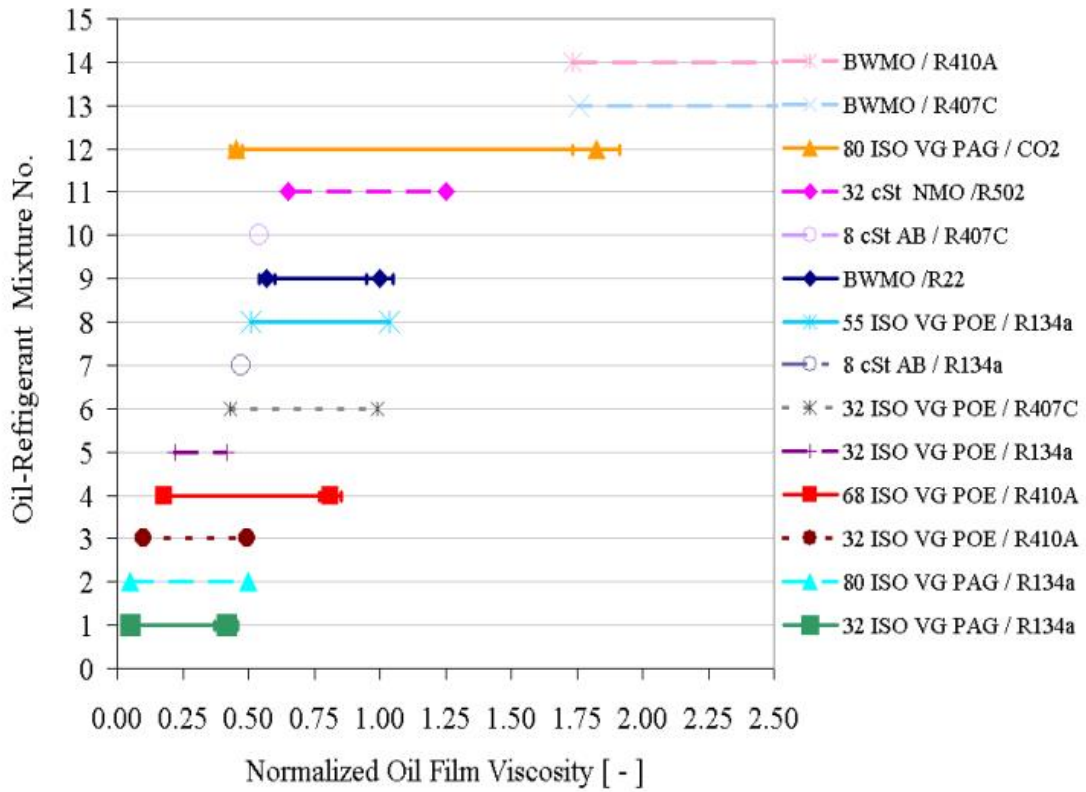
Figure 3.6: Viscosity (μ_f) Range for Different Oil-Refrigerant Film Mixtures
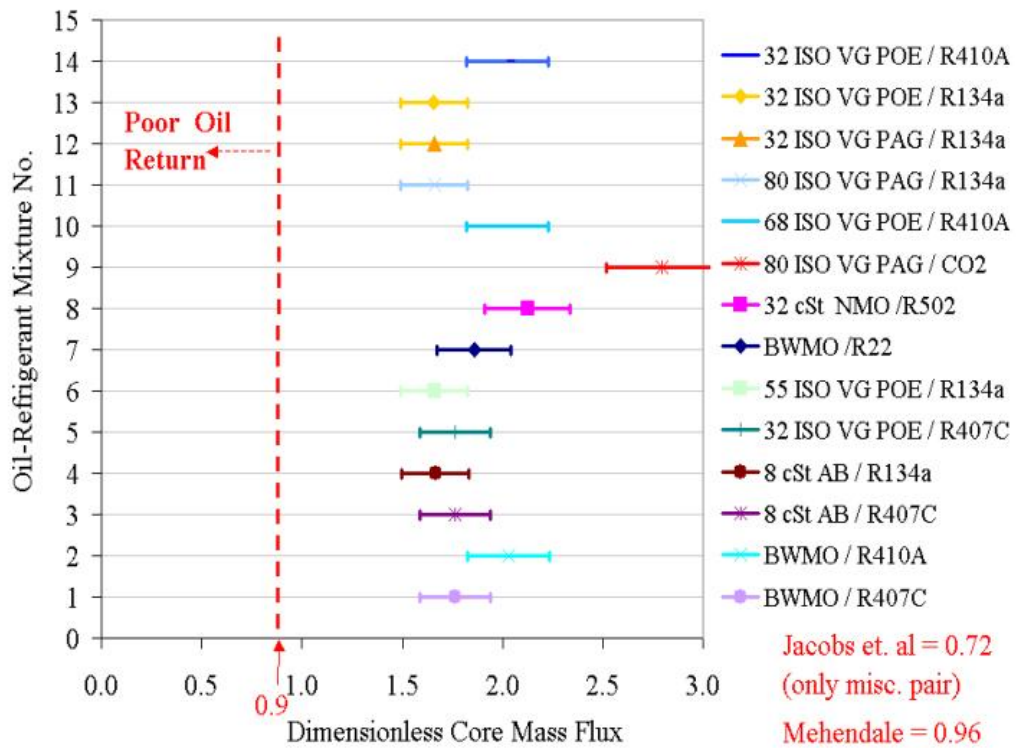
Figure 3.7: Dimensionless Transport Mass Flux for Different Refrigerant-Oil Mixtures
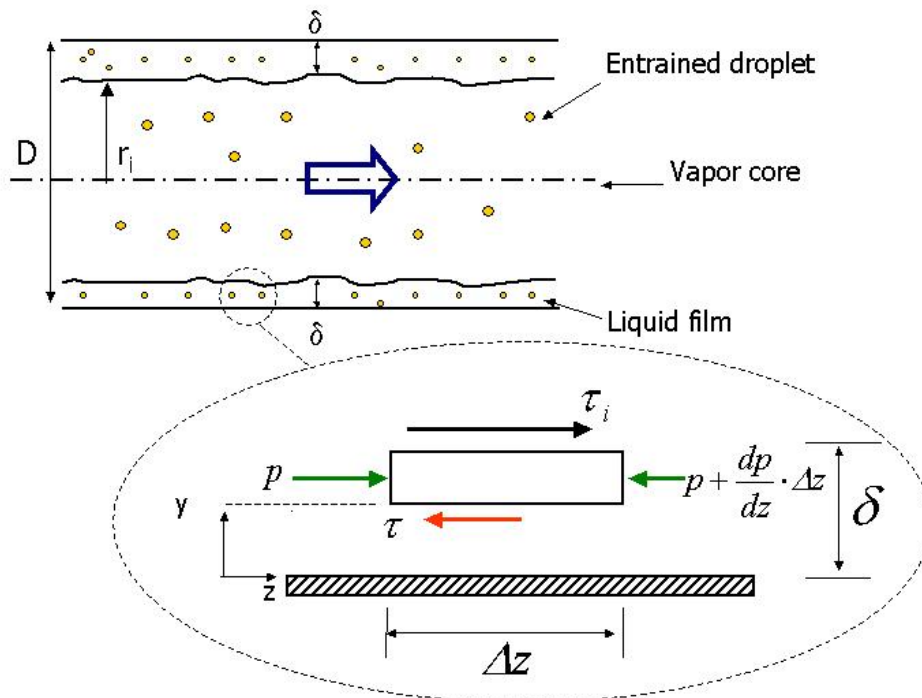
Figure 3.8: Oil Entrainment Simple Model

52
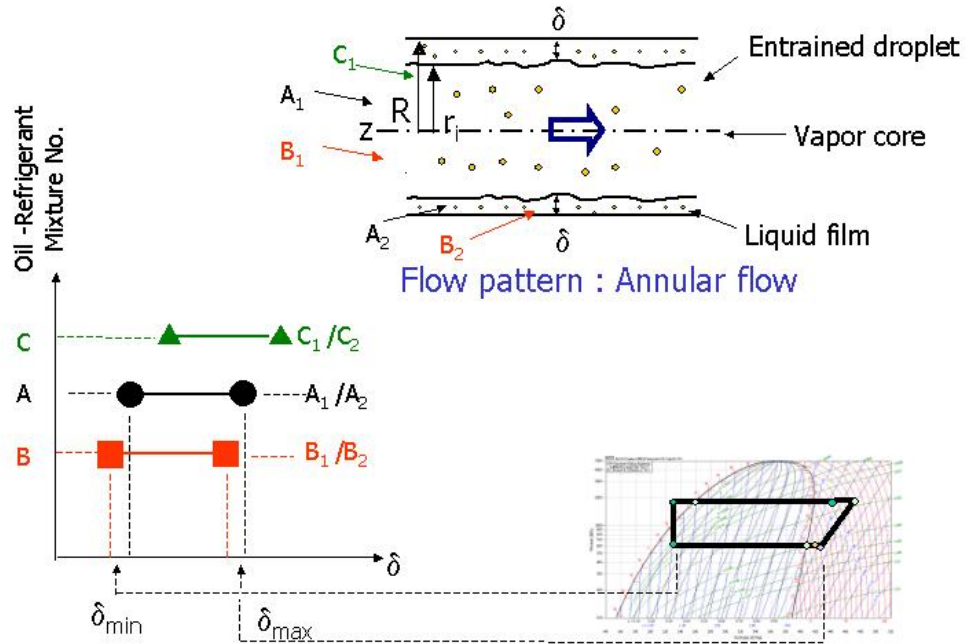
Figure 3.9: Schematic Model to Predict Oil Film Thickness δ
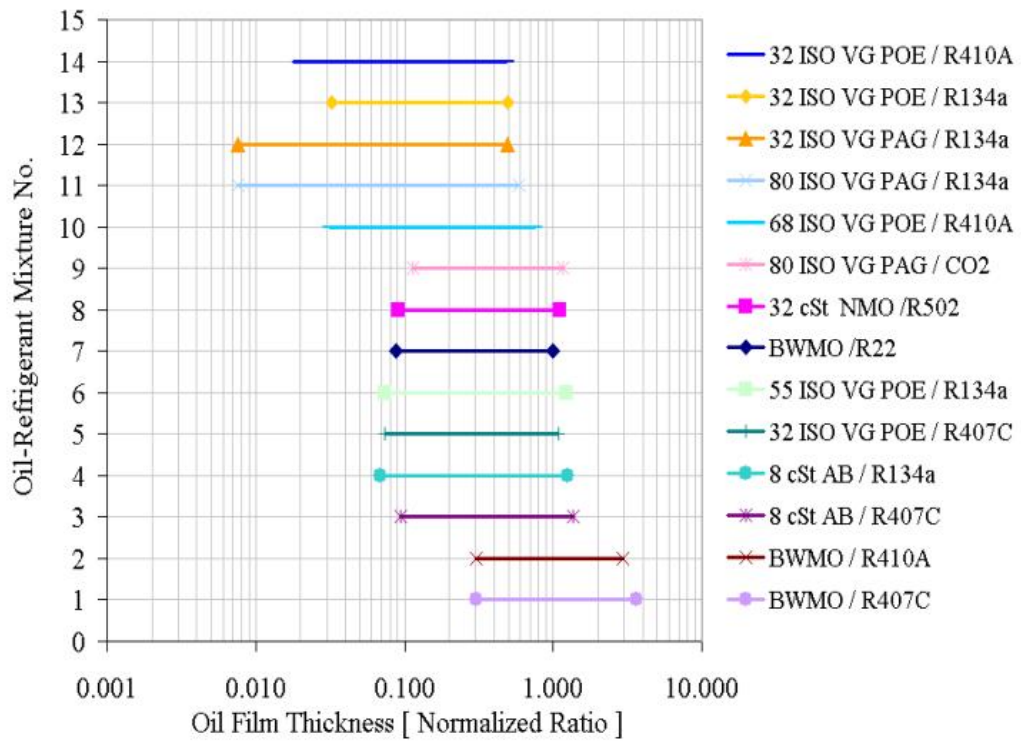
Figure 3.10: Estimated Oil Film Thickness for Different Refrigerant-Oil Mixtures

Chapter 4: Experimental Setup

4.1 Test Facility

The schematic diagram of the test facility is illustrated in Figure 4.1. The indoor (ID) unit (6) is located in a closed air-loop simulating indoor air conditions, while the outdoor (OD) unit (3) is placed in an environmental chamber that simulates outdoor conditions. The test unit is designed for R22 and is rated 10 kW. The ID heat exchanger has five passes of inlet and outlet, while the OD heat exchanger has four passes of inlet and outlet. The inside heat transfer coefficient is improved because of increased surface area and turbulation induced by integral helical ridges on the inside surface of the heat exchanger tubes. A modified scroll compressor (1) with a sight tube and a sight glass is used. The sight tube allowed the liquid volume in the compressor to be monitored. An oil loop system stands next to the residential air conditioning system. The oil injection and extractor device is schematically shown in Figure 4.2. The oil loop consists of an oil reservoir tank (11), a variable speed gear pump (13), a check valve along the injection line (15), an oil extractor (16), and an oil level sensor (17). The centrifugal oil pump has difficulty in passing gas bubbles and can lose its prime if the gas pocket is large enough. It should be ensured that R22 gas is not being drawn through its inlet to avoid pump cavitations and decoupling. The vertical tank, whose internal volume is about 2.25 liters, provides a proper prime for the oil pump and a 5/8 inches outer diameter pipe is installed at the pump suction. An electric tape heater (12) is placed around the oil reservoir tank

wall to help refrigerant-oil phase separation and minimize the solubility effects in the injection line.

4.1.1 Vapor Compression System and Oil Loop

Table 4.1 presents the specifications of the components used in the residential air conditioning system. Table 4.2 shows the specifications of the components that form the oil injection/extraction system. Four sight glasses before and after each heat exchanger provide windows to monitor the oil flow. The sight glass used for the visualization of the flow in the suction line is shown in Figure 4.5. Use of A/C dye and ultraviolet light enhances oil flow monitoring. In particular, the first sight glass after the discharge oil separator allows verification of whether oil is flowing out from the compressor. From the experimental tests, the measured OMF was less than 0.5 wt.% and no oil was observed in the sight glass after the compressor discharge. However, a small amount of oil is always circulating through the system, which creates the potential to measure incorrectly the oil retention amount. During the tests, if oil was not injected in the test section then the oil level in the level sensor tank remained constant. Consequently, it is assumed that the oil retained in each component, which is the difference between oil injected and oil extracted, is negligible when oil is not injected during the system run. In other words, the experimental oil retention results do not consider the oil amount that already exists in the test section due to compressor run. They can be shifted by constants, which represent the oil retention volumes at OMF equal or less than 0.5 wt.%. These oil retention volumes

are equal or less than 10 ml, which is the sensitivity of the oil level sensor. For example the oil retention volumes per unit length in the suction line can shift by an existing oil volume equal or less than 0.52 ml/m.

4.1.2   Measurements and Data Acquisition System

More than 100 sensors are distributed along the system to measure pressures, temperatures, flow rates, power consumptions, and air properties such as dew points and dry bulb temperatures. The pressure transducers are Setra Model 280E. Two Coriolis mass flow meters are used: the refrigerant mass flow meter is installed in the liquid line next to the OD unit, while the oil mass flow meter is placed along the oil injection line after the oil pump. All the sensors are connected to a Hewlett Packard (HP) 3497A data acquisition and control unit, and they are displayed in real time by Labview software graphic interface. A screenshot of the data acquisition system software interface is shown in Figure 4.6.

Temperature and Pressure Measurements

Thermocouples are used to measure temperature at several locations in the test facility. The data acquisition system uses hardware and software compensation to simulate the reference junction, thus eliminating the need for physical reference junction at constant reference temperatures. The voltages from the thermocouples are converted into temperature values using appropriate software in the data acquisition program. Table 4.3 shows the detailed specifications of the thermocouples.

Absolute pressure transducers are installed at the compressor discharge point, condenser inlet and outlet, expansion device inlet, evaporator inlet and outlet, and compressor suction sites. Detailed specifications are shown in Table 4.4.

Mass Flow Rate Measurements

Two Coriolis mass flow meters are used to measure refrigerant and oil mass flow rates. The refrigerant mass flow meter is installed at the condenser outlet. Since the mass flow meter does not provide reliable measurements for two-phase flows, a minimum degree of sub-cooling of about five degrees is necessary to guarantee always one-phase liquid flow through the instrument. The refrigerant mass flow meter specifications are shown in Table 4.5. In order to measure the amount of oil injected, the oil mass flow meter is installed in front of the oil injection port. The oil mass flow meter was scaled down and re-calibrated to measure mass flow rates ranging from 0.6 to 5 g/s. Indeed, during the preliminary tests, the oil injection flow rate was relatively smaller than the capacity of the mass flow meter. Specifications of the oil mass flow meter are given in Table 4.6.

Oil Level Measurements

The amount of oil taken from the extractor needs to be measured to compute the oil retention volume. The extractor drains the oil through a u-shape tube into the oil level sensor vessel. In-stream thermocouples measure the bulk temperature of the liquid oil-refrigerant mixture entering the level sensor vessel, which was properly insulated to minimize heat conduction effects. A capacitance probe measures the height of the

mixture in the vessel. A change in the value of the capacitor takes place because the dielectric constant between electrode and tank wall changes (Level Sensing Element Omega Operator's Manual, [86]). A radio frequency capacitance instrument detects this change and converts it into a relay actuation or proportional output signal from 4 to 20 mA. While the actual capacitive equation is very complex, it can be approximated as follows:

$$C = \frac{0.255 \cdot \left(K_{gas} \times A_{gas}\right)}{d} + \frac{0.255 \cdot \left(K_{oil} \times A_{oil}\right)}{d} \qquad (4.1)$$

where

C = capacitance [pF];

K_{gas} = dielectric constant of the gas [pF/m] (~ 1 pF/m)

K_{oil} = dielectric constant of the oil in the level sensor tank [pF/m] (~ 2 pF/m)

A_{gas} = inner area of the accumulator tank wall surrounded by gas [m^2]

A_{oil} = inner area of the accumulator tank wall surrounded by oil [m^2]

d = distance between the accumulator wall and electrode [m]

Since the electrode and tank wall are fixed in place, the distance between them does not vary and the following equation is obtained:

$$C = 2\pi \times 0.255 \cdot \left[K_{oil} \times h_{oil} + K_{gas} \times \left(1 - h_{oil}\right)\right] \qquad (4.2)$$

where h_{oil} is the dimensionless height of the oil in the vessel ($0 \leq h_{oil} \leq 1$).

When the oil accumulates in the levels sensor tank, h_{oil} increases in equation (4.2). If a higher dielectric constant material replaces a lower one, the total capacitance output of

the system will increase. Thus, the capacitance is directly proportional to the volume of the measured oil. The detailed specifications of the oil level sensor are shown in Table 4.7. The level sensor was calibrated by using the oil mass flow meter. The oil was injected directly into the oil level sensor vessel and measured by the oil mass flow meter. The output signal, which corresponds to the oil level in the oil vessel accumulator, was measured. Thus a linear calibration curve was calculated. Verifications of the oil amount measured by the oil level sensor were performed by manually pouring oil directly into the oil vessel. The influence of temperature on the dielectric constant K_{oil} and on the electronic noise of the transmitter was investigated. A calibration curve was computed at room and oil temperatures in equilibrium at 27 ºC. If the temperature of the oil changed to about ± 8ºC apart from 27ºC, the calibration results did not show a significant variation of the dielectric constant. If the temperature of the air around the electronic transmitter ranged between ± 8ºC from 27ºC, the output signal was influenced less than ±5%. However, more than ±6% of relative error was observed if oil and transmitter temperatures were equal to or higher than 43ºC. Figure 4.7 shows the calibration curves for the oil level sensor at different temperatures. The effects of density variations with temperature change have been included in the calibration curves. Thus, the difference between the two methods of oil volume measurement shown in Figure 4.7 can be due to the dielectric constant temperature dependence, $K_{oil}=K_{oil}(T)$ in the level sensor vessel.

Refrigerant dissolved into the oil and accumulated inside the oil level vessel affects the value of h_{oil} and K_{oil} in equation (4.2). Using temperature, solubility, and density charts, a compensation method can account for variations in h_{oil}. The change of K_{oil} should not

affect the measured volumes since the volume extracted is a relative difference between final and initial volume:

$$V_{exctracted} = V_{final} - V_{initial} = \Delta V_{oil} \qquad (4.3)$$

Thus, the difference in capacitance is proportional to:

$$\Delta V_{oil} \propto \Delta C \propto \left[K_{mixture, final} \times h_{mixture, final} - K_{mixture, initial} \times h_{mixture, initial} \right] \qquad (4.4)$$

In equation (4.4) the dielectric constants $K_{mixture, initial}$, and $K_{mixture final}$ are not the same as K_{oil} of equation (4.2) because the material is different in composition: oil-rich mixture in one case and pure oil in the other. However, if the mixture of oil and refrigerant maintains the same solubility from the beginning to the end of the extraction period, it is reasonable to assume

$$K_{mixture, initial} \approx K_{mixture, final} \approx K_{mixture} \qquad (4.5)$$

since the material in the vessel maintains similar composition. Thus, the change in capacitance reflects only a change in the mixture volume:

$$\Delta C \propto K_{mixture} \left[h_{mixture, final} - h_{mixture, initial} \right] \propto \Delta V_{mixture} \qquad (4.6)$$

A verification of the oil level calibration curve under realistic system operating temperatures and pressures has been performed to confirm the above assumption (4.5), which is of primary importance for the experimental part of this research work. The calibration curves for different oil and refrigerant pairs at various degrees of solubility are

60

given in Figure 4.8. As expected, the volume-voltage relation of the level sensor was different for each oil and refrigerant pair. It also depended on the amount of refrigerant dissolved into the oil. To obtain more accurate measurements, the proper calibration curve was selected depending upon type of mixture and degree of solubility.

4.2   Sources of Errors and Uncertainty Analysis of the Preliminary Results

During oil retention measurements, several sources of errors were identified. They are as follows:

- Pressure measurement accuracy

- Temperature measurement accuracy

- Mass flow rate (oil and refrigerant) measurement accuracy

- Accuracy of the amount of refrigerant dissolved in oil

- Oil viscosity and density values accuracy.

4.2.1   Temperature, Pressure, and Mass Flow Rate Measurement Accuracy

All the pressure transducers have been calibrated using a high precision pressure calibration machine. The accuracy achieved was about ± 10 kPa. The temperature measurement accuracy was about ± 0.5ºC. Copper-Constantan thermocouples have been installed in-stream mode to read the refrigerant bulk temperatures. The connecting lines,

the extractor and the level sensor tank were properly insulated to avoid any misreading of the temperature due to heat conduction.

During the preliminary tests, the oil mass flow rate changed from 0.7 to 5.2 g/s. The largest relative error of the oil mass flow meter was the following:

- ±10% at 0.4 g/s;

- ±6% at 0.7 g/s;

- ±1% at 5 g/s;

The refrigerant mass flow rate changed from 46 to 66 g/s. In this range, the accuracy of the mass flow meter was within ± 0.5% of the rate. The OMF has been computed by measuring the oil and refrigerant mass flow rates and by dividing them according to the definition (2.1).

In order to estimate the noise perturbation, all transducers have been checked in place at different chamber temperatures and with several electric loads working close by. The level sensor transmitter showed the highest sensitivity to temperature variations and to noise interferences. After electrical power cables and signal wires were positioned in separate channels, the electric noise interference on instrumentation output signals was negligible. The largest error of the oil level sensor was estimated from the calibration curves as follows:

±10% at volume equal to 100 ml;

± 7% at volume equal to 1000 ml;

4.2.2   Oil Retention Uncertainty

The Oil Retention volume (*OR*) is defined as the difference in two mass measurements divided by the average oil density, i.e.:

$$OR\,[\text{ml}] = \frac{1}{\overline{\rho}_{oil}}\left[Oil\ Amount\ Injected\,[\,g\,] - Oil\ Amount\ Extracted\,[\,g\,]\right]$$

$$= \frac{1}{\overline{\rho}_{oil}}\left[\int_{t_1}^{t_2}\dot{m}_{oil,inj}\,dt - \Delta m_{Level,Sensor}\Big|_{t_1}^{t_2}\right]$$

Thus, the uncertainty of the oil retention volume (u_{OR}) can be estimated as

$$u_{OR} = \sqrt{\left(u_{\dot{m}_o}\cdot\frac{\partial OR}{\partial \dot{m}_{oil}}\right)^2 + \left(u_{\overline{\rho}_{oil}}\cdot\frac{\partial OR}{\partial \overline{\rho}_{oil}}\right)^2 + \left(u_{dt}\cdot\frac{\partial OR}{\partial dt}\right)^2 + \left(u_{m_{Level,Sensor}}\cdot\frac{\partial OR}{\partial m_{Level,Sensor}}\right)^2}$$

where OR = oil retention volume; u_{OR} = uncertainty of the OR;

$\dot{m}_{oil}$ = oil mass flow rate; $u_{\dot{m}_o}$ = oil mass flow rate accuracy;

$\overline{\rho}_{oil}$ = average oil density; $u_{\overline{\rho}_{oil}}$ = average oil density accuracy;

dt = average time step; u_{dt} = average time step accuracy;

$m_{Level,Sensor}$ = oil mass in the level sensor; $u_{m_{Level,Sensor}}$ = level sensor accuracy.

From the experimental tests, several uncertainty values have been computed. The maximum overall uncertainty in oil retention volume has been estimated as follows:

±16% at volume equal to 50 ml;

± 5% at volume equal to 500 ml;

Using a dedicated Engineering Equation Solver (EES), uncertainty of the oil retention was computed. The model inputs were independent variables and their accuracies. Then, the model computed the propagation of error and predicted the uncertainty on the

dependent variables. The average estimated uncertainty on oil retention volume was about 12% relative error.

4.2.3   Solubility Effects and Oil Proprieties

The solubility effects of the refrigerant in corresponding oil have been included when computing the oil retention amount. Both the injected and extracted oil contain the refrigerant dissolved in it. The solubility was from 6 to 15 % in mass in the injected oil and from 10 to 20 % in mass in the extracted oil, depending on the test pressures and temperatures. The average oil film solubility was from 6 to 25 % in mass in the suction line, depending on pressure, temperature, and refrigerant-oil pair.

Density and viscosity of the liquid film have been computed according to temperature and pressure measurements and solubility effects. The thermodynamic proprieties of the oil and refrigerant mixtures were provided by the refrigeration companies that sponsored the research work at CEEE of the University of Maryland. Since they were available only in graphic form, surface fit interpolations were necessary. All the predicted values from the surface interpolations were within 90% confidence limit with respect to the measured data.

An oil presence increases the surface tension of the refrigerant-oil mixture significantly (Shen 2003 [98]). The actual values of the surface tension of the specific oil-refrigerant mixtures used in the experiments were unknown. The surface tension is the surface energy between a liquid and its own vapor, or air, or a metal surface. The static surface tension of oils on metals can be compared by placing a small drop on a clean metal

surface and observing if the drop has high contact angle (high surface tension) or very low contact angle (spreads out, low surface tension). Interfacial tension exists between the oil and another fluid. Dynamic surface tension of pure lubricant and dynamic interfacial tension of refrigerant-lubricant mixture can be measured experimentally using the maximum bubble pressure technique. This method involves injecting a gas (air for dynamic surface tension and refrigerant gas for dynamic interfacial tension) into the liquid while monitoring the pressure inside the bubbles formed. However, measuring the surface tension is only feasible for static oils and not for flowing flows. The dynamic surface tension of the film of oil and refrigerant mixture was estimated according to the equation recommended by Shen and Groll (2003 [98]):

$$\sigma_{\mathrm{m}} = \sigma_{ref,liq} + \left(\sigma_{oil} - \sigma_{ref,liq}\right) \cdot \sqrt{\omega_{local}}$$

where ω_{local} is the local oil mass fraction of the oil-refrigerant mixture. The surface tension of a generic pure mineral oil is equal to about 33 mN/m in air. The surface tension of POE oil is about 46 mN/m while the surface tension of PAG oil is about 31.5 mN/m. These are common values for compressor lubricants used in different A/C applications, but they can vary depending on the chemicals added to the oil. Oil surface tension values are the static surface tension of pure oils on clean metal surface in air, which usually are the most common surface tension data available from the manufacture.

Table 4.1: Component Specifications of the Air Conditioning System

	Components	Manufacturer	Description
1	Compressor	-	Type: Scroll Compressor; HCFC R22, 60 Hz, 1-Phase, 208 V; N = 3500 RPM ; Max Power = 3 kW; Volume Flow Rate = 9.68 m^3/h ($\approx$ 342 ft^3/hr) Mass Flow Rate = 63 – 65 g/s $\qquad$ ($\approx$ 500 – 515 lbs/hr) Max Oper. Pressure = 27.5/20 H/L (bar); Tube Diameter = ¾" In, 3/8" Out; Oil = 42 oz Mineral (~1242 cm^3);
2	Oil Separator	Henry Technologies	Type: Helical Oil Separator with floating valve 5/8" O.D. (Model S-5185)
3	Condenser	-	Type: 4 passes of inlet and outlet Cross Flow, Fin-and-Tube Heat exchanger Tube O.D. Vapor = ¾" ; Tube O.D. Liquid = 3/8" Axial Fan (1/5 hp, 825 RPM, 2800 cfm) Face Area: 18.5 Sq ft
4	Mass Flow Meter	Micromotion	Type: Coriolis Mass Flow Meter Model: DH025S119SU Mass Flow rate: 1 – 100 g/s ($\approx$ 8 – 794 lbs/hr)
5	Expansion Device	Swagelok	3/8" O.D. Integral Bonnet Needle Valves Model: SS-1RS6
6	Evaporator	-	Type: Slope-Coil, fin-and-tube, 5 passes inlet and outlet, down-flow air Fan: Part of Indoor Loop Pipe O.D. Inlet = 3/8"; Pipe O.D. Outlet = ¾"

			Face Area ≈ 0.25 m^2 (= 2.7 Sq ft)
7	Accumulator	Henry Technologies	Tube Diameter: 7/8" In, 7/8" Out
8	Gas Line	-	Pipe O.D. = ½"
9	Liquid Line	-	Pipe O.D. = 3/8"; Total Pipe length = 23 m; (Vertical = 5 m; Horizontal = 17 m)
10	Suction Line	-	Pipe O.D. = 7/8" ; Total Pipe length = 19 m; (Vertical = 5 m; Horizontal = 14 m)

Table 4.2: Component Specifications of the Oil Injection/Extraction System

Component		Manufacturer	Description
11	Oil Reservoir Tank	Swagelok	Internal Volume ≈ 3 liters (≈ 0.8 gallons) (1 tank of 1 liter plus 1 tank of 2 liters)
12	Electric Heater	Omega	Type: Electrical Tape Heater Power = 600 W
13	Oil Pump	MicroPump	Type: Series 220 Magnetically Driven Gear Pump Motor: 1/3 HP variable speed DC motor Speed= 1750 – 4000 RPM Flow rate:1 – 58 cm^3/s (0.06 – 3.5 liters/min) (≈ 3.66 – 214 in^3/min)
14	Mass Flow Meter	Micromotion	Type: Coriolis Mass Flow Meter Model D-12 Mass Flow rate = 0.4 – 5.5 g/s
15	Check valve	Swagelok	Size: ¼" O.D.
16	Extractor	Henry Technologies	Type: Helical Oil separator Pipe Dimension: 1 and 3/8 O.D. Model: S-5190
17	Level Sensor	Omega	Type: Capacitor Level Probe Model: LV5204-Y0-15-Z5 Internal Volume ≈ 2 liters Actual Volume ≈ 1.5 liters
18	Injection Line	-	Pipe O.D. = ½" O.D.
19	Oil Pump Suction Line	-	Pipe O.D. = 5/8" O.D.

Table 4.3: Specifications of Thermocouples

Item	Specification
Thermocouple type	T-type
Alloy Combination	Copper-Constantan
Temperature range	-270 to 400 ºC
Accuracy	± 0.5 ºC
Manufacturer	Omega Engineering, Inc.

Table 4.4: Specifications of Absolute Pressure Transducers

Item	Specification
Model	280E
Pressure Range	0-500 psia (0-3.4 MPa)
Accuracy	± 0.11 % Full Scale
Output	0-5 VDC
Excitation	24 VDC Nominal
Manufacturer	Setra System, Inc.

Table 4.5: Specifications of Refrigerant Mass Flow Meter

Item	Specification
Sensor Model	DH025S119SU
Transmitter Model	1700C11ABUEZZZ
Type of Sensor	Coriolis Mass Flow Meter
Flow Range	$1 - 100$ g/s ($\approx 8 - 794$ lbs/hr)
Accuracy	± 0.5 % of rate
Maximum Operating Pressure	3000 psig (20.7 MPa)
Maximum Operating Temperature	150 ºC
Output	4 to 20 mA
Manufacturer	Micro Motion Inc.

Table 4.6: Specifications of Oil Mass Flow Meter

Item	Specification
Sensor Model	D-12 Series
Transmitter Model	Elite Model RFT9739
Type of Sensor	Coriolis Mass Flow Meter
Flow Range	$0.4 - 5.5$ g/s
Accuracy	Max ± 10% at minimum rate
Maximum Operating Pressure	11.7 MPa
Maximum Operating Temperature	204 ºC
Output	4 to 20 mA
Manufacturer	Micro Motion Inc.

Table 4.7: Specifications of Oil Level Sensor

Item	Specification
Sensor Model	LV5200
Transmitter Model	LV5900
Type of Sensor	Capacitance Sensor
Range	0 – 38 cm
Linearity	± 0.5% of full scale
Maximum Operating Pressure	6.89 MPa
Maximum Operating Temperature	232 ℃
Output	4 to 20 mA
Manufacturer	Omega Engineering,Inc.
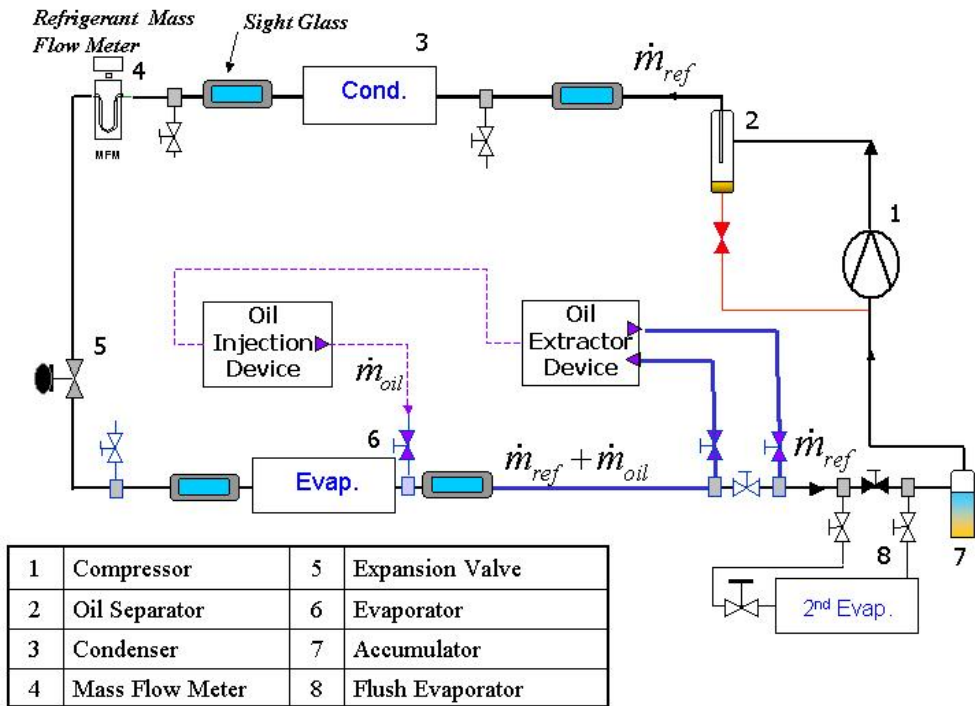
Figure 4.1: Schematic Diagram of the Test Facility

1	Compressor	5	Expansion Valve
2	Oil Separator	6	Evaporator
3	Condenser	7	Accumulator
4	Mass Flow Meter	8	Flush Evaporator

9	Oil Reservoir
10	Electric Heater
11	Gear Pump
12	Oil Mass Flow Meter
13	Check Valve
14	Oil Extractor
15	Oil Level Sensor
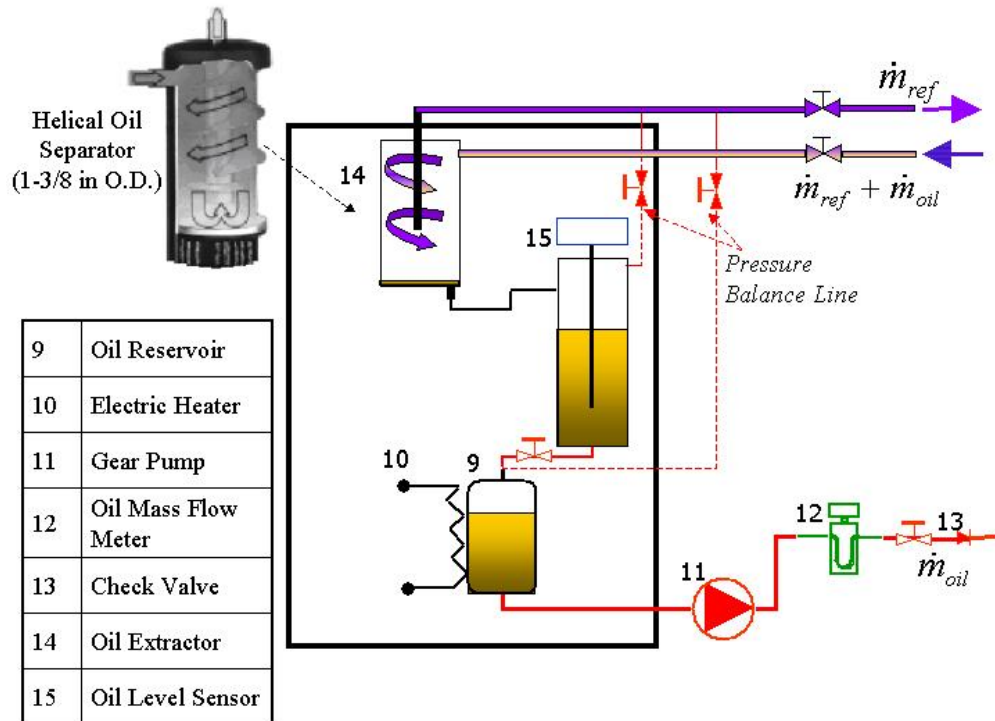
Figure 4.2: Schematic Diagram of the Oil Injection/Extraction Device

Figure 4.3: Slope Coil Heat Exchanger used as Evaporator in the Oil Retention Test
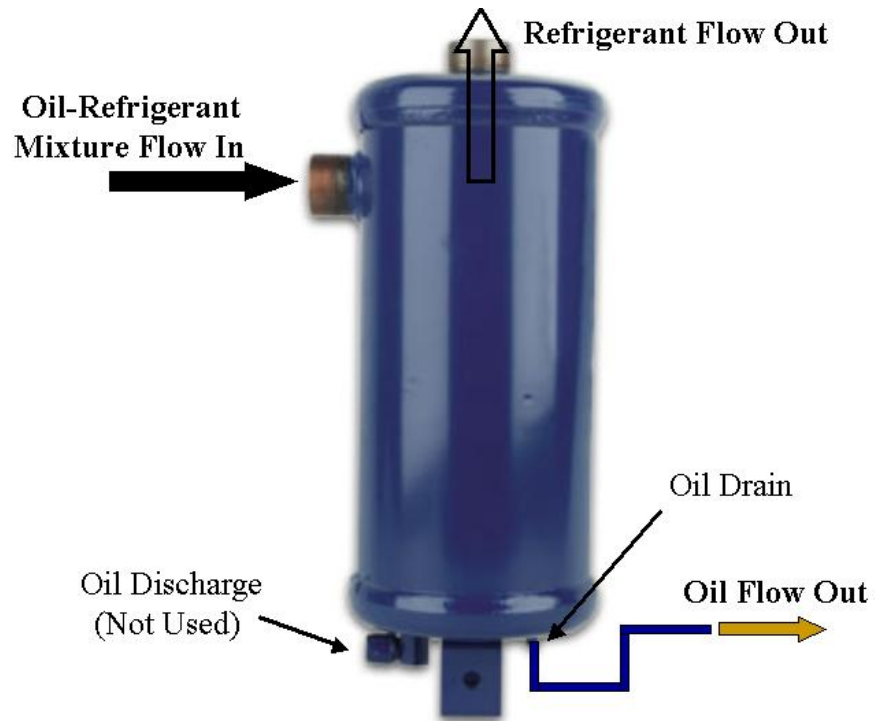
Figure 4.4: Oil Extractor (Modified Helical Oil Separator, Henry Technologies)
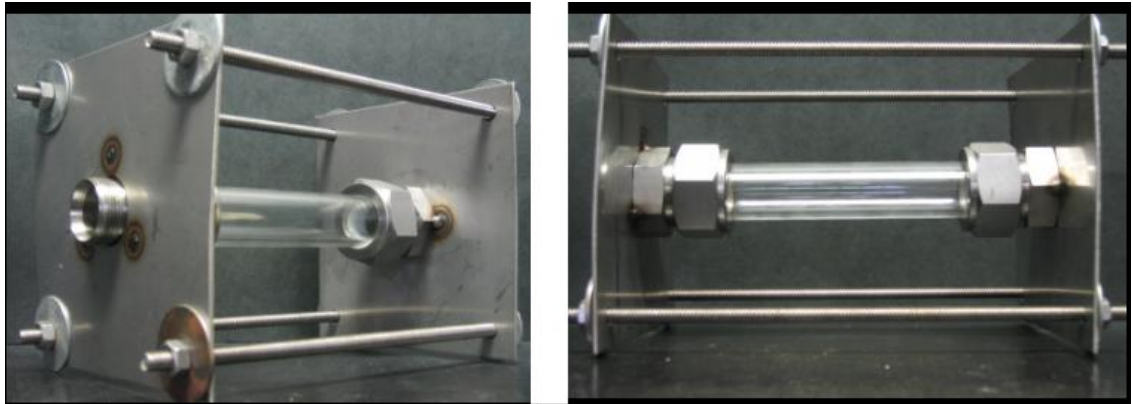
Figure 4.5: Sight Glass Tube for Flow Visualization
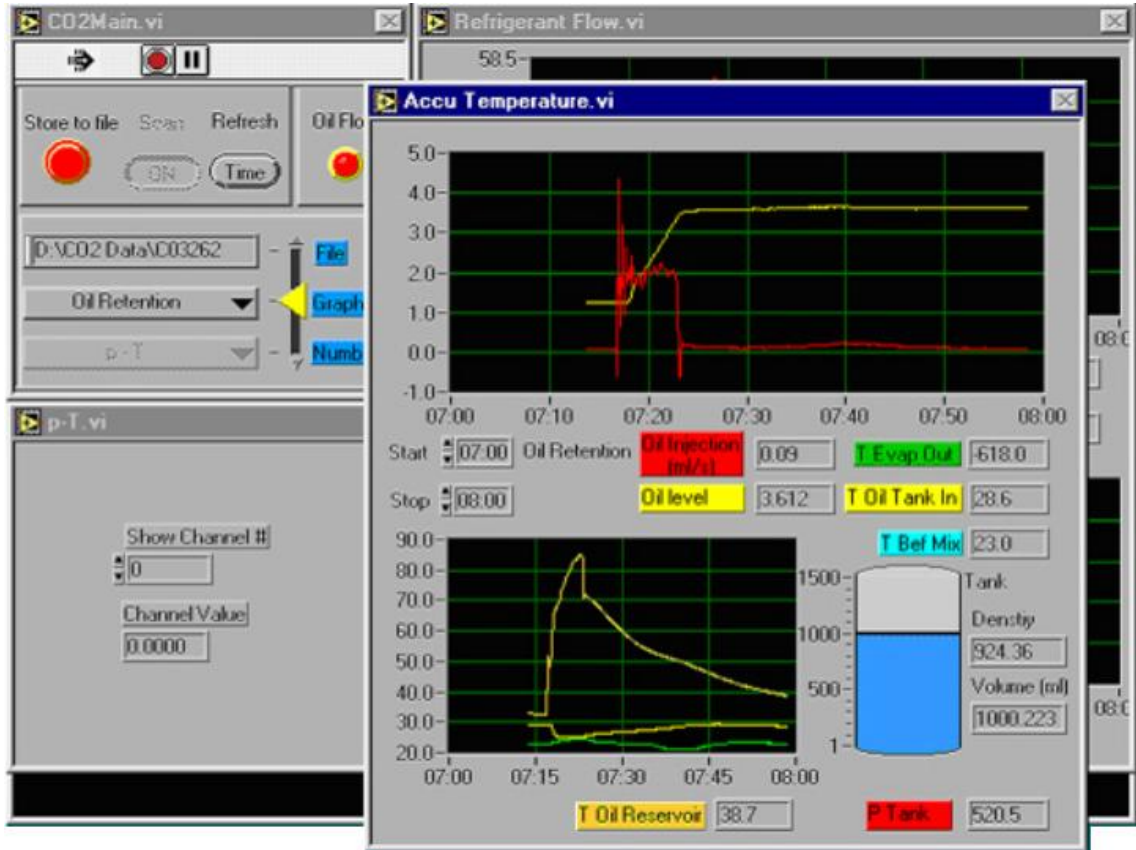
Figure 4.6: LabView Software for DAS
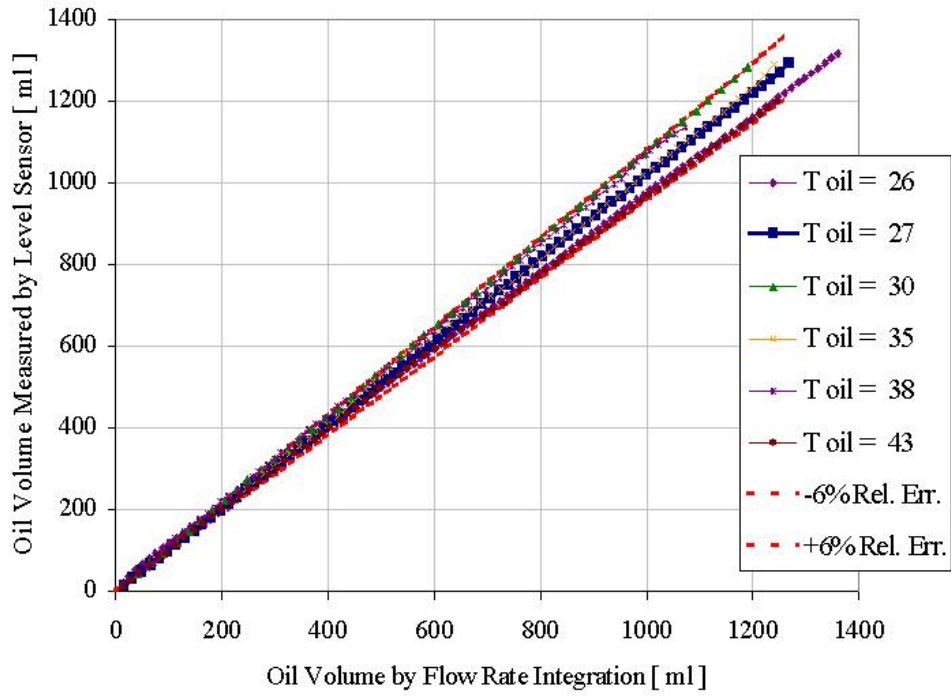
Figure 4.7: Oil Level Sensor Calibration Curves at Different Temperatures
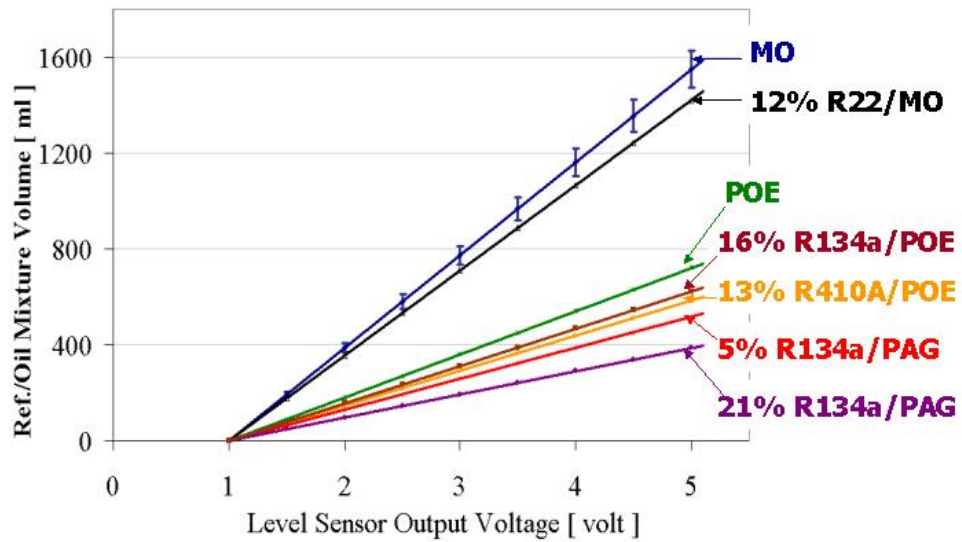
Figure 4.8: Oil Level Sensor Calibration Curves for Different Oil-Refrigerant

Mixtures at Various Degrees of Solubility

Chapter 5: Experimental Procedures

The experimental aspect of this work is similar to that used by Lee (2002, [68]) during oil retention investigations in CO_2 air conditioning systems. Basically, the information used to calculate the oil retention are the oil injection flow rate at the inlet of the test section and the rate of increasing oil volume inside the oil level accumulator at the end of the test section. During the experimental work, the following variables are changed to perform a parametric study:

- OMF from 1 to 8 wt.%

- Refrigerant Mass Flow Rate

The operating limitations of the experimental test facility used for the preliminary tests determined the range of the refrigerant flow rate. For example, when using the R22/MO mixture, at refrigerant flow rates lower than 40 g/s, the discharge temperature exceeds the maximum tolerable limit. On the other hand, for refrigerant flow rates higher than 60 g/s the refrigerant side capacity is higher than the maximum air side capacity that the facility can handle. Thus, refrigerant liquid exits the evaporator and enters the compressor, which is not recommended. With fixed displacement compression volume and RPM, closing the metering expansion valve modifies the refrigerant flow rate and affects the cycle temperatures and pressures. In particular, a decrease of refrigerant mass flow rate leads to an increase of the degree of superheat at the evaporator outlet if air side conditions are kept constant. Thus, mass flow rate can decrease due to variations in refrigerant density and refrigerant velocity along the test section. It is the purpose of the present research to

isolate each effect, so that the main parameters affecting oil entrainment can be traced. The refrigerant charge and the indoor air side conditions were changed to maintain similar temperatures and pressures in the test section while varying the refrigerant mass flow rate, as explained in the next section.

5.1   Experimental Test Conditions

The air side test conditions changed depending on the refrigerant mass flow rate and the type of tests performed. For refrigerant mass flow rates of 42, 51, and 59 g/s, the air side test conditions have been fixed to the ASHRAE B Conditions. The R22 charge was constant and only the expansion valve opening was changed. As a result, the pressure and temperature levels changed for each series of data. For fixed boundary air-side conditions, these three series of tests are meant to simulate the real operating conditions of a residential air conditioning system, which can work at minimum, medium, and full load. Two more series at refrigerant mass flow rates of 46 and 53 g/s were carried out by changing the expansion valve opening, refrigerant charge, and indoor air-side conditions. Combinations of these system variables allowed preserving similar degrees of superheat and evaporation pressures during the tests. Thus, if the refrigerant density is constant, the variation of the mass flow rate is caused by a change in the refrigerant velocity in test section. Table 5.1 summarizes the test conditions for both refrigerant-side and air-side in each test series.

5.2 Test Procedure during Preliminary Tests

Before each test, the system was flushed by running the compressor for about an hour and collecting the residual oil in the extractor. Once the oil was drained from the level sensor tank, the test started. The gear pump injected oil into the injection port at specified flow rates. The oil was carried over with the refrigerant and formed a homogeneous mixture or an annular thin film on the pipe wall, depending upon the injection port location. After a few minutes, the oil was separated at the extractor and collected in the oil level sensor accumulator. Meanwhile the oil level in the sensor vessel was monitored on line and the rate of increase of oil is recorded as shown in Figure 5.1

During the test period, the law of conservation of mass is applied to the oil-loop system of Figure 5.2 and it yields the following relation:

$$m_{ret}(t) = m_{oil,in}(t) - [m_{oil,out}(t) + m_{oil,by-pass}(t)] \qquad (5.1)$$

where m_{ret} = oil mass retained in the test section at a given time;

$m_{oil,in}$ = cumulative oil mass injected at a given time;

$m_{oil,out}$ = cumulative oil mass drained from the extractor and stored inside the level sensor vessel;

$m_{oilby-pass}$ = cumulative oil mass that by-passed the extractor at a given time;

t = time

In the equation (5.1), $m_{oil,in}$ is experimentally measured by integrating the oil flow rate injected over the time. $m_{oil,out}$ and $m_{oilby-pass}$ can be estimated by measuring the mass of oil-

78

refrigerant mixture in the level sensor vessel and by using the solubility proprieties of the oil-refrigerant mixture and extractor efficiency. Each term of equation (5.1) is plotted in Figure 5.3. The solid line with circles represents the cumulative oil amount injected at a given time, while the dashed line with squares is the cumulative mixture of oil and refrigerant that is extracted. In the example, after 5 minutes, the pump was shut off and the oil injection port was closed promptly. Pressures and temperatures were measured both at the injection and extraction ports so that solubility effects could be accounted for. By using the solubility propriety (s) of the oil-refrigerant mixture, the mass of pure oil inside the level sensor vessel has been calculated as described below:

$$s = \frac{m_{ref,dissolved}}{m_{mixture,oil+ref}} = \frac{m_{ref,dissolved}}{m_{ref,dissolved} + m_{oil,pure}} \Leftrightarrow s(t) = f\big(pressure(t),temperature(t)\big) \quad (5.2)$$

If the mass of oil-refrigerant mixture ($m_{mixture,oil+ref}$) stored in the level sensor vessel is known then the mass of pure oil extracted is:

$$m_{oil,out}(t) = \big(1 - s(t)\big)\cdot m_{mixture,oil+ref}(t) \quad (5.3)$$

One hour after the oil pump was turned off, all residual oil in the test section was collected inside the vessel and the oil-refrigerant mixture volume did not increase anymore. The oil mass retained in the test section is assumed to be zero after this time, i.e., $m_{oil,ret} \approx 0$ grams at $t \geq 60$ minutes.

During the test, some amount of oil bypassed the extractor, and extractor efficiency of separation needed to be considered. While the nominal efficiency of separation was approximately 99%, it actually depended on the oil mass fraction. For the

ideal injection and extraction test and if the extractor efficiency of separation is 100%, then one hours after the oil pump was turned off, the following equation applied (which is the law of conservation of mass for oil):

$$m_{oil,out,ideal}\left(t \geq 60\right) = m_{oil,in}\left(t \geq 60\right) \quad \Leftrightarrow \quad \varepsilon_{extractor} = 100\% \tag{5.4}$$

Consequently, for the actual oil retention tests, the actual extractor efficiency was estimated as follows:

$$\varepsilon_{extractor} = \frac{m_{oil,out}\left(t \geq 60\right)}{m_{oil,in}\left(t \geq 60\right)} = 1 - \frac{m_{oil,by-pass}\left(t \geq 60\right)}{m_{oil,in}\left(t \geq 60\right)} \tag{5.5}$$

that leads to the following equation

$$m_{oil,by-pass}\left(t\right) = \left(1 - \varepsilon_{extractor}\right) \cdot m_{oil,in}\left(t\right) \tag{5.6}$$

If the oil mass fraction was higher than 5 wt.% then the extractor efficiency was verified. It decreased to 80% if the OMF was between 2 and 5 wt.% while it dropped drastically to 50% or less if the concentration became lower than 2 wt.%. The efficiency of separation in the extractor depends also on the solubility and miscibility between refrigerant and oil and on the refrigerant mass flow rate. Higher mass flow rates and lower degrees of solubility and miscibility increased the efficiency of separation.

The mass of oil retained can be experimentally found by rearranging the previous equations as follow:

$$m_{oil,ret}(t) = m_{oil,in}(t) \cdot \varepsilon_{exctractor} + m_{mixture,oil+ref} \cdot \left[1 - s(t)\right]$$ (5.7)

An example of an oil retention test is in Figure 5.4. The cumulative oil mass injected and the actual cumulative oil mass extracted in and from the test section respectively are plotted. It should be noted that the oil injected has some refrigerant dissolved in it. By using an electrical heater, the oil was preheated in the oil reservoir. The solubility in the injection line depends on temperatures and pressures but usually is between 5 and 8 %. The refrigerant dissolved in the oil injected has already been accounted for in the curve with circles of Figure 5.4. In steady state, the oil retention is defined as

$$OR \ [g] \ = m_{oil,in} \ [g] - m_{oil,out} \ [g]$$ (5.8)

Consequently, in order to compute a mean oil retention value, it is important that the two curves of injection (circles) and extraction (squares) be parallel and at steady state for several minutes at least. The slope of these two curves is computed and compared in Figure 5.4. The oil mass retained is found by taking the average difference between the two curves after they become steady state. Finally the oil volume retained is defined as:

$$OR \ [ml] = \frac{OR \ [g]}{\bar{\rho}_{oil} \left[g / ml\right]}$$ (5.9)

where $\bar{\rho}_{oil}$ is the time and space average oil density in the test section. Since the mass is conserved, it is more accurate to deal with masses rather than volumes. The mass basis method produced a coherent set of results and the oil retention was converted to units of

volume (ml) by simply dividing by an average oil density in the final step using equation (5.9).

Table 5.1: Test Conditions for Oil Retention in Suction Line and Evaporator

Refrigerant Side				Air Side				
Ref.	R22	Evap. Out	Super	Indoor			Outdoor	
MFR	Charge	Pressure	Heat	T	RH	AFR	T	RH
[g/s]	[kg]	[kPa]	[°C]	[°C]	[%]	[m^3/h]	[°C]	[%]
42	6.3	530	24	26.7	50	1800	27.8	56
46	6.1	561	18	24.5	50	1470	27.8	56
51	6.3	612	16	26.7	50	1800	27.8	56
53	5.5	640	16	28.5	50	2100	27.8	56
59	6.3	658	0	26.7	50	1800	27.8	56

Note: Temperature Tolerance = ± 0.5 °C

Relative Humidity Tolerance = ± 1 % RH

Pressure Tolerance = ± 5 kPa
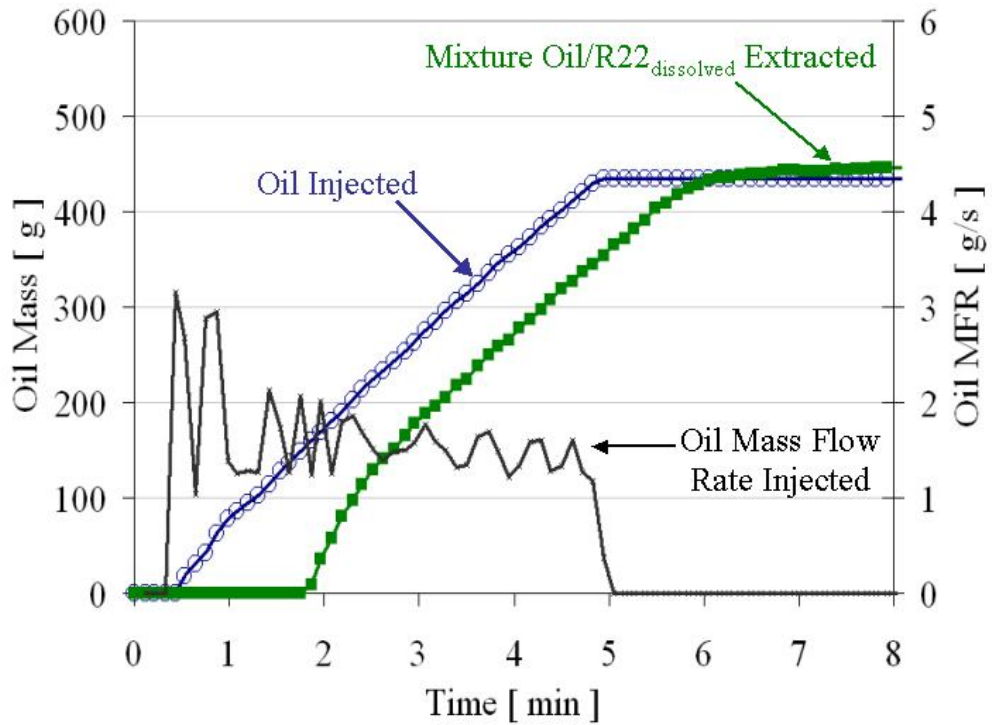
Figure 5.1: Example of Oil Injection and Oil-Refrigerant Mixture Extraction
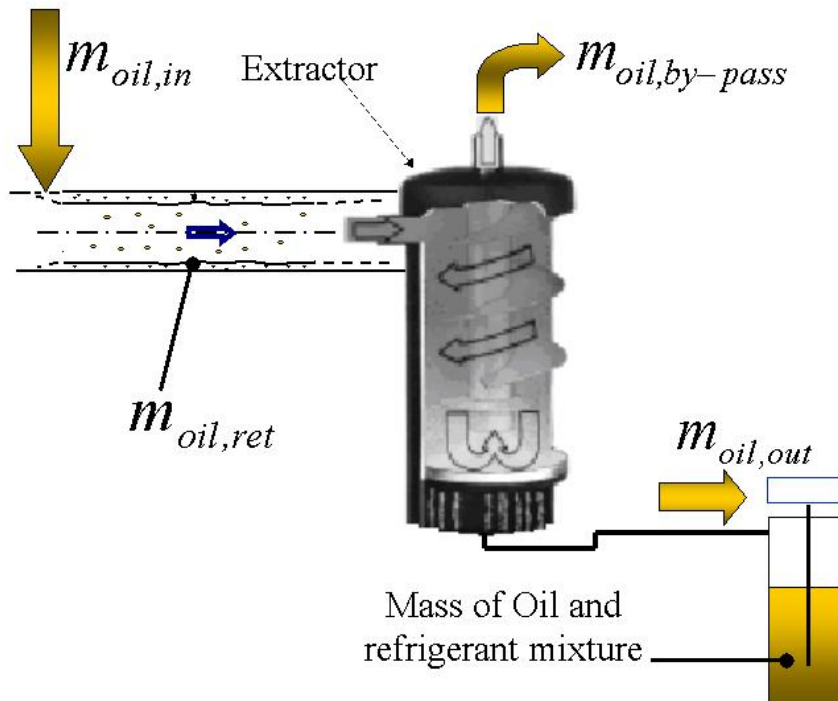
Figure 5.2: Oil Mass Balance during the Oil Retention Test
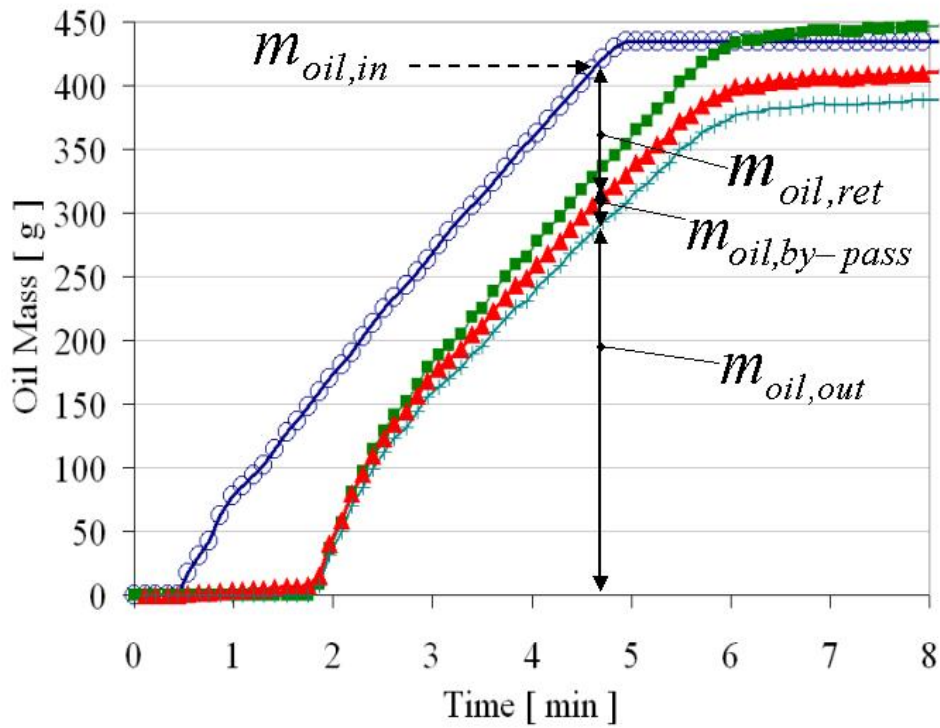
Figure 5.3: Effects of the Oil-Refrigerant Solubility and Extractor Efficiency
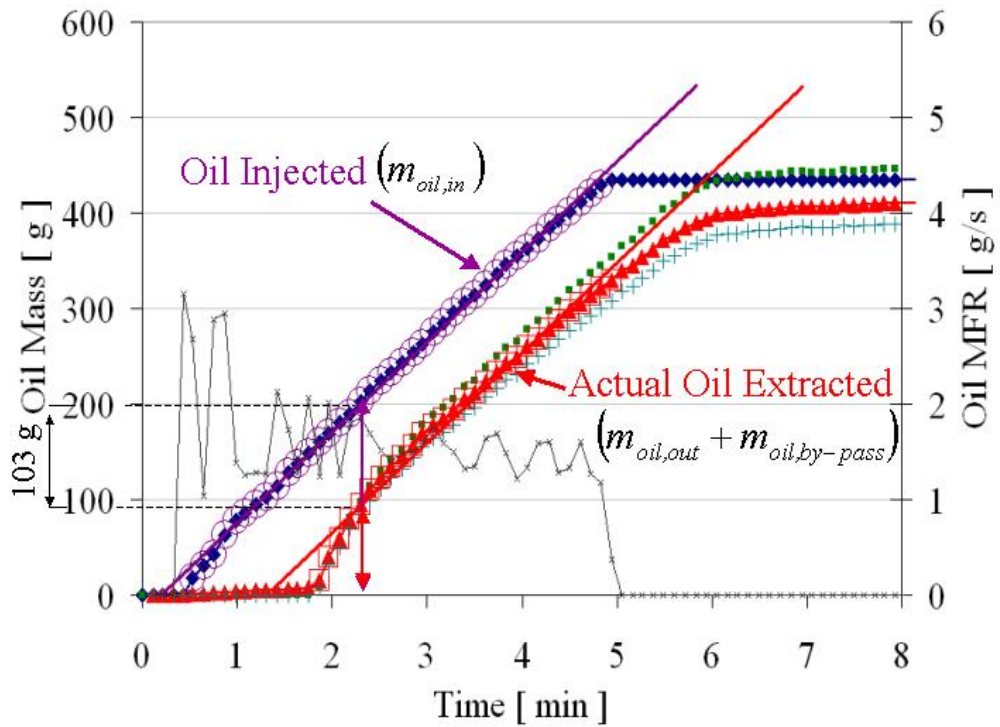
Figure 5.4: Example of Oil Retention Test

Chapter 6: Experimental Results

6.1   Oil Retention in R22/MO Residential Air Conditioning System

This section describes the experimental results of oil retention and pressure drops for the R22/MO air conditioning system. Figure 6.1 represents the cumulative oil retention distribution in each component of a typical 10 kW rated cooling capacity R22 air conditioning system. The suction line was about 14 meters long and its internal diameter was 19 mm. The overall length of the evaporator pipe was about 36 m while the liquid line was 19 m long. If the OMF increased from 1 to 5 wt.%, the oil retained in the condenser varied from 5% to about 50% of the initial oil charge. This was because of the overall pipe length of the condenser, which is equal to about 70 m. The oil retention mass is given in both absolute value on the primary y-axis and percentage with respect to the initial design mass of oil charged into the compressor in the secondary y-axis. If the OMF increases from 1 to 8 wt%, the oil retention in the suction line increases from 2% up to 28% of the initial oil charge. Only a few percent of oil are retained in the evaporator while the cumulative oil retention in the liquid line, evaporator, and suction line can rise to 40%. At OMF = 1 wt.%, about 10% of the initial oil charged resides outside the compressor.

Figure 6.2 shows the relation between OMF and cumulative oil retention mass in the suction line and evaporator while Figure 6.3 shows cumulative oil retention mass in the liquid line and condenser at various refrigerant mass flow rates.   The cumulative percentage of oil present in the components with respect to the oil mass initially charged

into the compressor is shown in the secondary y-axis of the charts. While the oil retention is strongly dependent upon the mixture oil mass fraction, it is not much affected by the refrigerant mass flow rate. However at higher refrigerant mass flow rates, lower oil retention values have been observed. In the suction line, an increase of refrigerant flow rate from 42 to 59 g/s led to a decrease of oil retention of about 23% at OMF=1wt.% and about 28% at OMF=5wt.%. The variations in mass flow rates (or mass fluxes) affect slightly the oil mass retained and, from this point of view, these experimental results are in agreement with the research results of Schlager *et al*. (1990, [95]) about oil retention in smooth and micro-fin tubes during evaporation and condensation of R22/MO mixtures.

The flow in the liquid line was visualized using a sight glass tube located before the mass flow meter at the condenser outlet. The oil was rather homogeneously mixed with the liquid refrigerant, and oil retention did not depend on the refrigerant mass flow rate. The solid lines on the graph of Figure 6.3 represent oil retention in the liquid line at various refrigerant mass flow rates. The results show very similar oil retention characteristics in the liquid line at each flow rate.

Table 6.1 summarizes the oil retention experimental results of the R22 air conditioning system. The values represent oil retention mass per unit length of tube in each component. As shown here, the suction line is the most critical component with the highest values of oil retention per unit length.

6.2 Oil Retention in R410 Residential Air Conditioning Systems

This section describes the oil retention experimental results of R410A/POE and R410A/MO air conditioning systems. Figure 6.4 shows the relations between OMF and cumulative oil mass retained in the suction line and evaporator while Figure 6.5 shows cumulative oil retention mass in the liquid line and condenser at various refrigerant flow rates. The system components were not modified with respect to the R22 test facility. Thus the geometry and length of the pipes were invariant. The evaporation and condensation pressures of the R410A system were higher than those of the R22 system. At fixed outdoor air side conditions, the refrigerant flow rate increased in the range of 46 to 77 g/s. Thermophysical properties were determined by pressure, temperature, and the solubility of the refrigerant and oil mixture. The density of the injected oil was also experimentally measured by the oil mass flow meter. At the suction line, the average Reynolds number of the refrigerant vapor was between $23 \times 10^4 \leq Re_{R410A} \leq 40 \times 10^4$ .An increase of refrigerant flow rate from 46 to 77 g/s led to a decrease of oil retention in the suction line of about 18% at OMF=1wt.% and about 10% at OMF=5wt.%. At the highest mass flow rate of 77 g/s, conditions at the evaporator outlet were nearly saturated. Oil retention in the evaporator decreased of about 33% as compared to the tests with MFR=46 g/s. This oil retention reduction was due to the fact that liquid refrigerant was mixed with pure oil along the entire length of the tubes of this component. Consequently the reduced liquid film viscosity and the highest vapor refrigerant mass flux enhanced the oil transport. If the refrigerant flow rate increased from 46 to 77 g/s, the oil retention in the evaporator decreased to approximately 32% and 34% at OMF equal to 1 and 5 wt.%,

respectively. A similar trend has been observed in the condenser. Oil retention decreases in the condenser but not as significantly as in the evaporator. For the three different mass flow rates, the condensation pressure varied from 2260 to 2400 kPa. At the highest mass flow rate of 77 g/s, the condenser outlet condition was nearly saturated. Since the outdoor air side conditions were kept constant, an increase of refrigerant flow rate caused a reduction of the degree of subcooling. On the other hand, the correspondent discharge temperature decreased as well. The condenser inlet temperature decreased by more than 20ºC,that is, from 101ºC to 80 ºC, shifting the entire vapor compression cycle toward the two-phase dome. As a result of these two opposite effects, (reduction in the degree of subcooling on one side and a decrease of condenser inlet temperature on the other) oil retention in the condenser dropped from 15% to 20% when the refrigerant flow rate rose from 46 to 77 g/s.

Table 6.2 summarizes oil retention experimental results of the R410A/MO air conditioning system while Table 6.3 shows oil retention experimental results for the R410A/POE mixture.

6.3 Oil Retention in R134a Residential Air Conditioning System

Oil is retained in each component of a air conditioning system and oil distribution maps can be developed when the system runs in steady state conditions. Figure 6.6 shows an example of oil distribution map for R134a/POE system. Two different OMFs and refrigerant mass flow rates are plotted in the x-axis and the oil retention ratio, which is

the ratio between the measured oil retention and initial oil charged into the compressor, is given on the y-axis. If OMF increased from 1 to 5 wt.%, oil retained in the major system components outside the compressor crankcase increased from 10% to 30% of the initial oil charge, respectively. Some components are more sensitive to the refrigerant flow rate than others. For example, at OMF = 1wt.%, while oil retention decrease of about 21% in the suction line and 15% in the evaporator, oil retention in the condenser did not vary with the refrigerant flow rate. In contrast, oil retention in the liquid line increased of about 36% with the refrigerant flow rate at constant OMF = 1wt.%, that is, at constant oil concentration in the mixture. The results in Figure 6.6 proved that for R134a/POE mixtures the cumulative oil retention in the entire system reduced only few percents if the refrigerant flow rate increased because oil retention reductions in some components were compensated with retention increases in the liquid line. These results depend on the length of the liquid line with respect to dimensions of the other components. Short liquid lines are beneficial since they can reduce oil retention in the overall system, especially if the refrigerant flow rate increases. Figure 6.7 shows a more general relation between OMF and cumulative oil mass retained in the suction line, evaporator, liquid line, and condenser for two different refrigerant flow rates of R134a/POE mixture. The geometry, orientation, and length of the pipes were invariant with respect to the R22 test facility. The evaporation and condensation pressures of the R134a system were lower than those of the R22 system. The refrigerant flow rate decreased between 30 to 45 g/s. At the suction line, the average Reynolds number of the refrigerant vapor was between 17×10^4 $\leq Re_{R134a} \leq 26 \times 10^4$ depending on the refrigerant flow rate. In the suction line and

evaporator, an increase of refrigerant flow rate from 30 to 46 g/s decreased oil retention more than 10% only if the OMF was greater than 2 wt.%. For example, at OMF = 5wt.%, oil retention decreased about 32% and 30% in the suction line and evaporator, respectively. These results stem from the combined effect of increased refrigerant vapor mass flux and reduced liquid film viscosity associated with a refrigerant mass flow rate of 45 g/s. Oil retention reduction in the suction line, evaporator and condenser was compensated by oil retention increase in the liquid line, so the overall cumulative oil retention in the major system components did not change if the refrigerant flow rate increased.

Figure 6.8 shows a comparison of cumulative oil retention mass between the miscible refrigerant and oil pair R134a/POE and the partially miscible pair R134a/PAG. The geometry and refrigerant mass flow rate were invariant and the operating conditions of the system were quite the same. Oil retention was similar in all system components. The main difference was observed in the condenser where the mixture R134a/PAG had about 15% smaller oil mass retained than the mixture R134a/POE. Table 6.4 summarizes oil retention experimental results of the R134a/POE air conditioning system while Table 6.5 shows oil retention experimental results for the R134a/PAG mixture.

6.4   Parametric Study of the Oil Retention in the Suction Line

Oil retention is a complex function of multiple variables. Pipe geometry and orientation, oil mass fraction, refrigerant velocity, oil solubility and miscibility are only

some examples. An experimental parametric study was performed in order to understand the physics of the oil transport phenomena. The study focused on the suction line where the flow was in the annular flow regime. The refrigerant and oil mixture was R22 and MO for most of the tests while a different combinations of refrigerant and oil pair were tested to perform a parametric analysis at various liquid film viscosities and surface tensions.

Oil retention depends on the following independent variables according to a more or less complicated analytical function (f):

$$OR = f\left(g, \rho_{ref}, \vec{v}_{ref}, \mu_{ref}, D, \sigma_{film}, \mu_{film}, \rho_{film}, \bar{\varepsilon}_{pipe}, \gamma_{misc}\right) \tag{6.1}$$

where g = gravity; ρ_{ref}= refrigerant density;

v_{ref}= refrigerant vapor velocity; μ_{ref}= refrigerant dynamic viscosity

D = Inner Pipe diameter; σ_{film}= liquid film surface tension

μ_{film}= liquid film viscosity; ρ_{film}= liquid film density

ε_{pipe}= pipe surface roughness; γ_{misc} = degree of miscibility between ref. and oil.

The experimental parametric study focused on the effect on oil retention by the following variables:

- Inner pipe diameter
- orientation of the pipe
- refrigerant vapor velocity
- oil and refrigerant mixture viscosity ratio
- degree of mutual miscibility and solubility of oil and refrigerant mixture.

Each single variable affected oil transport in a unique way and they can be grouped in dimensionless characteristic numbers. The main dimensionless groups were identified in two-phase flow literature. In the suction line, they are the refrigerant vapor Reynolds number (Re_g), the mixture Weber number (We_m), the oil mass fraction (OMF), and the film over refrigerant vapor viscosity ratio ($\tilde{v}$) defined as

$$Re_g = \frac{\rho_{ref} v_{ref} D}{\mu_{ref}} = \frac{G_{ref} \cdot D}{\mu_{ref}}; \qquad\qquad We_m = \frac{G_{ref}^2 D}{\rho_m \sigma_m};$$

$$OMF = \frac{\dot{m}_{oil}}{\dot{m}_{oil} + \dot{m}_{ref}}; \qquad\qquad \tilde{v} = \frac{v_{liquid, film}}{v_{ref, vapor}}.$$

where G_{ref} is the refrigerant mass flux. Re_g represents the ratio between the inertia and viscous forces in the vapor region while We_m is the ratio between the inertia force of the vapor core and the surface tension force of the liquid film of oil-refrigerant mixture in the annular region. $\tilde{v}$ is the liquid film over the refrigerant vapor kinetic viscosity ratio and for air conditioning applications it is always greater than one.

The experimental parametric analysis provided useful information about how the dimensionless groups controlled the oil transport phenomena in the suction line. For example, it was possible to study the effect of the Re_g on oil retention volume. An increase of Re_g should always lead to a decrease of oil retention volume but different mixtures with identical Re_g do not necessarily have the same oil retention volume. Moreover Re_g can increase due to a rise in refrigerant velocity or a change in pipe diameter. It is the purpose of the next section to analyze if both ways of increasing Re_g similarly reduce the oil retained in the suction line. In realistic applications, it is not

possible to decouple one single effect from the other. A change in one variable will cause a variation in some others. During the experiments, tricks were adopted such as creation of a by-pass line, reduction of pipes diameters, and variation of air side conditions. The set up allowed artificial reproduction of the desired conditions in the suction line and simulation of the actual realistic applications.

6.4.1   The Effect of Changing Pipe Diameter

Inner pipe diameter affects refrigerant mass flux. At a constant refrigerant flow rate, a decrease of the pipe diameter causes a restriction of the cross section area and augments refrigerant mass flux. The refrigerant Reynolds number increases as well since refrigerant viscosity changes less than 4% during the tests. The temperature and pressure at the inlet to the test section were similar for all tests. The length of the suction line changed depending on pipe diameter. A minimum amount of oil retention is required by the experimental injection–extraction methodology used in the experiments. Thus, if the tube diameter was reduced, the length of the tube was increased. In the graph of Figure 6.9, oil retention volume per unit length of tube is plotted versus the OMF and for different refrigerant mass fluxes in both the horizontal suction line (Gh) and the vertical suction line (Gv). The inner suction pipe diameter was reduced from 19 mm to 13 mm causing the refrigerant mass flux to increase from 150 to 409 kg/(m^{2}s) and the refrigerant vapor Reynolds number to raise from 21×10^4 to 40×10^4. In the graph of Figure 6.9, an increase of mass flux from 181 kg/(m^{2}s) to 206 kg/(m^{2}s) led to a decrease of oil retention by about 20% in the horizontal test section. In the upward vertical suction line, oil

retention reduction has been observed only if the OMF was higher than 2 wt.%. For example, at OMF = 5 wt.%, oil retention decreased to about 22% in the horizontal line and 19% in the upward vertical suction line. The reduction in pipe diameter promoted oil transport in both horizontal and vertical suction lines.

6.4.2   The Effect of the Gravity Force

The effect of the gravity force on oil retention has been investigated experimentally by changing the orientation of the suction line. Figure 6.10 shows oil retention volume per unit length versus OMF at different refrigerant mass fluxes G, and the solid line represents the horizontal line while the dotted line represents the upward vertical suction line. The mass flux was between 150 kg/(m^{2}s) $\leq G \leq$ 206 kg/(m^{2}s) and the Reynolds number was between $21 \times 10^4 \leq Re_g \leq 31 \times 10^4$. At the same refrigerant mass flux, pressure, and temperature, oil retention in the vertical upward suction line was higher than that of the horizontal line. At specific OMF, oil retention in the vertical upward suction line increased more than 50% with respect to the horizontal suction line due to the gravity force. The vapor core inertia force, which is the driving force for oil transport, has to overcome the shear stress viscous resistance as well as the gravity forces in the vertical upward suction line. Mehendale (1998, [78]) investigated vertical upward suction lines extensively, using different combination of refrigerant-oil mixtures. He concluded that if the oil mass flow rate was held constant, as the mass flux decreased the average film thickness increased. In his work, the refrigerant mass flow rate ranged from 1 to 18

g/s since he focused in oil-flow reversal phenomena. A quick comparison is made between his work and the experimental results of this section. Mehendale estimated the oil film thickness for various OMFs. The maximum refrigerant mass flux was G=74 kg/(m^{2}s) and the liquid film viscosity was 12 cSt. At OMF=0.4 wt.%, the average dimensionless film ratio ε ($=\delta/R$) was ε =0.0202. In the experimental results of Figure 6.10, the minimum mass flux was G=150 kg/(m^{2}s) and the corresponding liquid film viscosity was 18 cSt. For this data series both mass flux and liquid film viscosity are higher than those of Mehendale's work, and the average dimensionless liquid film thickness at OMF=0.4 wt.% was about ε =0.0053. This value is about one fourth of the value computed by Mehendale. Since the minimum mass flux in Figure 6.10 is still more than double with respect to Mehendale's mass flux, the corresponding inertia force is stronger and lower oil film thickness was expected.

6.4.3   The Effect of Refrigerant Vapor Velocity

Refrigerant mass flux is the product of refrigerant density and velocity. The latter directly affects the shear stress gradient inside the flow. Figure 6.11 compares oil retention volume per unit length versus OMF for different refrigerant vapor velocities. The graph refers to the vertical upward suction line of R22/MO mixture. The mass fluxes were G$\cong$ 150 kg/(m^{2}s) and G $\cong$ 213 kg/(m^{2}s) and the corresponding Reynolds numbers were 21 $\times$ 10^4 and 26 $\times$ 10^4. At G = 150 kg/(m^{2}s), refrigerant velocity changed from 7.2 m/s to 8.8 m/s while at G = 213 kg/(m^{2}s) the refrigerant velocity changed from 10.4 m/s

to 12.5 m/s. By comparing the two series at G = 213 kg/(m²s), it seems that the highest refrigerant velocity of 12.5 m/s, which is represented by the dotted line with squares in Figure 6.11, led to lower oil retention when refrigerant velocity was equal to 10.4 m/s, as represented by the dotted line with diamonds. At G=150 kg/(m²s), the difference on oil retention was less than 7% if the refrigerant velocity increased from 7.2 to 8.8 m/s. The general trend of the curves seems to suggest that if vapor velocity increased, oil retention decreased slightly. For the same mass flux or similar Reynolds number, at constant OMF, the difference of oil retention for various vapor velocities was less than 7%, so that final conclusions cannot be drawn. The measurement relative error of data plotted in Figure 6.11 was ±7% and the sensitivity limits of the experimental apparatus were reached during the tests.

6.4.4   The Effect of Oil Viscosity

This section describes experimental results for how the thermodynamic proprieties of the liquid film affect the oil retention volume in the widest possible range of viscosity, density, and surface tension. The viscosity of the liquid film is the most important parameter affecting oil retention volume. More viscous liquid films are more resistant to the refrigerant driving force and are therefore more difficult to carry. Various combinations of the refrigerant and oil mixture provided a wide range of liquid film viscosity and density. In particular, some combinations used the same refrigerant but different types of oil while others adopted the same oil but different refrigerants. By

changing the oil and refrigerant mixture in a systematic order, a parametric study was performed with the purpose of identifying the liquid film characteristics that promote oil transport. Figure 6.12 shows oil retention volume per unit length of horizontal suction pipe versus the OMF at different liquid film kinetic viscosities. The results are normalized with respect to the viscosity ratio of MO oil and R22. The viscosity ratio ($\tilde{v}$) and the viscosity ratio factor (vfr) are defined as

Viscosity Ratio: $\tilde{v}_{oil-ref} = \dfrac{v_{oil,film}}{v_{ref}}$;

Viscosity ratio Factor : $vrf = \dfrac{\tilde{v}_{oil-ref}}{\tilde{v}_{MO-R22}}$.

In the graph of Figure 6.12, the refrigerant mass flux and Reynolds number were constant to G $\cong$ 160 kg/(m^{2}s) and Re $\cong$ 24 $\times$ 10^4 for all tests. The degree of solubility and miscibility between the oil and refrigerant affected the thermodynamics proprieties of the liquid film. The average viscosity ratio factor during the tests was 1.55 for R410A/MO and 1.17 for R410A/POE mixture. Poor solubility and miscibility between oil and refrigerant, such as the mixture R410A/MO, caused the oil retained in the test section to increase of about 55%. This mixture represents an obsolete combination adopted in commercial vapor compression systems. Sundaresan *et. al.* (1996, [105]) provided experimental results showing that immiscible oil-refrigerant mixtures, such as R410A/MO, caused oil return problems and that potential lack of proper lubricant inside the compressor crankcase affected system reliability. This result is in agreement with the current research finding since R410A/MO caused the highest oil retention volume in the suction line. At constant OMF= 3 wt.% if the viscosity ratio factor increased from about

97

17% to 55%, the oil retention volume increased from about 30 to 120%, respectively. More soluble oil refrigerant pairs, such as R134a/POE and R134a/PAG, have reduced liquid film viscosity compared to R22/MO. In the graph of the Figure 6.12, a decrease of viscosity ratio factor from 1 to 0.8 caused a reduction in oil retention of about 20%. POE and PAG synthetic oils had different degrees of solubility and miscibility with R134a. The PAG oil was ISO VG 46 grade lubricant while the POE oil viscosity was slightly less (ISO VG 32). The average PAG oil solubility in the suction line was about 28 mass % and the POE oil solubility was only 21 mass %. As a result, the liquid film viscosities in the data of Figure 6.12 were very similar for both mixtures and equal to approximately 14 cSt for R134a/POE and 15 cSt for PAG/R134a. These two mixtures provided identical oil retention characteristics as shown by the two curves with circles and stars plotted in the graph of Figure 6.12. This is due to the fact that they have similar refrigerant Reynolds numbers and viscosity ratios.

6.4.5   The Effect of Oil and Refrigerant Miscibility on the Mixture Viscosity

This section describes the experimental results of oil retention when an immiscible refrigerant-oil pair and the corresponding miscible mixture were tested. Every substance is miscible to some degree but the refrigeration industry refers to immiscible pairs as mixtures in which the refrigerant and oil have very poor miscibility characteristics. For these mixtures, the annular flow regime in the suction line consists not only of the vapor and liquid region but also has three distinct regions: the vapor core refrigerant zone, the

liquid refrigerant rich film, and the oil rich film on the wall of the pipe. The effect of increased mutual miscibility between oil and refrigerant on the oil retention volume reduction is quite difficult to predict. In the simplest model, the liquid region can still be treated as a homogeneous mixture with average thermodynamic proprieties. However, this model is more an engineering approach than a realistic model since the viscosity of the liquid near the wall is higher than the average bulk liquid film viscosity. Figure 6.13 shows a comparison of cumulative oil retention in each component of the vapor compression system between miscible refrigerant and oil pair, such as R410A/POE, and immiscible pairs, such as R410A/MO. The geometry and refrigerant mass flow rate were invariant and the operating conditions of the system were similar. The condensation and evaporation pressure were about 2370 kPa and 1010 kPa, respectively. The degree of subcooling was 5 K for R410A/MO and 6K for R410A/POE. The degree of superheat was 18K for R410A/MO and 22 K for R410A/POE. The refrigerant mass flow rate was 45 g/s, while at the suction line, the mass flux was G $\cong$ 160 kg/(m^{2}s) and the Reynolds number was Re $\cong$ 24 $\times$ 10^4. The average solubility of R410A in MO oil in the suction line was about 6 mass % while the solubility of R410A in POE oil was 11 mass %. The estimated average liquid film viscosity in the suction line was 28 cSt for MO/R410A and the actual liquid film viscosity of POE/R410A was 22 cSt. The degree of miscibility is different and directly affects local liquid film viscosity near the wall of the suction pipe. Poorly miscible mixtures have substantially higher oil retention mass in each component of the system. At OMF=5wt.%, R410A/MO had an oil retention mass in the suction line of about 31% higher than that of R410A/POE. An increase of more than 60% was

observed in the evaporator, liquid line, and condenser. Oil retention in the overall system for the mixture R410A/MO was about double compared to the R410A/POE mixture. This significant increase of oil retention is due to both the difference in the liquid film viscosity, which is about 27%, and the degree of mutual miscibility between refrigerant and oil.

6.5   Oil Retention Comparison among Different Refrigerant and Oil Mixtures

Figure 6.14 presents a comparison of the oil retention volume between R22 and R410A systems. The suction line inner diameter was approximately 19 mm. The oil retention volume in the figure is an average value per unit length of pipe. The results are plotted versus the OMF, which ranges from 0.7 to 5.5 wt.%. The mass flux changed from 150 to 206 kg/(m^{2}s) for R22/MO and from 160 to 276 kg/(m^{2}s) for R410A/POE. The Reynolds numbers were between $21 \times 10^4 \leq Re_{R22} \leq 32 \times 10^4$ for R22/MO and between $24 \times 10^4 \leq Re_{R410A} \leq 40 \times 10^4$ for R410A/POE mixture. The dotted area represents the oil retention volume for R410A/POE mixture, while the striped area includes the oil retention experimental results of the R22/MO mixture. The R410A/POE mixture has higher oil retention volume at OMFs less than 2 wt.% but lower oil retention volume at OMFs greater than 5 wt.%. The R410A/POE mixture has a higher oil film viscosity but also a higher refrigerant mass flux. The balance between oil film viscous force and refrigerant core inertia force depends on the oil film thickness. Viscous forces seem to be a predominant factor at OMFs less than 2 wt.%.

Table 6.6 compares oil retention volume per unit length of tube for the R22/MO and R410A/POE mixtures in each component of the system. The results show that the R410A/POE mixture has a higher oil retention volume in the evaporator but a lower oil retention volume in the liquid line and condenser.

6.6 Pressure Drop Penalty Factor due to Oil Retention

The amount of oil retained in the test section offers an additional resistance to refrigerant flow. If the OMF increases, oil retention in the test section increases as well. Consequently, in single-phase flows, the pressure drops depend upon the refrigerant flow rate and the OMF of the mixture. In two-phase flows, additional terms need to account for gravitational pressure drops, acceleration pressure drops, and frictional pressure drops as summarized in literature by Shen and Groll (2003, [98]). From an experimental point of view, it is possible to quantify the increase of pressure drop due to the oil retained in the pipe. The oil effect on pressure drop can be experimentally estimated by measuring the pressure drop in the test section at specific mass flow rates and OMFs. Then, the pressure drop can be compared with the corresponding pressure drop in the test section at the same mass flow rate but at an OMF= 0 wt.%. The pressure drop penalty factor (PDPF) represent the ratio of the two measurements and it is defined as

$$\textbf{PDPF } [-] = \frac{\varDelta P\big|_{OCR=x\,wt.\%}^{component(i)}}{\varDelta P\big|_{OCR\approx 0\,wt.\%}^{component(i)}} \tag{6.2}$$

where $i = 1$ is the suction line and $i = 2$ is the evaporator. Figure 6.16 shows the PDPF in the suction line and evaporator of a R22 air conditioning system.

If the OMF increases to 8 wt.%, the pressure drop increases about 40% in the suction line and 15% in the evaporator with respect to the case of OMF≈0 wt.%, i.e., no oil is injected in the test section. A more significant increase of pressure drop occurred in the suction line rather than in the evaporator. This may be due to less mutual solubility between the refrigerant core and the oil film in the suction line, which leads to higher values of liquid film viscosity. At OMF= 1 wt.%, the PDPF in the suction line increases by 10% while in the evaporator it increases less than 2%.

For R410A air conditioning systems, the PDPF for the suction line and evaporator have trends similar to those observed for the R22 system. At OMF=1.5 wt.%, the PDPF increased about 18% in the suction line and less than 2% in the evaporator while at OMF=5wt.%, the PDPF increased about 33% in the suction line and 9% in the evaporator.

Figure 6.16 shows the PDPF in the suction line versus OMF for different refrigerant and oil mixtures. The suction line has an inner diameter of about 19 mm and a length of 14 m. For all tests plotted in the graph of the figure, refrigerant mass flow rate was 46 g/s, mass flux was $G \cong 160$ kg/(m^{2}s) and Reynolds number was $Re \cong 24 \times 10^4$. The measured pressures drop along the suction line at OMF $\cong$ 0 wt.% were the following:

- R22 $\rightarrow \Delta P\big|_{OCR \approx 0 \, wt.\%}^{suction} = 66$ kPa.(refrigerant velocity vR22 = 8.1 m/s)

- R410A $\rightarrow \Delta P\big|_{OCR \approx 0 \, wt.\%}^{suction} = 78$ kPa .(refrigerant velocity vR410A = 8.3 m/s)

- R134a $\rightarrow \Delta P\big|_{OCR\approx 0\, wt.\%}^{suction} = 80$ kPa .(refrigerant velocity vR134a = 8.6 m/s)

An increase of OMF from 0 to 5 wt.% caused a rise of pressure drop of about 50% for R410A/MO, which was the mixture that had the most viscous liquid film. The pressure drop increased 33% for R22/MO and 22% for R134a/POE mixture. The latter was the mixture with the least viscous liquid film.

Figure 6.17 shows the PDPF for the condenser versus OMF for different refrigerant and oil mixtures. The mass flow rate in the condenser varied from 46 g/s ≤ MFRc ≤ 76 g/s. The condenser used in the experiments was slightly oversized with respect to the capacity of the vapor compression system. The pressure drop across this component ranged from 2 to 25 kPa. At OMF = 0 wt.%, the pressure drops were approximately 16 kPa for R22 and R410A and 14 kPa for R134a. The mixture R410A/MO still had the highest PDPF, reaching PDPF ≅ 1.5 at OMF = 5 wt.%. If the OMF increased from 0 to 5 wt.%, the pressure drop in the condenser increased about 30% for both R134a/PAG and R22/MO mixtures while the maximum PDPF is only 18% for R410A/POE. It should be noted that, for the same mixture R410A/POE, the higher the flow rate, the lower the PDPF at a constant OMF. In Figure 6.17, the dotted lines with stars, circles, and triangles represent the pressure drops across the condenser for refrigerant flow rates equal to 46, 59, and 76 g/s, respectively. This PDPF reduction can be due to the fact that an increase of mass flow rate caused a decrease in the discharge temperature and the degree of subcooling. While reduced subcooling is unfavorable for oil transport in the condenser, lower inlet temperature had a predominant influence on the oil retained in the condenser. The vapor compression cycle was shifted toward the two-phase dome and the liquid phase covered a

higher portion of the condenser. Since in miscible refrigerant and oil pairs, the liquid refrigerant drastically decreases oil film viscosity, oil transport is promoted and the pressure drop penalty factor is reduced.

6.7   Conclusion

In this chapter, experimental test results for various refrigerant an oil mixtures were presented and discussed. Oil retention mass was measured by using the oil injection-extraction method for all components of the vapor compression system including the suction line, evaporator, liquid line, and condenser. The conclusions from the experiments are summarized next.

☐ Oil retention volume depends on the oil mass fraction (OMF); if the OMF increases then the oil retention volume also increases.

☐ The most critical component for oil transport is the suction line. In this component the reduction of the oil driving force and the increase of the liquid film viscous resistance create unfavorable conditions for oil transport.

☐ If the OMF increases from 1 to 5 wt.%, oil retention in the suction line of R22 systems increases from 2% to 20% of the initial oil charged inside the compressor. At OMF = 1 wt.%, about 10% of the initial oil charge is retained in the overall system components and resides outside the compressor.

☐ If the OMF increases from 1 to 5 wt.%, oil retention in the suction line of R410A/POE systems increases from 4% to 16% of the initial oil charged inside

the compressor. Similarly to R22 systems, R410A/POE air conditioners have about 11% of the initial oil charge retained in the overall system components if OMF = 1 wt.%.

☐ If the OMF increases from 1 to 5 wt.%, oil retention in the suction line of R134a/POE and R134a/PAG systems increases from about 2% to 16% of the initial oil charged inside the compressor. For R134a/POE mixture, oil retention in the overall system components increases from 8% at OMF=1wt.% to 30% of the initial oil charge at OMF=5wt.%.

☐ R410A/MO mixture, which is a very poorly soluble and miscible mixture, has from 33% to 71% higher oil retention in the system as compared to other refrigerant-oil mixtures tested. If the OMF increases from 1 to 5 wt.%, oil retention in the suction line of R410A/MO systems increases from 4% to 24% of the initial oil charged inside the compressor. At OMF = 1 wt.%, about 18% of the initial oil charge is retained in the overall system components and resides outside the compressor.

☐ A parametric study of oil retention in the suction line was performed. The oil retention volume is a function of four dimensionless groups: the refrigerant vapor Reynolds number, the oil mass fraction, the mixture viscosity ratio, and the mixture Weber number. The last dimensionless group accounts for secondary effects due to liquid film surface tension.

☐ A reduction of pipe inner diameter promotes oil transport but also increases frictional pressure drop along the pipe. If the OMF is constant, an increase of

the refrigerant Reynolds number reduced the oil volume retained. At OMF = 5 wt.%, the maximum reduction observed was 44% in the horizontal suction line and 21% in the upward vertical suction line.

☐ Oil retention volume depends on pipe orientation and upward vertical suction lines can have up to 50% more oil retained compared to horizontal lines in the same operating conditions.

☐ The mixture viscosity ratio is the predominant parameter affecting oil retention in horizontal pipelines. If the viscosity ratio of the mixture increases then oil retention also increases. Mixtures that have similar viscosity ratios tend to have similar oil retention characteristics, as exemplified by R134a/POE and R134a/PAG.

☐ Due to viscosity effects, R410A/POE systems have slightly higher oil retention volumes than R22 systems, especially at OMFs less than 2 wt.%. R134a systems have lower oil retention because of the increased degree of solubility and miscibility between the refrigerant and synthetic oils.

☐ The pressure drop increase due to oil retention was experimentally measured. The most sensitive component to the oil is the suction line. In this component, the pressure drop can increase by up to 40% as compared to when no oil is circulating through the system. While the pressure drop increased less than 15% in the evaporator, it can reach 30% in the condenser, as compared to oil-free conditions.

☐ Liquid film thermodynamic proprieties also affect the pressure drop penalty factor. In all components of the system, an increase of liquid film viscosity caused an increase of pressure drop at given fixed mass flow rates and OMFs.

Table 6.1: Summary of Oil Retention Results in R22/MO Air Conditioning System

Component	OR at OMF=1wt.%	OR at OMF=5wt.%	I.D.	Length	Min OR	Max OR
Suction Line	37 g (3 %)	223 g (20 %)	19 mm	14 m	2.6 g/m	15.9 g/m
Evaporator	18 g (2 %)	40 g (4 %)	9 mm	36 m	0.5 g/m	1.1 g/m
Liquid Line	21 g (2 %)	105 g (10 %)	8 mm	19 m	1.1 g/m	5.5 g/m
Condenser	112 g (10%)	375 g (34 %)	8 mm	70 m	1.6 g/m	5.4 g/m
Overall System	188 g (17%)	742 g (68 %)	-	139 m	-	-

Table 6.2: Summary of Oil Retention Results in R410A/MO Air Conditioning System

Component	OR at OMF=1wt.%	OR at OMF=5wt.%	I.D.	Length	Min OR	Max OR
Suction Line	97 g (9 %)	333 g (30 %)	19 mm	14 m	6.9 g/m	23.8 g/m
Evaporator	75 g (7 %)	129 g (12 %)	9 mm	36 m	2.1 g/m	3.6 g/m
Liquid Line	21 g (2 %)	120 g (11 %)	8 mm	19 m	1.1 g/m	6.3 g/m
Condenser	56 g (5%)	177 g (16 %)	8 mm	70 m	0.8 g/m	2.5 g/m
Overall System	260 g (24%)	759 g (69%)	-	139 m	-	-

Table 6.3: Summary of Oil Retention Results in R410A/POE Air Conditioning System

Component	OR at OMF=1wt.%	OR at OMF=5wt.%	I.D.	Length	Min OR	Max OR
Suction Line	49 g (4 %)	197 g (16 %)	19 mm	14 m	3.5 g/m	14.1 g/m
Evaporator	18 g (1 %)	105 g (9 %)	9 mm	36 m	0.5 g/m	2.9 g/m
Liquid Line	28 g (2 %)	28 g (2 %)	8 mm	19 m	1.5 g/m	1.5 g/m
Condenser	10 g (1%)	98 g (8 %)	8 mm	70 m	0.1 g/m	1.4 g/m
Overall System	105 g (9 %)	428 g (35 %)	-	139 m	-	-

Table 6.4: Summary of Oil Retention Results in R134a/POE Air Conditioning System

Component	OR at OMF=1wt.%	OR at OMF=5wt.%	I.D.	Length	Min OR	Max OR
Suction Line	41 g (3 %)	190 g (16 %)	19 mm	14 m	2.9 g/m	13.6 g/m
Evaporator	10 g (1 %)	38 g (3 %)	9 mm	36 m	0.3 g/m	1.1 g/m
Liquid Line	32 g (3 %)	17 g (1 %)	8 mm	19 m	1.7 g/m	0.9 g/m
Condenser	28 g (2%)	159 g (13 %)	8 mm	70 m	0.4 g/m	2.3 g/m
Overall System	111 g (9 %)	404 g (33%)	-	139 m	-	-

Table 6.5: Summary of Oil Retention Results in R134a/PAG Air Conditioning System

Component	OR at OMF=1wt.%	OR at OMF=5wt.%	I.D.	Length	Min OR	Max OR
Suction Line	40 g (3 %)	143 g (12 %)	19 mm	14 m	2.9 g/m	10.2 g/m
Evaporator	20 g (2 %)	36 g (3 %)	9 mm	36 m	0.6 g/m	1.0 g/m
Liquid Line	17 g (1 %)	93 g (8 %)	8 mm	19 m	0.9 g/m	4.9 g/m
Condenser	7 g (1%)	82 g (7 %)	8 mm	70 m	0.1 g/m	1.2 g/m
Overall System	84 g (7 %)	354 g (29%)	-	139 m	-	-

Table 6.6: Comparison of Oil Retention Volume for R22/MO and R410A/POE Air Conditioning Systems

Component	Oil Ret. Volume R22/MO System [ml/m]		Oil Ret. Volume R410A/POE System [ml/m]	
	OMF = 1 wt.%	OMF = 5 wt.%	OMF = 1 wt. %	OMF = 5 wt.%
Suction Line	3.9	18.6	5.0	15.2
Evaporator	< 0.2	1.4	1.0	3.0
Liquid Line	2.5	7.9	1.7	2.2
Condenser	1.6	6.2	0.6	3.0
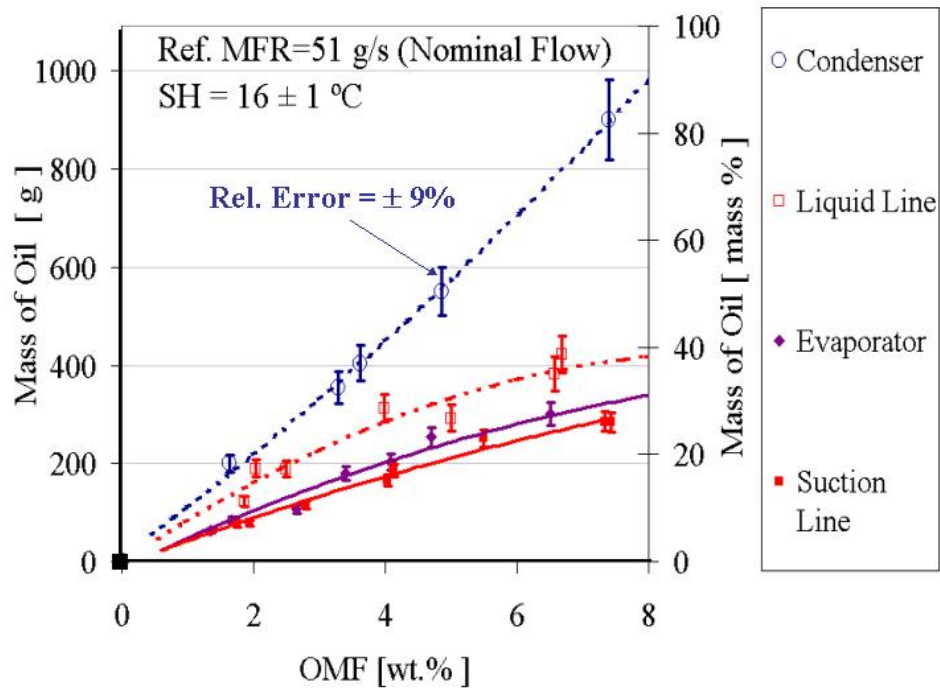
Figure 6.1: Oil Distribution in R22 Air Conditioning System at Nominal Capacity
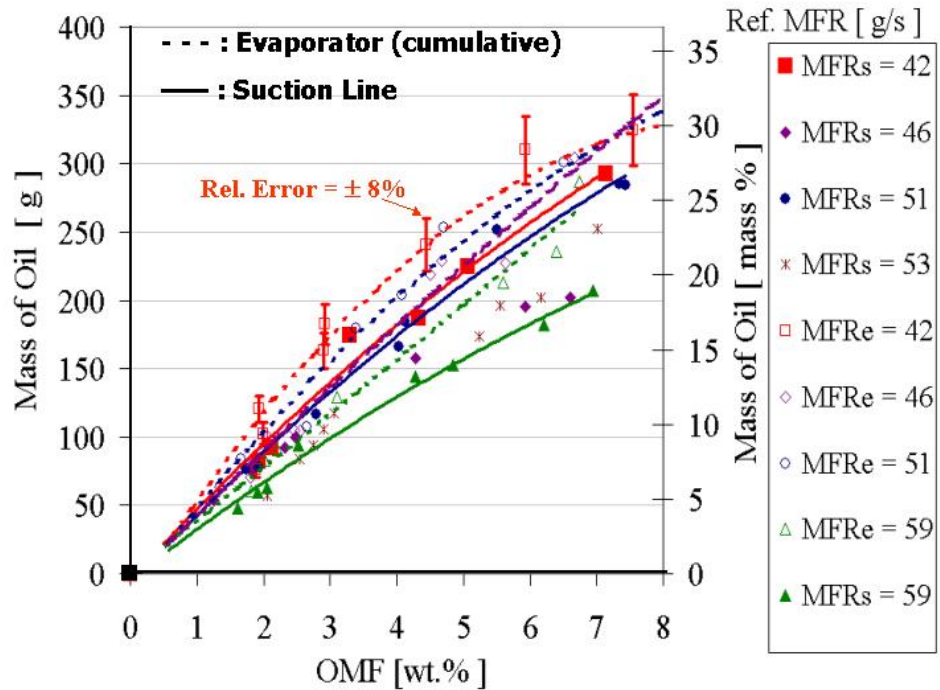
Figure 6.2: Cumulative Oil Retention in Suction Line, Evaporator of R22 System
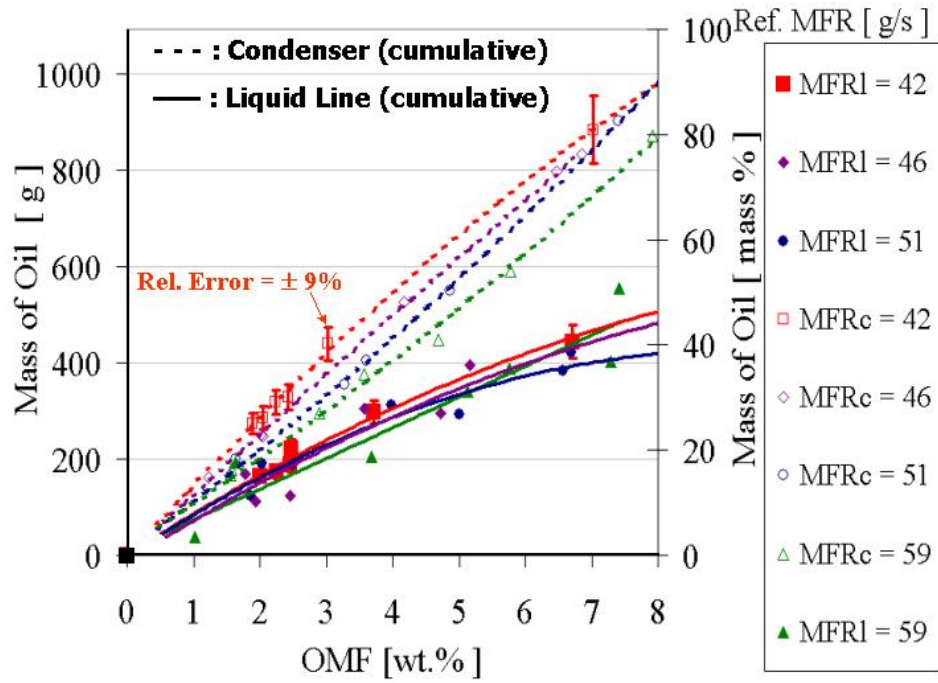
Figure 6.3: Cumulative Oil Retention in Liquid Line and Condenser of R22 System
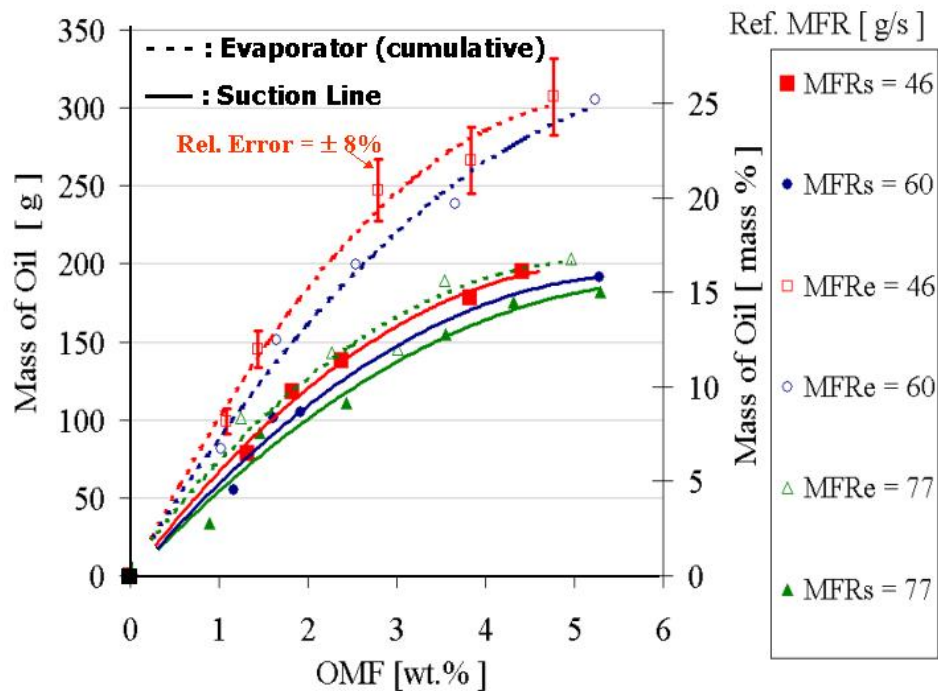
Figure 6.4: Cumulative Oil Retention in Suction Line and Evaporator of R410A/POE System
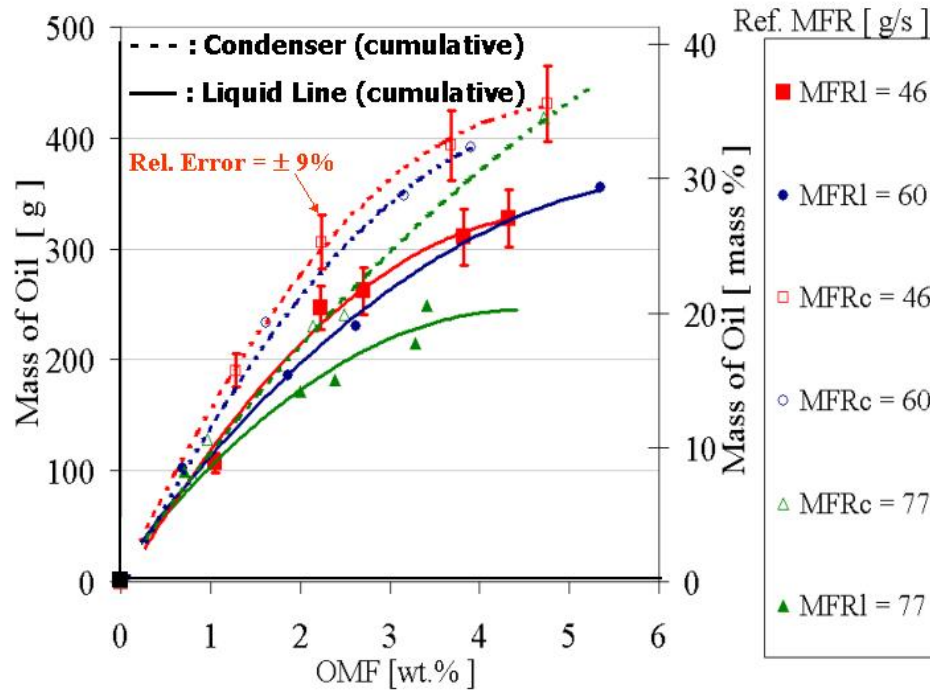
Figure 6.5: Cumulative Oil Retention in Liquid Line and Condenser of R410A/POE System
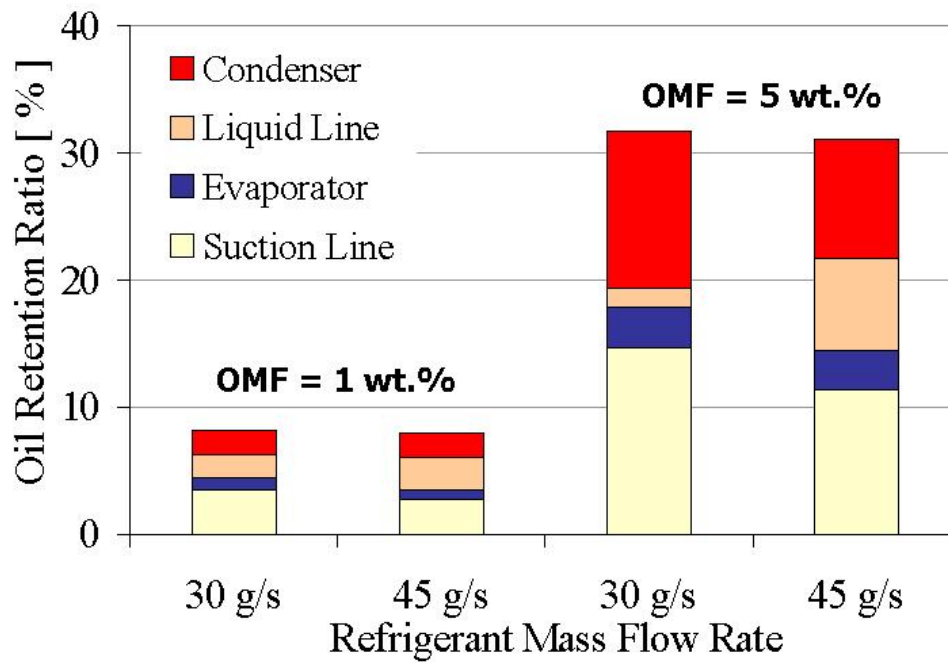
Figure 6.6: Oil Distribution for R134a/POE System

113
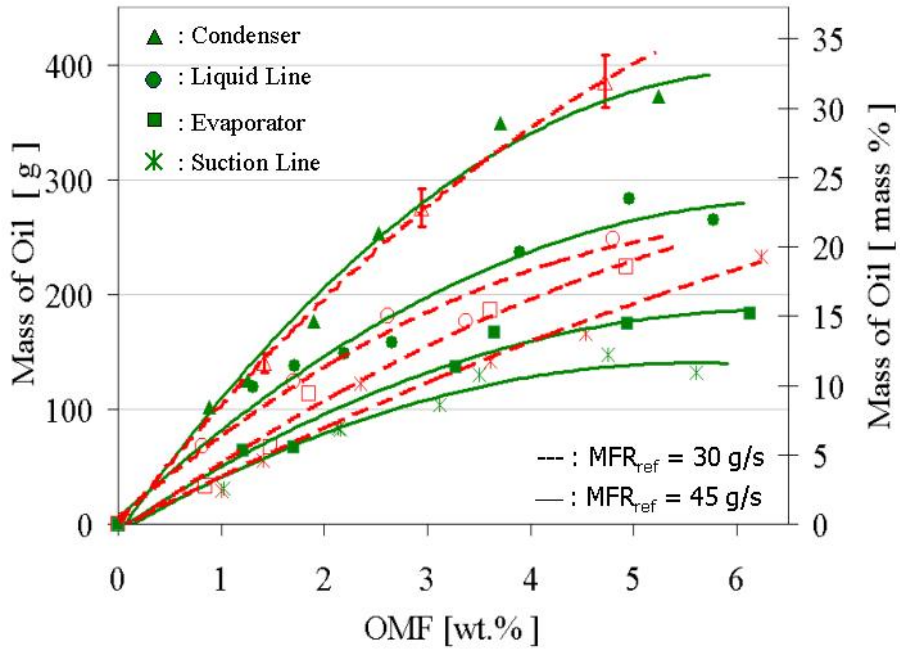
Figure 6.7: Cumulative Oil Retention in Suction Line and Evaporator, Liquid Line and Condenser of R134a/POE System
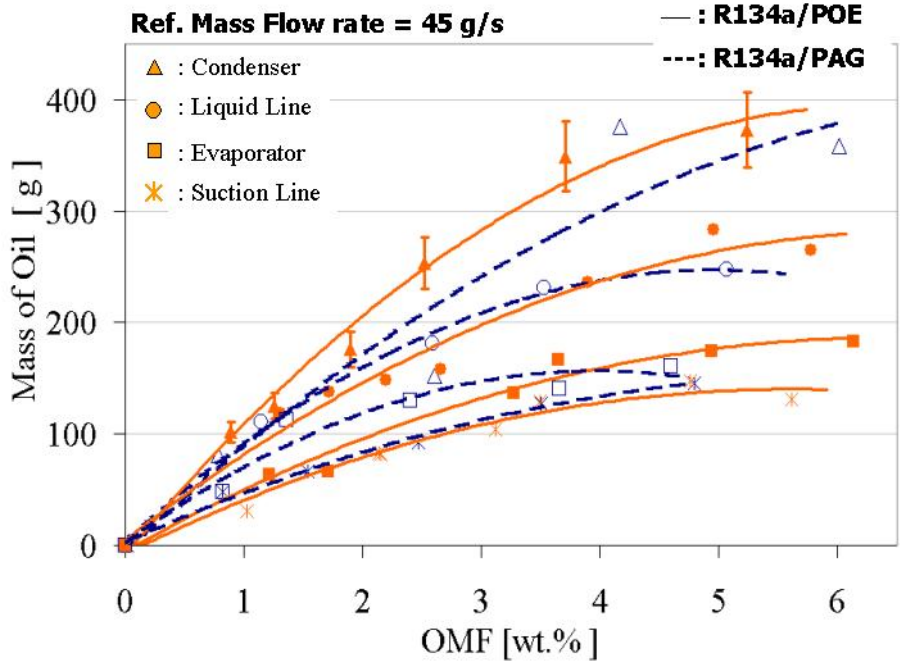
Figure 6.8: Comparison of Oil Retention between R134a/POE and R134a/PAG Systems
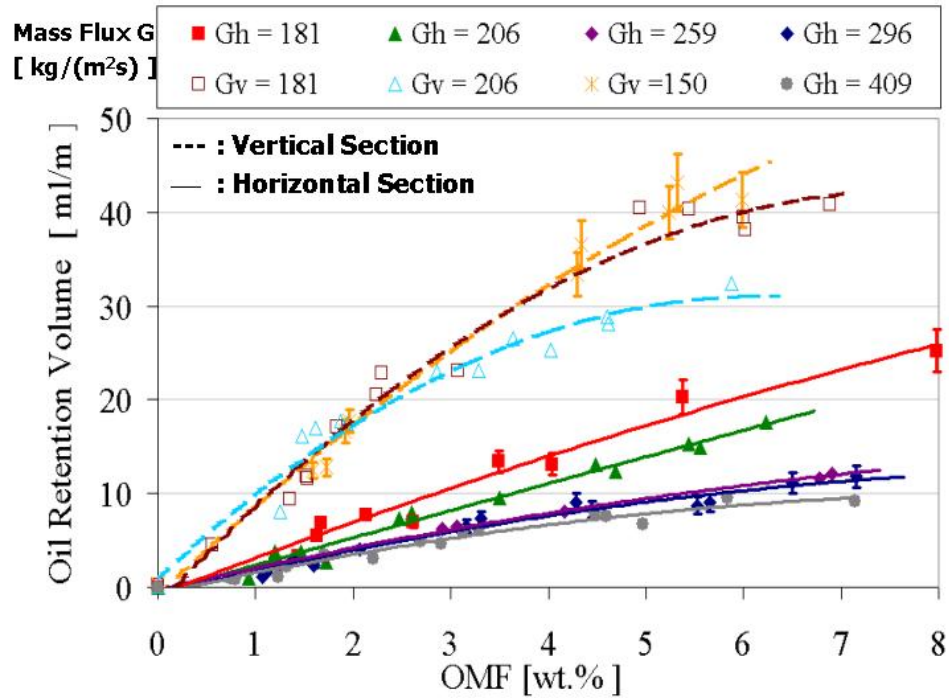
Figure 6.9: Effect of the Refrigerant Mass Flux on the Oil Retention Volume
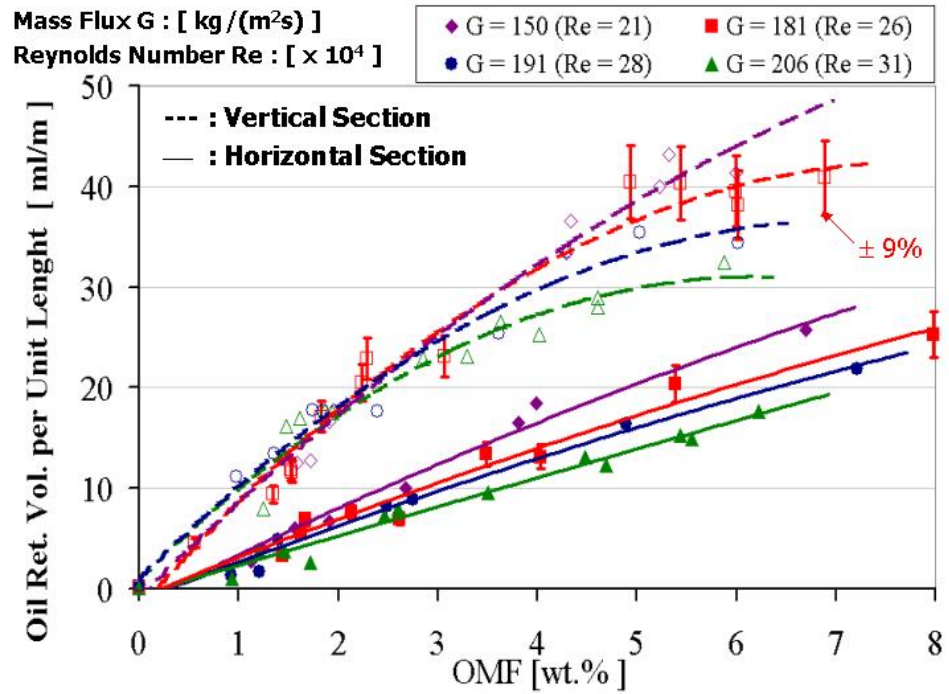
Figure 6.10: Effect of the Gravity Force on the Oil Retention Volume in the Suction
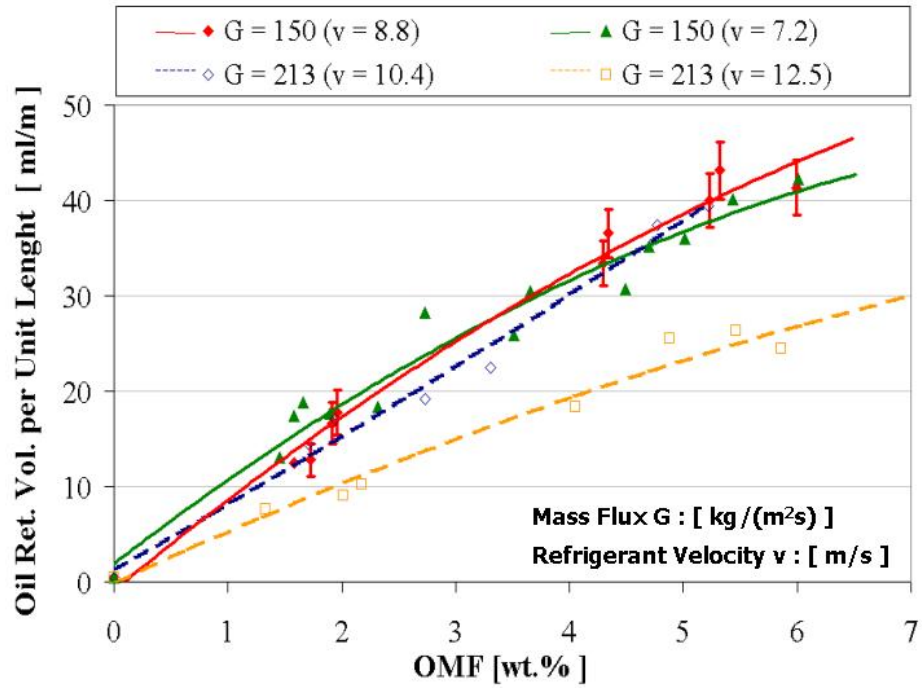
Line of R22 System

Figure 6.11: Effect of the Refrigerant Vapor Velocity on the Oil Retention in the Vertical Upward Suction Line of R22 System
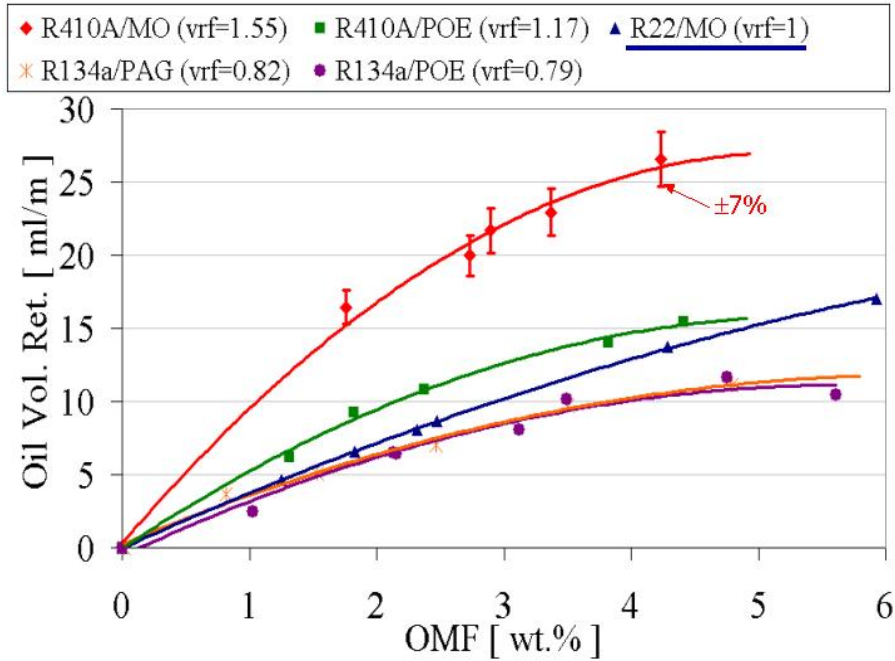
Figure 6.12: Effect of the Mixture Viscosity Ratio on the Oil Retention Volume in the Suction Line
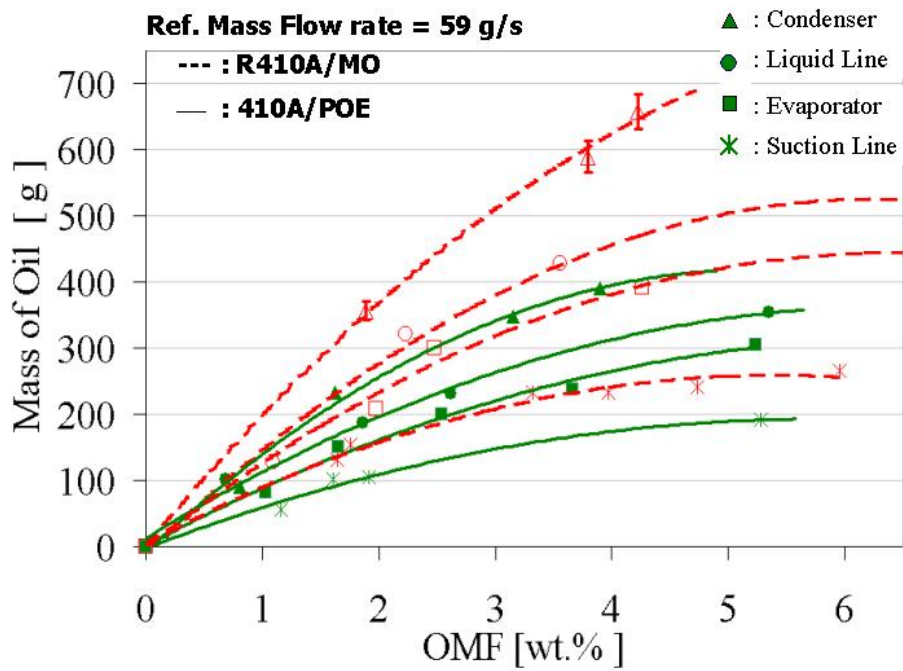
Figure 6.13: Comparison of Oil Retention Characteristics in R410A/POE and R410A/MO Air Conditioning Systems
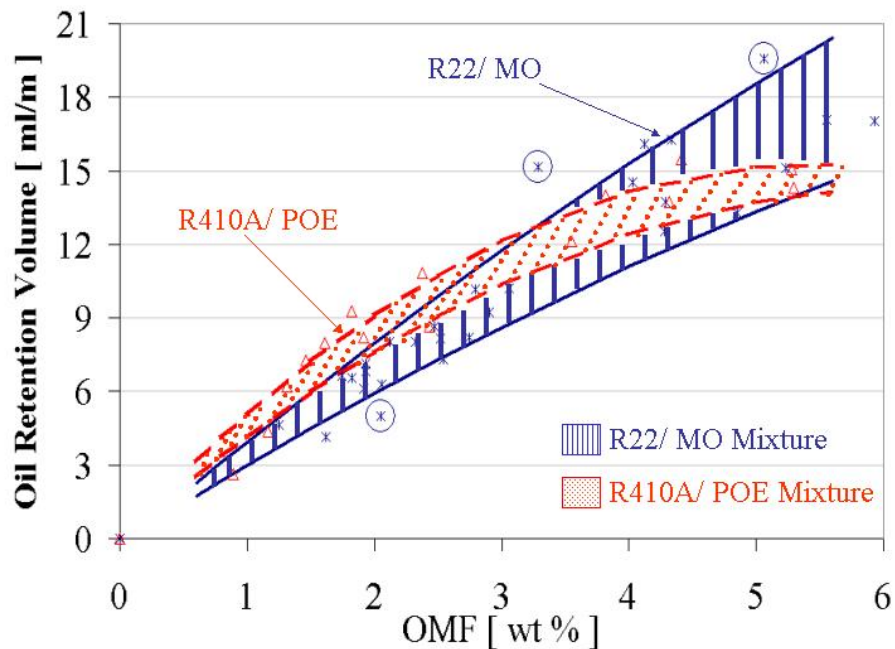
Figure 6.14: Comparison of Oil Retention Volume in the Suction Line for Different Refrigerant and Oil Mixtures

117
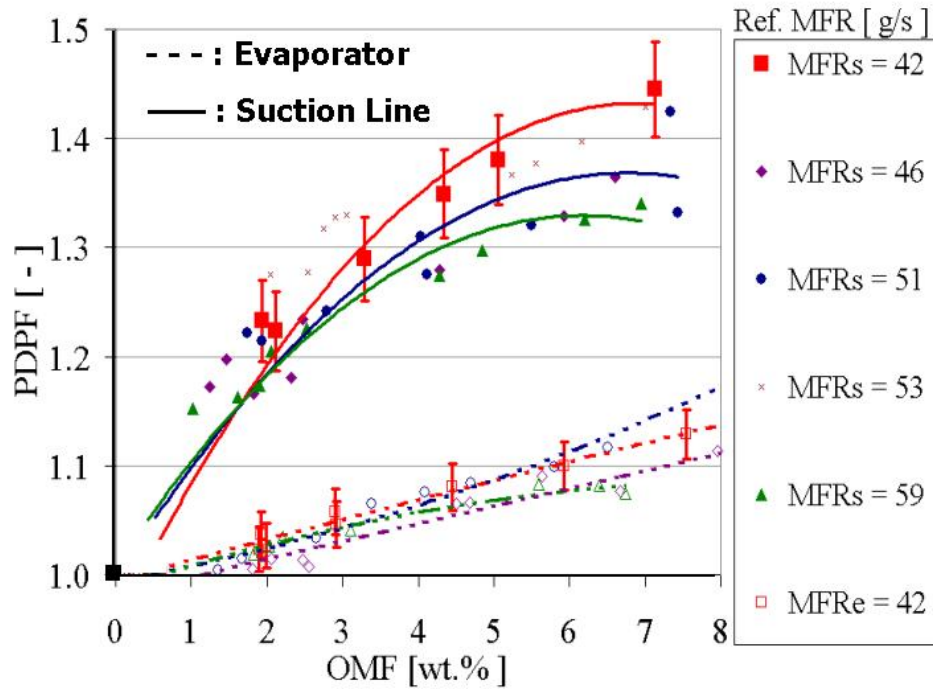
Figure 6.15: Pressure Drop Penalty Factor in the Suction Line and Evaporator of

R22 System
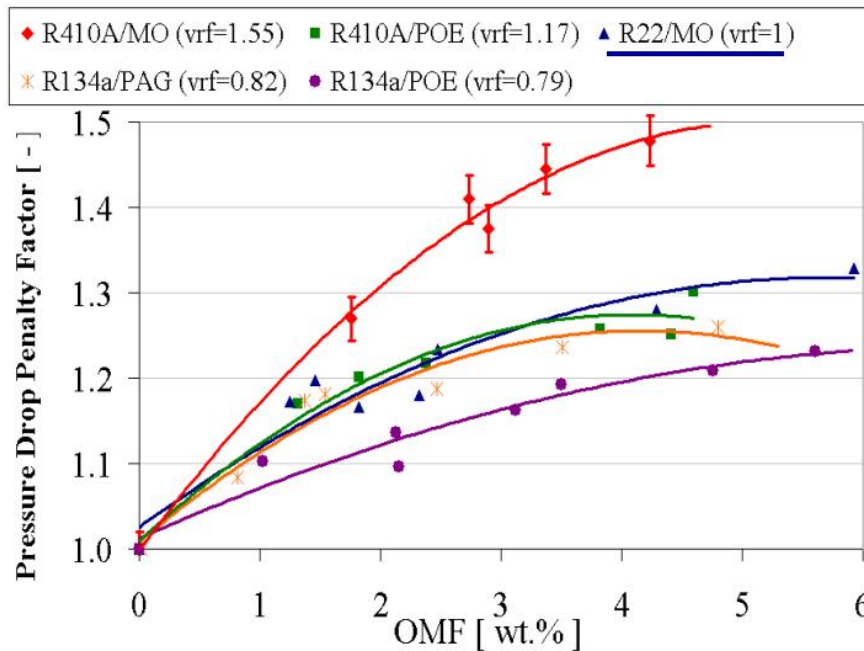
Figure 6.16: Pressure Drop Penalty Factor in the Suction Line for Different

Refrigerant and Oil Mixtures

118
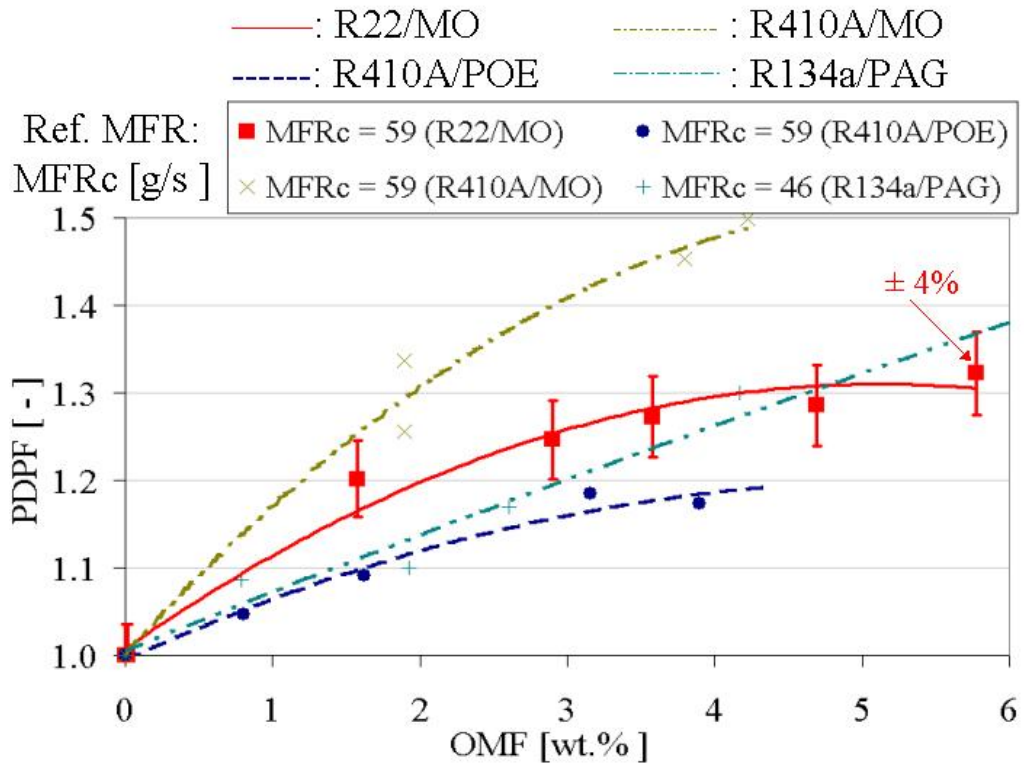
Figure 6.17: Pressure Drop Penalty Factor in the Condenser for Different Refrigerant and Oil Mixtures

Chapter 7: Modeling of Oil Retention in the Suction Line

`

Two-phase flows obey all of the basic laws of fluid mechanics. The equations are merely more complicated or more numerous than those for single-phase flows. The techniques for analyzing one-dimensional flows fall into several classes. They can conveniently be arranged in ascending order of sophistication, depending on the amount of information which is needed to describe the flow: correlations, simple analytical models, integral analysis, differential analysis, and universal phenomena. In this chapter a theoretical approach to estimate the oil retention is proposed and the governing equations are explained. Oil entrainment is a complex function of refrigerant and oil velocities, densities, mutual solubility, and miscibility. Moreover geometry, orientation, and surface roughness of the pipe affect the oil transport characteristics. From literature review, the models for oil entrainment are mainly divided in two types: separated flow models for gas and liquid two-phase flows and homogeneous models for liquid and liquid two-component flows. In vapor compression system pipe flows, the core region is usually the refrigerant-rich phase while the liquid film at the pipe wall is the oil-rich phase. The adiabatic annular two-phase flow will be described next since it usually occurs in the suction line. It is a simple engineering approach that leads to empirical correlations useful in air conditioning applications. Further investigations will focus on homogeneous, stratified, and slug flow models, which applied to liquid lines, condensers, and evaporators. The next chapter will consider the phase change processes that occur in heat exchangers of a vapor compression system.

7.1 Navier-Stokes Equations for Annular Laminar Flow

Simple analytical models, which take no account of the details of the flow, can be quite successful, both for organizing experimental results and for predicting design parameters. In a separated-flow model the phases are assumed to flow side by side. Separate equations are written for each phase and the interaction between the phases is considered. The price that is paid for greater accuracy in prediction of results is an increase in complexity. However, it is useful to write down the Navier-Stokes equations and look for an analytical solution. Coutris *et al.* (1989, [28]) proved successfully this approach and analytical and numerical solutions exist. For simplicity, core gas and liquid film are considered first. Two-phase separated annular flow is schematically represented in Figure 7.1. Both core and film flows are laminar and the droplets entrainment in the core region is assumed to be zero. Circumferential secondary flows as described by James *et al.* (1987, [55]) are neglected. Phase inversion instabilities as described by Brauner and Ullman (2002, [19]) are also neglected. Thus, finding the film thickness of separation between the two phases appears trivial but ultimately is not.

7.1.1 Flow Pattern in the Suction Line

Numerous studies have shown that no single theory or correlation can satisfactorily predict the pressure gradient or liquid hold-up over all possible flow regimes encountered in two-phase gas-liquid flow in pipes. This fact was also mentioned in the research work

by Mandhane *et. al.* (1974, [75]). From the designer's point of view, it is important to be able to predict accurately what flow pattern will occur from given input flow rates, pipe sizes, and fluid proprieties. Many methods have been presented in the literature for this purpose, usually in the form of two-dimensional maps in which the location of the boundaries between flow pattern regions are based on empirical observations.

In this research work, the modified Baker's map (1954, [6]) is used to identify the flow pattern in the suction line. The data have been plotted in the map of Figure 7.2 and the circles represent empirical observations of the flow pattern. The x- axis represents the corrected ratio of liquid mass flux (G_l) to the vapor mass flux (G_g), while the and y- axis represents the corrected vapor mass flux. The map was originally developed for air-water two-phase flows. However the correction factors λ, ψ allow researchers to compensate for different proprieties and to apply the map for other fluid mixtures. The correction factors are given as follows:

$$\lambda = \sqrt{\left(\frac{\rho_g}{\rho_a}\right) \cdot \left(\frac{\rho_L}{\rho_W}\right)}; \qquad \psi = \left(\frac{\sigma_W}{\sigma_L}\right) \cdot \left[\left(\frac{\mu_L}{\mu_W}\right) \cdot \left(\frac{\rho_W}{\rho_L}\right)^2\right]^{1/3} \qquad (7.1)$$

where

ρ_g, ρ_L = gas and liquid density ; ρ_a, ρ_W = air and water density;

μ_L, μ_W = liquid and water viscosity ; σ_L, σ_W= liquid and water surface tension

The subscripts *a* and *w* refer to the values of proprieties for air and water at atmospheric pressure. In the map of Figure 7.2, the x-and y-axes were corrected according the relations (7.2):

$$X = \left(\frac{G_l}{G_g}\right) \cdot \lambda \cdot \psi; \qquad Y = \frac{G_g}{\lambda}. \qquad\qquad (7.2)$$

As shown in the map, the mixture flow pattern in the suction line is mostly annular flow for each operating condition tested. In annular flow, the oil-rich liquid flows in a film along the tube wall while the refrigerant vapor flows in the core region. Figure 7.3 presents the flow pattern in the upward vertical suction line for the R22/MO mixture. During the experiments the minimum mass flux was about G = 106 kg/(m^{2}s) and the observed flow pattern was always annular-spray flow. The liquid film climbed the wall surface and some droplets were entrained in the core region. Figure 7.3 compares the flow pattern when the mass flux reached the critical value of about 63 kg/(m^{2}s). At this critical mass flux, the flow became annular-wavy flow and the oil started to reverse its flow causing wavy pattern on the pipe wall. Mehendale (2000, [77]) studied extensively the critical mass flux for oil reversal and the observations in the current work verified his conclusions. Since the mass flux during the experiments was always higher than the critical value, it can be assumed that annular flow is the flow type in the suction line. Figure 7.4 shows the annular flow pattern for the R410A/POE mixture in horizontal suction lines. Different OMFs are shown in the figure to investigate potential changes in the flow patterns due to the oil. However, the flow pattern remained annular for all OMFs. An increase of OMF caused the oil film thickness to rise. This effect was qualitatively detected by an increase of the intensity of the reflecting light from the sight glass. Figure 7.5 shows the flow pattern for R134a/POE and R134a/PAG mixtures. The

refrigerant Reynolds number and the refrigerant mass flux were Re = 17 x 10^4 and G = 106 kg/(m^{2}s), respectively. Moreover the two images have the same geometry as well as similar pressures and degrees of superheat. The degree of solubility and miscibility between refrigerant and oil affected liquid film viscosity, density, and surface tension. The liquid film kinetic viscosities were 25 cSt for R134a/POE and 28 cSt for R134a/PAG.For the two refrigerant-oil mixtures, different types of waves flowing on the wall of the pipe were observed at OMFs of about 1.0 wt.% for R134a/POE and 1.4 wt.% for R134a/PAG. The type of the waves can be seen in Figure 7.5, especially in the upper part of the tube. R134a/PAG had stretched waves along the flow axial direction due to higher viscous resistance of the liquid film, while R134a/POE exhibited numerous tiny separate waves moving slowly on the pipe wall surface.

7.1.2   Analytical Model for Gas-Liquid Annular Flow in the Suction Line

First, the Navier-Stokes equations are applied to both fluid phases. The following assumptions simplified further the problem:

- Axisymmetric flow.

- Steady state, adiabatic, and fully developed flow.

- Oil droplets entrainment is neglected.

- The proprieties of the oil and liquid refrigerant mixtures are uniform along the liquid film thickness. The oil film has some refrigerant dissolved in it. Since the oil properties are not the same as those of the pure oil, properties of oil

124

with refrigerant solution are estimated based on the solubility data from the manufacturers.

The oil retention volume ratio in the suction line can be calculated by the integration of oil film thickness with respect to the cross sectional area (tube inner diameter~19 mm) as well as the entire length (~19 m) of the suction line tube, as shown in equation (7.3)

$$Oil\ Retention\ Volume\ Ratio = L \cdot A \cdot \left[1 - \left(1 - \frac{\delta}{R}\right)^2\right] \cdot \frac{1}{V_{ini}} \tag{7.3}$$

where

L : total suction line length [m] ; A: tube inner cross sectional area [m^2]

R: Inner tube radius [m]; δ: oil film thickness [m]

V_{ini}: oil volume initially charged in the compressor [m^3]

The properties of fluids change from section to section along the pipe, and the suction line consists of horizontal (~14 m) as well as vertical (~5 m) sections. The proprieties of the mixture were estimated by averaging pressure and temperature in the test section. The problem of estimating the oil retention in the suction is reduced to the problem of finding the oil film thickness δ in the pipe at given refrigerant pressures and temperatures.

For steady state incompressible flows, the continuity equation for the liquid film region is:

$$\frac{\partial}{\partial r}(ru_r) = 0 \tag{7.4}$$

while the z-momentum equation is

$$\frac{\mu_l}{r}\frac{\partial}{\partial r}\left(r\frac{\partial u}{\partial r}\right) = \frac{dp}{dz} + \rho_l g_z \qquad (7.5)$$

By integrating equation (7.4), we obtain

$$r \cdot u_r = const \quad \Rightarrow \quad no\,slip\,condition\,at\,the\,wall \quad \Rightarrow R \cdot u_r(r = R) = 0$$

which yield to

$$u_r = 0 \qquad R - \delta \leq r \leq R \qquad (7.6)$$

The equation (7.5) becomes

$$\frac{\mu_l}{r}\frac{d}{dr}\left(r\frac{du}{dr}\right) = \frac{dp}{dz} + \rho_l g_z$$

which can be integrated leading to the following equation:

$$\mu_l\left(r\frac{du}{dr}\right) = \left(\frac{dp}{dz} + \rho_l g_z\right)\frac{r^2}{2} + C_1 \qquad (7.7)$$

For Newtonian fluid, the relation between shear stress tensor and velocity gradient is linear:

$$\tau_{rz} = \tau = -\mu_l\frac{du}{dr} \qquad (7.8)$$

Similarly for the core region, due to the conservation of mass and momentum and with the assumption of zero droplets entrainment, the core velocity has no component along the radial direction of the pipe (i.e., $u_{core,radial}$=0). Consequently, the following system of equations describes the film and the core regions:

Liquid Film

$$\mu_f \frac{du_f}{dr} = \left(\frac{dp}{dz} + \rho_f g_z\right)\frac{r}{2} + \frac{C_1}{r} \qquad\qquad R - \delta < r < R \qquad\qquad (7.9)$$

Core Region

$$\mu_c \frac{du_c}{dr} = \left(\frac{dp}{dz} + \rho_c g_z\right)\frac{r}{2} + \frac{C_3}{r} \qquad\qquad 0 < r < R - \delta \qquad\qquad (7.10)$$

The following boundary conditions need to be satisfied:

(1) Symmetry boundary condition: $\left.\dfrac{du_c}{dr}\right|_{r=0} = 0$

(2) Interface core-film boundary condition: $\left[\mu_c \dfrac{du_c}{dr}\right]_{r=R-\delta} = \left[\mu_f \dfrac{du_f}{dr}\right]_{r=R-\delta}$

(3) No slip boundary condition at the wall: $\left.u_f\right|_{r=R} = 0$

(4) No slip condition at the core-film interface: $\left.u_f\right|_{r=R-\delta} = \left.u_c\right|_{r=R-\delta}$

Using the four boundary conditions, the problem can be mathematically solved. The symmetry B.C. yields to

$$\mu_c \frac{du_c}{dr} = \left(\frac{dp}{dz} + \rho_c g_z\right)\frac{r}{2} + \frac{C_3}{r} \quad\underset{r\to 0}{\longrightarrow}\quad 0 \;\Rightarrow\; C_3 = 0$$

Thus, integrating equations (7.9) and (7.10) yields the following velocity profiles

$$u_f = \frac{1}{\mu_f}\left[\frac{1}{2}\left(\frac{dp}{dz} + \rho_f g_z\right)\frac{r^2}{2} + C_1 \ln r + C_2\right] \qquad\qquad R - \delta < r < R$$

$$u_c = \frac{1}{\mu_c}\left[\frac{1}{2}\left(\frac{dp}{dz} + \rho_c g_z\right)\frac{r^2}{2} + C_4\right] \qquad\qquad 0 < r < R - \delta$$

Applying the boundary conditions (2), (3), and (4), the velocity profiles can be obtained.

For simplicity, define the dimensionless variables variables as follows:

$$\tilde{\rho} = \frac{\rho_f}{\rho_c} = \text{density ratio}; \qquad \tilde{\mu} = \frac{\mu_c}{\mu_f} = \text{viscosity ratio};$$

$$\xi = \frac{r}{R} = \text{dimensionless radial coordinate: } 0 \le \xi \le 1;$$

$$\varepsilon = \frac{\delta}{R} = \text{dimensionless oil film thickness: } 0 \le \varepsilon \le 1;$$

Introducing these dimensionless variables in the above velocity profiles, and after some algebra, the resulting velocity profiles are as follows:

$$u_c = -\frac{1}{4}\frac{R^2}{\mu_c}\frac{dp}{dz}\left[\left(\tilde{\mu} - \xi^2\right) + \left(1 - \tilde{\mu}\right)\left(1 - \varepsilon\right)^2\right] +$$

$$-\frac{1}{4}\frac{R^2}{\mu_c}\rho_c g_z\left[\left(\tilde{\mu}\tilde{\rho} - \xi^2\right) + \left(1 - \tilde{\rho}\tilde{\mu}\right)\left(1 - \varepsilon\right)^2 + 2\tilde{\mu}\left(\tilde{\rho} - 1\right)\left(1 - \varepsilon\right)^2 \ln\left(1 - \varepsilon\right)\right] \qquad (7.11)$$

$$0 \le \xi \le 1 - \varepsilon$$

$$u_f = -\frac{1}{4}\frac{R^2}{\mu_c}\frac{dp}{dz}\tilde{\mu}\left[\left(1 - \xi^2\right)\right] +$$

$$-\frac{1}{4}\frac{R^2}{\mu_c}\rho_c g_z\tilde{\mu}\left[\left(1 - \xi^2\right)\tilde{\rho} + 2\left(\tilde{\rho} - 1\right)\left(1 - \varepsilon\right)^2 \ln\left(\xi\right)\right] \qquad (7.12)$$

$$1 - \varepsilon \le \xi \le 1$$

Integration of the velocity profiles yields the volume flow rates of the core refrigerant and liquid oil film:

$$Q_c = \int_0^{2\pi}\int_0^{R-\delta} u_c(r)\,r\,dr\,d\vartheta = 2\pi R^2 \int_0^{1-\varepsilon} u_c(\xi)\,\xi\,d\xi$$

$$Q_f = \int_0^{2\pi} \int_{R-\delta}^{R} u_f(r)\,rdrd\vartheta = 2\pi R^2 \int_{1-\varepsilon}^{1} u_f(\xi)\xi d\xi$$

The results are shown in the equations below:

$$Q_c = -\frac{\pi}{2}\frac{R^4}{\mu_c}\frac{dp}{dz}(1-\varepsilon)^2\left[\frac{3}{4}(1-\varepsilon)^2 + \frac{\tilde{\mu}}{2} - \tilde{\mu}(1-\varepsilon)^2\right] +$$
$$-\frac{\pi}{2}\frac{R^4}{\mu_c}\rho_c g_z(1-\varepsilon)^2\left\{-\frac{1}{4} + \tilde{\mu}\tilde{\rho} + \frac{1}{2}\left[\begin{array}{l}(1-\tilde{\rho}\tilde{\mu})(1-\varepsilon)^2 + \\ +2\tilde{\mu}(\tilde{\rho}-1)(1-\varepsilon)^2 \ln(1-\varepsilon)\end{array}\right]\right\}$$

(7.13)

$$Q_f = -\frac{\pi}{2}\frac{R^4}{\mu_c}\frac{dp}{dz}\tilde{\mu}\left[\frac{1}{4} + -\frac{1}{2}(1-\varepsilon)^2 + \frac{1}{4}(1-\varepsilon)^4\right] +$$
$$-\frac{\pi}{2}\frac{R^4}{\mu_c}\rho_c g_z\tilde{\mu}\left\{\tilde{\rho}\left[\frac{1}{4} + -\frac{1}{2}(1-\varepsilon)^2 + \frac{1}{4}(1-\varepsilon)^4\right] +\right.$$
$$\left. + (\tilde{\rho}-1)(1-\varepsilon)^2\left[\frac{1}{2} + (1-(1-\varepsilon)^2 + (1-\varepsilon)^2 \ln(1-\varepsilon))\right]\right\}$$

(7.14)

Once the volume flow rates and the proprieties of core and film are known, the equations

(7.13) and (7.14) set a system of two equations in two unknown variables (*dp/dz* and ε).

If the pressure gradient, *dp/dz*, is obtained from one equation and then substituted in the

other, the analytical solution for this problem is reduced to look for a solution ε of the

form $\varepsilon = \varepsilon(\tilde{q}, \tilde{\rho}, \tilde{\mu})$, such that it satisfies a 4th order polynomial equation of the following

form:

$$\varepsilon^4 + a\varepsilon^3 + b\varepsilon^2 + c\varepsilon + d = 0$$

(7.15)

Where *a*, *b*, *c*, and *d* are coefficients that depend on the volume flow rate ratio

($\tilde{q} = Q_f/Q_c$), the density ratio ($\tilde{\rho}$) and the viscosity ratio ($\tilde{\mu}$) of the two phases. This

analysis was provided first by Wallis in 1970 ([113],[114]) and numerical solutions for stratified flow of gas and water and oil and water between flat plates and inside pipes were given by Coutris *et al.* a few years later (1989, [28]). Given the polynomial equation of the form (7.15), the numeric solutions showed that the film thickness tends to increase if the volume flow rate ratio ($\widetilde{q}$) increases or if the viscosity ratio ($\widetilde{\mu}$) decreases.

Hall and Hewitt (1993, [42]) proposed an approximate model to solve two-phase stratified gas-liquid and oil-water flows in between flat plates and circular pipes. They compared their results with the exact solution, which was derived either analytically or numerically. The results showed that film thickness tended to increase when the Martinelli's parameter increased. The Martinelli parameter (*X*) was defined as

$$X^2 = \frac{u_f}{u_c}\frac{\mu_f}{\mu_c} = \frac{1}{\widetilde{Q}\widetilde{\mu}} \; .$$

Moreover, for the same Martinelli parameter, oil-water two-phase flows showed higher dimensionless liquid height than gas-water two-phase flows.

7.2 The Interfacial Shear Stress Model

The simple theory described in the previous section provides a starting point for further developments. It offers approximate predictions, which are adequate for preliminary estimates. It provides a conceptual framework that puts more detailed investigations in perspective. It is generally compatible with the results of other researchers except where deviations can be traced to physical effects, which are not

accounted for in the theory. The structure of such theory may well be too awkward for it to be useful in practice. It is often simpler and cheaper to perform a suitable experiment. Correlations of experimental data in terms of chosen variables are a convenient way of obtaining design equations with a minimum of analytical work. The crudest correlations are mere mathematical exercises, readily performed with modern computers while more advanced techniques use dimensional analysis or grouping of several variables together on a logical basis.

From the previous analysis, it appears that dimensionless film thickness is proportional to the liquid/vapor mixture's volume flow rate ratio and viscosity ratio. In real oil entrainment phenomena, the flow regime at the suction line is usually annular-wave flow and the wavy drag force of the core refrigerant on the film is the main factor responsible for oil entrainment. Turbulence, instability effects, and boundary effects may change the oil transport characteristics appreciably. The complexity of the problem increases and looking for analytical solutions seems hopeless. Several researchers follow a different approach based on interfacial shear stress definition. The developed models are supported by experimental data and the correlations are easy to use. As long as the correlations are applied to situations similar to those that were used to obtain the original data, they can be quite satisfactory, within statistical limits, which are usually known. However, experimental correlations can be quite misleading if used indiscriminately in a variety of applications. Furthermore, since little insight into the basic phenomena is achieved by data correlations, no indication is given of ways in which performance can be improved or prediction accuracy increased.

For steady state fully developed laminar film flow in pipes, the governing equations for the oil film region do not change. However the boundary conditions can be specified on the shear stress forces instead of on the velocities gradient.

Interfacial core-film boundary condition: $\tau = \left[\mu_f \dfrac{du_f}{dr} \right]_{r=R-\delta} = \tau_i$ at $r = R - \delta$

where τ_i is the interfacial shear stress. The above boundary condition can be used in equation (7.7), which becomes

$$-\tau \cdot r = \left(\frac{dp}{dz} + \rho_f g_z \right) \cdot \frac{r^2}{2} + C_1, \text{ at } r=R-\delta.$$

So the following equation is obtained:

$$-\tau_i (R - \delta) = \left(\frac{dp}{dz} + \rho_f g_z \right) \frac{(R-\delta)^2}{2} + C_1 \tag{7.16}$$

Eliminating C_1 between equations (7.7)and (7.16) leads to the equation

$$\tau = \tau_i \frac{(R-\delta)}{r} - \frac{1}{2} \left(\frac{dp}{dz} + \rho_f g_z \right) \left(\frac{r^2 - (R-\delta)^2}{r} \right) \tag{7.17}$$

which is the equation (3.1) previously obtained by using the force balance approach described in Chapter 3.3. If the shear stress term is expressed by the velocity gradient, Equation (7.17) becomes

$$-\mu_l \frac{du}{dr} = \tau_i \frac{(R-\delta)}{r} - \frac{1}{2} \cdot \left(\frac{dp}{dz} + \rho_f g_z \right) \left(\frac{r^2 - (R-\delta)^2}{r} \right) \tag{7.18}$$

Integrating Equation (7.18) with respect to r and using a no-slip boundary condition for the oil film at the wall ($u(r = R) = 0$) shows, respectively,

$$-\mu_l u = \tau_i \, ln \, r \cdot (R-\delta) - \frac{1}{2} \cdot \left(\frac{dp}{dz} + \rho_f g_z \right) \left(\frac{r^2}{2} - (R-\delta)^2 \cdot ln \, r \right) + C_2$$

$$0 = \tau_i \, ln \, R \cdot (R-\delta) - \frac{1}{2} \cdot \left(\frac{dp}{dz} + \rho_f g_z \right) \left(\frac{R^2}{2} - (R-\delta)^2 \cdot ln \, R \right) + C_2$$

Eliminating C_2, the velocity profile of the liquid film is specified as follows:

$$u_f = \frac{1}{\mu_l} \begin{bmatrix} \left[\left(\tau_i \cdot (R-\delta) + \frac{(R-\delta)^2}{2} \cdot \left(\frac{dp}{dz} + \rho_f g_z \right) \right) \cdot ln \frac{R}{r} + \right] \\ -\frac{1}{4} \left(\frac{dp}{dz} + \rho_f g_z \right) (R^2 - r^2) \end{bmatrix} \tag{7.19}$$

The oil mass flow rate can be obtained by integrating the velocity profile over the cross sectional area:

$$\dot{m}_o = \frac{2\pi\rho_f}{\mu_f} \left(\tau_i (R-\delta) + \frac{(R-\delta)^2}{2} \left(\frac{dp}{dz} + \rho_f g_z \right) \right) + $$
$$\frac{2\pi\rho_f}{\mu_f} \left(\frac{R^2 - (R-\delta)^2}{4} - \frac{(R-\delta)^2}{2} ln \frac{R}{R-\delta} \right) + \tag{7.20}$$
$$-\frac{\pi\rho_f}{8\mu_f} \left(\frac{dp}{dz} + \rho_f g_z \right) (R^2 - (R-\delta)^2)^2$$

For given fluid properties and tube diameter, equation (7.20) contains three unknown quantities, which are:

- oil film thickness (δ)

- pressure gradient ($\frac{dp}{dz}$)

- interfacial shear stress (τ_i).

Since the only known value in equation (7.20) is the oil mass flow rate ($\dot{m}_o$) for a certain

oil mass fraction at given refrigerant mass flow rates, the interfacial shear stress and

pressure gradient should be correlated to obtain oil film thickness as described next.

7.3   Core Analysis

Figure 7.1 shows a force balance on the vapor refrigerant core region. It is assumed that

oil film thickness δ uniformly covers the inside tube wall while the gas flows through the

core. When the force balance applied to the gas core is drawn,

$$\frac{dp}{dz} + \rho_g g_z + \frac{\tau_i \pi D_c}{A_c} = 0$$

where D_c is the outer vapor core diameter and A_c is the vapor core cross sectional area.

The void fraction α is defined as follows:

$$\alpha = \frac{A_c}{A} = \left(\frac{D - 2\delta}{D}\right)^2 \tag{7.21}$$

The previous force balance equation can be written as:

$$\frac{dp}{dz} = -\frac{4\tau_i}{D - 2\delta} - \rho_g g_z \tag{7.22}$$

Consequently, the pressure gradient of the core is a function of oil film thickness δ (or

the void fraction α) and interfacial shear stress τ_i.

7.4 Interfacial Friction Factor

The refrigerant core mass flux acts on the liquid film by transmitting axial momentum outward in the radial direction. The interfacial shear stress exerted by the gas core on the liquid film is given by

$$\tau_i = \frac{1}{2} f_i \rho_c \left(u_c - u_f \right)^2 \tag{7.23}$$

In case of gas-liquid two-phase flow, the velocity of the gas core is much larger than the oil film surface velocity. The interfacial shear stress can be approximated as

$$\tau_i = \frac{1}{2} f_i \rho_c u_c^2 \tag{7.24}$$

The interfacial friction factor f_i in equation (7.24) is the most important parameter in estimating oil film thickness. It is usually obtained from empirical correlations produced by suitable experimental tests. For example, Wallis (1969, [113]) proposed the following correlation valid for annular two-phase flow with thin liquid film in smooth pipes:

$$f_i = 0.005 \left(1 + 300 \frac{\delta}{D} \right) \tag{7.25}$$

Newton *et al*. (1999, [80]) investigated two-phase flows of air with different liquids, water, kerosene, and Propar-22, which is a light machine oil. They proposed two different friction factors depending on interface roughness:

$$f_i = 6.5 \times 10^{-4} \cdot Re_g^{0.3} \quad \text{for a smooth interface}$$

(7.26)

$$f_i = 0.003 \cdot Re_g^{0.2} \qquad \text{for a wavy interface}$$

Wongwise and Kongkiatwanitch (2001, [116]) suggested a new empirically correlated interfacial friction factor with air and water. Like fully developed single-phase turbulent flows in vertical pipes, the friction factor can be expressed as a function of the gas Reynolds number and dimensionless liquid film thickness:

$$f_i = 17.172 \cdot Re_g^{-0.768} \cdot \left(\frac{\delta}{D} \right)^{-0.253}$$

(7.27)

Equation (7.27) was developed for vertical upward air-water flow using a 29 mm inner diameter pipe. It was developed for gas Reynolds that varied $2 \times 10^4 < Re_g < 8\ 10^4$ and the liquid film thickness ranged from $0.10 \leq \delta/D < 0.17$. The flow pattern was annular flow with large disturbance waves that formed as the liquid flow rate increased. The droplets entrainment in the gas core regions was experimentally measured and it was taken into account in the model proposed by Wongwise and Kongkiatwanitch.

Lee (2002, [68]) studied oil retention in air conditioning systems using CO_2/PAG mixtures. He proposed a similar form for the friction factor but with different exponents:

$$f_i = 9.287 \times 10^{-5} \cdot Re_g^{0.2976} \cdot \left(\frac{\delta}{D} \right)^{-0.6515}$$

(7.28)

The correlation (7.28) was obtained for Reynolds numbers varying from $16 \times 10^4 < Re_g < 35 \times 10^4$, which was the range of gas core Reynolds numbers in CO_2 air conditioning systems. The liquid film thickness ranged from $0.02 \leq \delta/D < 0.10$ and the suction line was horizontal.

7.5 Suction Line Simulation Results

The degree of solubility and miscibility between refrigerant and oil determines oil film density, viscosity, and surface tension. Different refrigerant and oil mixtures may have modified or more complex shear stress relations, depending upon the degree of interaction and affinity between the phases.

The approach used in the current research work was the following:

- All the liquid and vapor mixture proprieties were estimated using the manufacturer's data or correlations.

- Liquid film thickness and oil and refrigerant mass flow rates were measured in the experimental part of the current work.

- The system of equations (7.20), (7.22), and (7.24) was solved using Engineering Equation Solver software (EES). Thus, the experimental friction factor was obtained.

- The experimental friction factor was correlated to different parameters such as liquid film thickness, refrigerant vapor Reynolds number, mixture Weber number, and mixture viscosity ratio.

- New correlations were developed for horizontal and upward vertical suction pipes.

- Using the new correlations, oil retention was predicted and compared with experimental data.

The above mentioned systems of non linear equations formed an ill-posed system with system determinant nearly singular. By setting the measured δ into the system of equations according to experimental data, the friction factor f_i was obtained in EES. Then various friction factor correlations were used in an attempt to accord closely with the data. Figure 7.6 shows the interfacial friction factor versus the dimensionless liquid film thickness. The correlations that better described the friction factor characteristic were the ones developed by Lee and Wongwise. The latter was developed for lower Reynolds numbers and higher liquid film thicknesses compared to those observed in the current work. Lee developed an empirical correlation for CO_2 and PAG oil mixture but he did not consider the solubility effects. In his work, the proprieties of oil and oil retention characteristics were estimated without accounting for the mass of CO_2 dissolved into the oil. After re-considering this effect in Lee's data, the experimental friction factors for CO_2/PAG mixture was plotted in Figure 7.6. The results show that CO_2/PAG mixture has higher liquid film thickness and lower interfacial friction factor than conventional refrigerants. The main deviation was observed at very low liquid film thicknesses. New semi-empirical correlations for various refrigerant and oil mixtures are proposed based on experimental results in the suction line. The newly developed correlation represents an extension of the previous correlations for low liquid film thickness.

Figure 7.7 presents the variation of interfacial shear stress with refrigerant vapor velocity. The refrigerant velocities during experiments with horizontal lines were 9, 12.6 and 19 m/s while the velocity varied from 6 to 15 m/s in vertical line tests. Interfacial shear stress varied significantly for given fixed refrigerant vapor velocities due to friction

138

factor changes. Parametric analysis was performed to investigate the main parameters that affect the friction factor and provide the best possible correlations. After some preliminary study, the friction factor was correlated with the dimensionless liquid film thickness (δ/D), the refrigerant vapor Reynolds number (Re_g), and the mixture Weber number (We_m). More complex forms of the friction factor have been developed but they increased the accuracy of the results less than 1%. Moreover, as a result of the increased complexity of the correlation, the system of equations to predict the oil retention became more and more singular. The correlations that best fit the data and that were easy but accurate enough to be employed in engineering applications were the following:

- R22/MO mixture in horizontal suction line

$$f_i = 8.915 \times 10^{-6} \cdot Re_g^{0.365} \cdot \left(\frac{\delta}{D}\right)^{-1.273} \cdot We_m^{-0.512} \tag{7.29}$$

- R22/MO mixture in vertical suction line

$$f_i = 3.103 \times 10^{-4} \cdot Re_g^{0.366} \cdot \left(\frac{\delta}{D}\right)^{-0.750} \cdot We_m^{-1.011} \tag{7.30}$$

- All refrigerant and oil mixtures in horizontal suction line (including R22/MO)

$$f_i = 4.686 \times 10^{-2} \cdot Re_g^{-0.335} \cdot \left(\frac{\delta}{D}\right)^{-1.056} \cdot We_m^{-0.255} \tag{7.31}$$

The equation (7.31) is plotted in Figure 7.6. It fits closest the experimental data for conventional refrigerants obtained from the current work and estimates quite well the friction factor of CO_2 and PAG oil mixture obtained from Lee's experimental work. Moreover, as the liquid film thickness increases, it converges to Wongwises's correlation.

In the suction line of air conditioning systems, if $\delta/D > 0.1$ then Wongwises's correlation can be used to estimate the interfacial friction factor, while if $\delta/D < 0.1$ then the new correlation (7.31) can be applied to approximate the interfacial friction factor for both conventional refrigerants and CO_2.

The experimental versus the correlated friction factors are plotted in Figure 7.8. The average relative error due to the uncertainty on the measured variables was estimated using the model in EES. The final results showed that the correlations predicted the friction factor within an uncertainty of about $\pm 26\%$.

Equation (7.31) represents the most general equation that can be adopted to predict oil retention in the suction line of vapor compression systems. It has been developed and verified in the following range:

- $0.001 \leq \dfrac{\delta}{D} < 0.06$; • $17{,}000 \leq Re_g \leq 40{,}000$;

- $13.8 \leq We_m \leq 221$; • $20 \leq \dfrac{v_{liquid,film}}{v_{ref,vapor}} \leq 48$;

which represents the widest possible ranges of liquid thicknesses, Reynolds numbers, Weber numbers, and viscosity ratios for most common refrigerant and oil mixtures in air-conditioning systems. Figure 7.9 compares experimental oil retention volume versus predicted oil retention volume, which was obtained by using the relation (7.31) to close the problem specified by the system of equations (7.20), (7.22), and (7.24). The simulation results were within $\pm$ 31 % average relative error. The friction factor correlation (7.31) should be used only for horizontal suction lines while, for vertical suction lines, the friction factor correlation (7.30) provides more accurate results.

However the specific friction factor correlation for upward vertical suction lines has been developed only for R22/MO mixture and its accuracy has not been verified for other refrigerant-oil mixtures. In the future, more studies should focus on the correlations for vertical suction lines, and on verifying them for different oil and refrigerant mixtures.
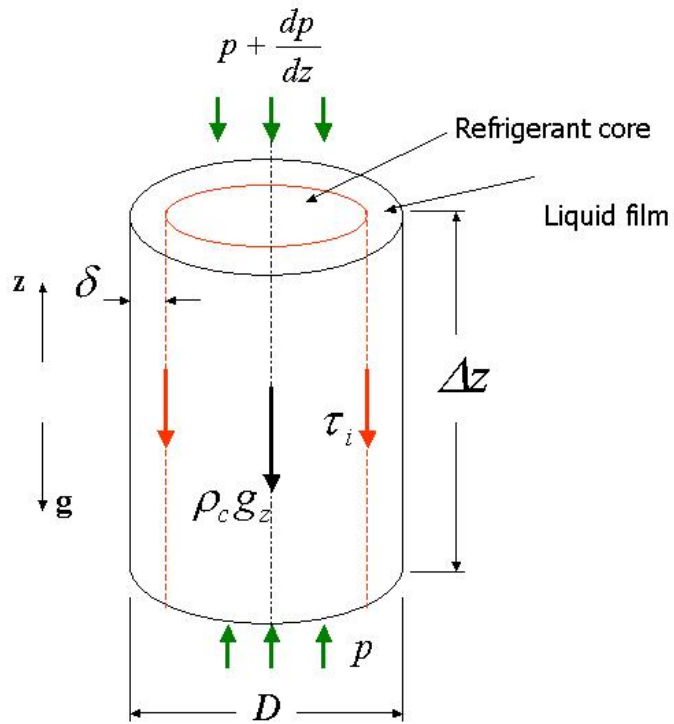
Figure 7.1: Force Balance on Refrigerant Core in Annular Flow
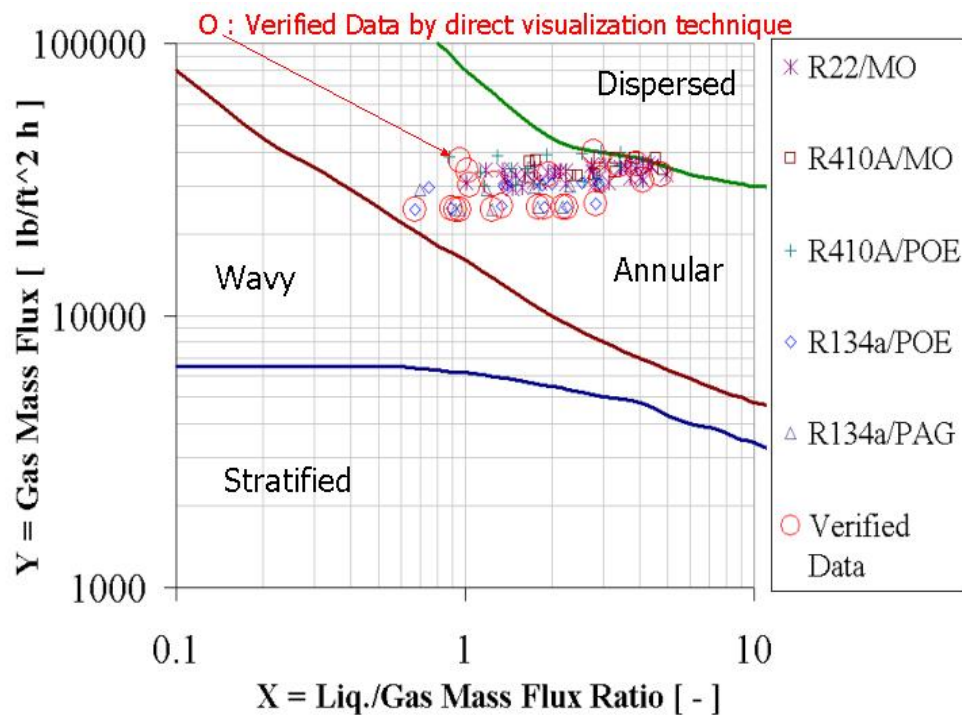
Figure 7.2: Modified Baker's Flow Map for Horizontal Suction Line of Vapor Compression Systems

Re	$= 25 \times 10^4$
G	$= 211$ kg/(m^{2}s)
OMF	$\cong 6$ wt.%
D	$\cong 19$ mm
Type of Flow	Spray-Annular Flow
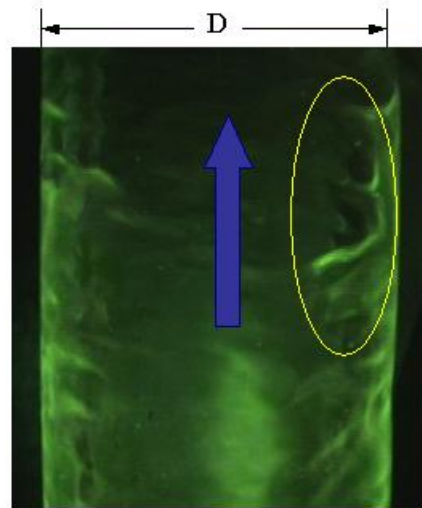
Re	$= 9 \times 10^4$
G	$= 63$ kg/(m^{2}s)
OMF	$\cong 4$ wt.%
D	$\cong 19$ mm
Type of Flow	Annular-Wavy Flow

Figure 7.3: R22/MO Mixture Annular Flow in Vertical Suction Line
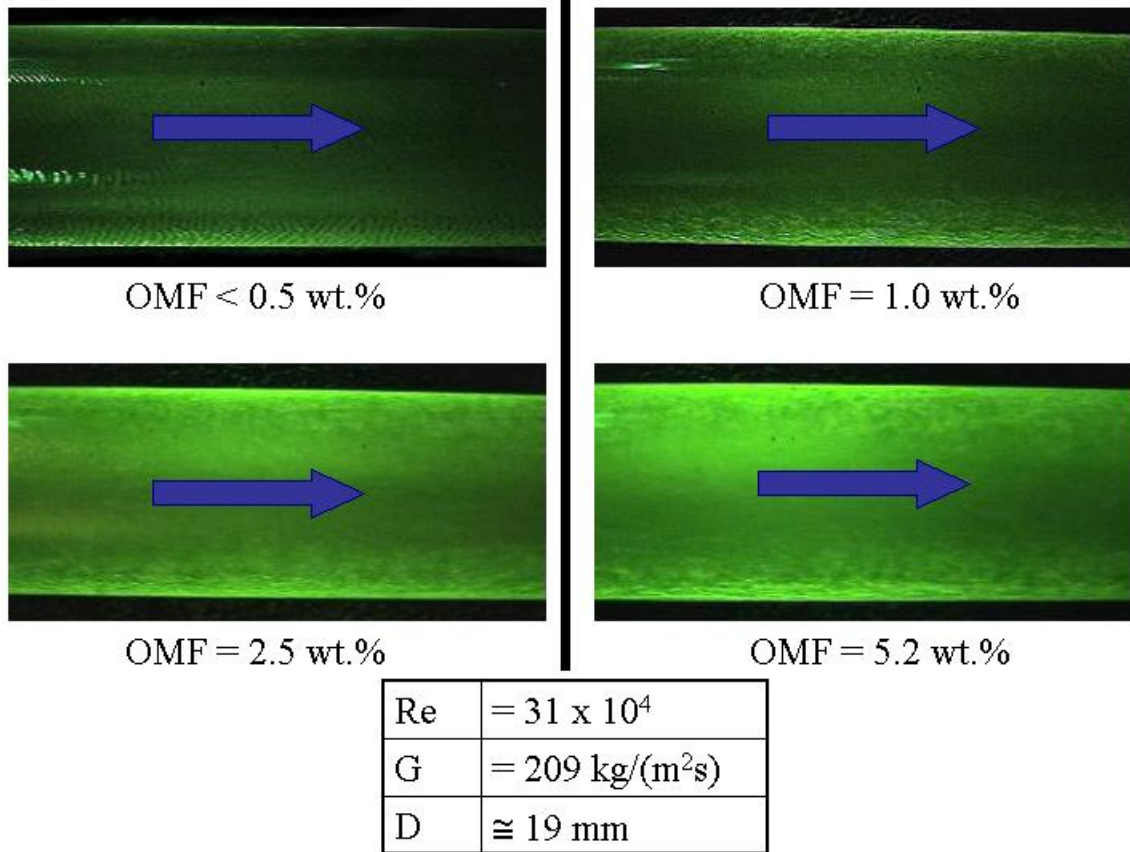
Figure 7.4: R410A-POE Mixture Annular Flow in Horizontal Suction Line

R134a/POE
OMF = 1.0 wt.%

Re	$= 17 \times 10^4$
G	$= 106 \ kg/(m^2s)$
D	$\cong 19 \ mm$

Similar Pressure (~320 kPa)
and SH~20°C for both mixtures
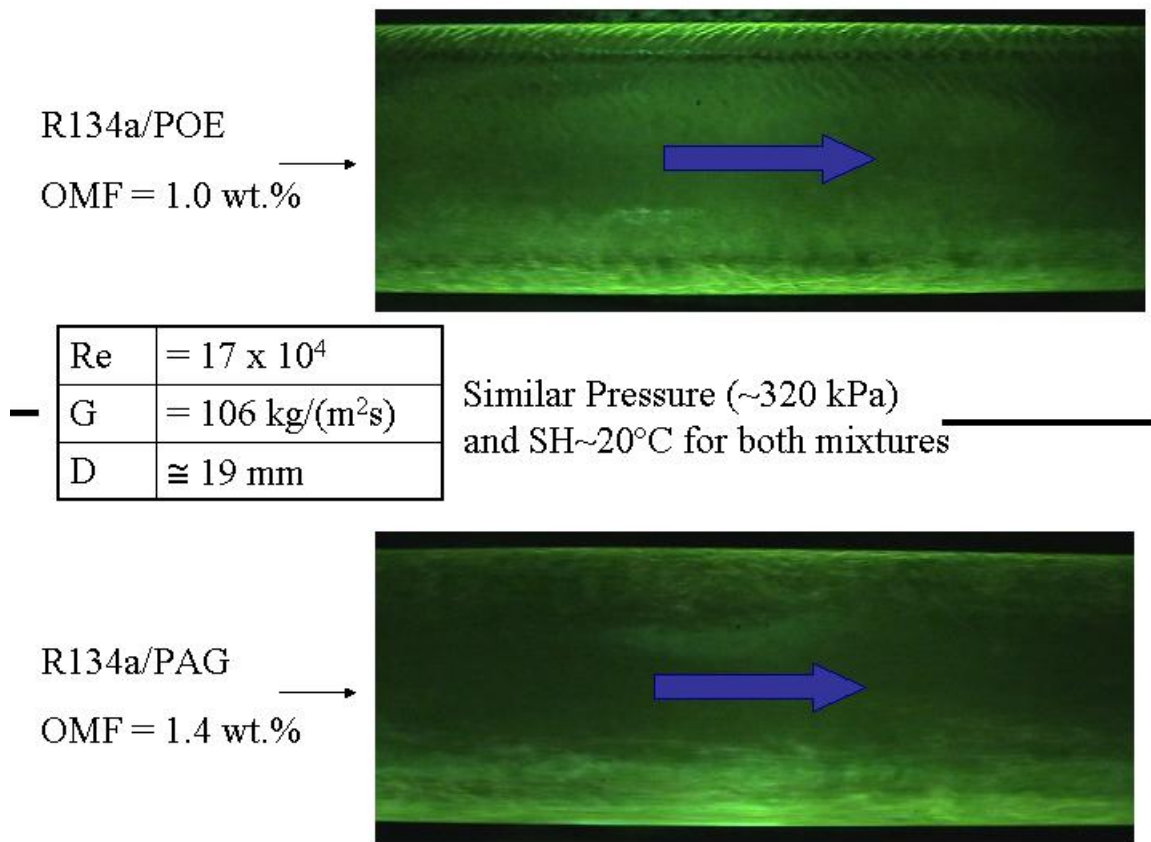
R134a/PAG
OMF = 1.4 wt.%

Figure 7.5: R134a-POE and R134a-PAG Mixture Annular Flows in Horizontal Suction Line
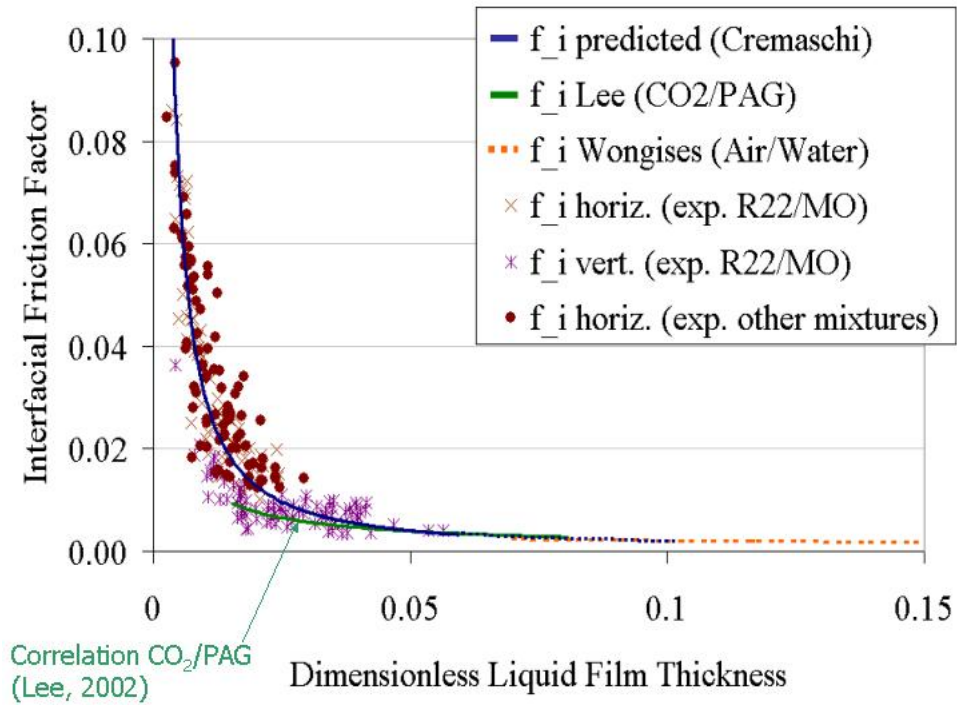
Figure 7.6: Interfacial Friction Factor versus Dimensionless Liquid Film Thickness in the Suction Line
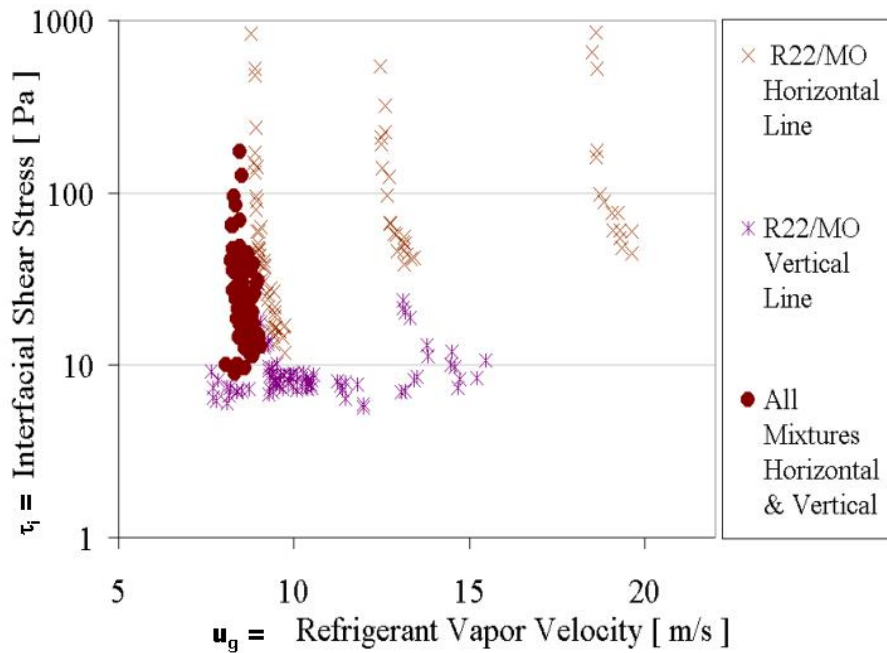
Figure 7.7:Interfacial Shear Stress versus Refrigerant Vapor Velocity
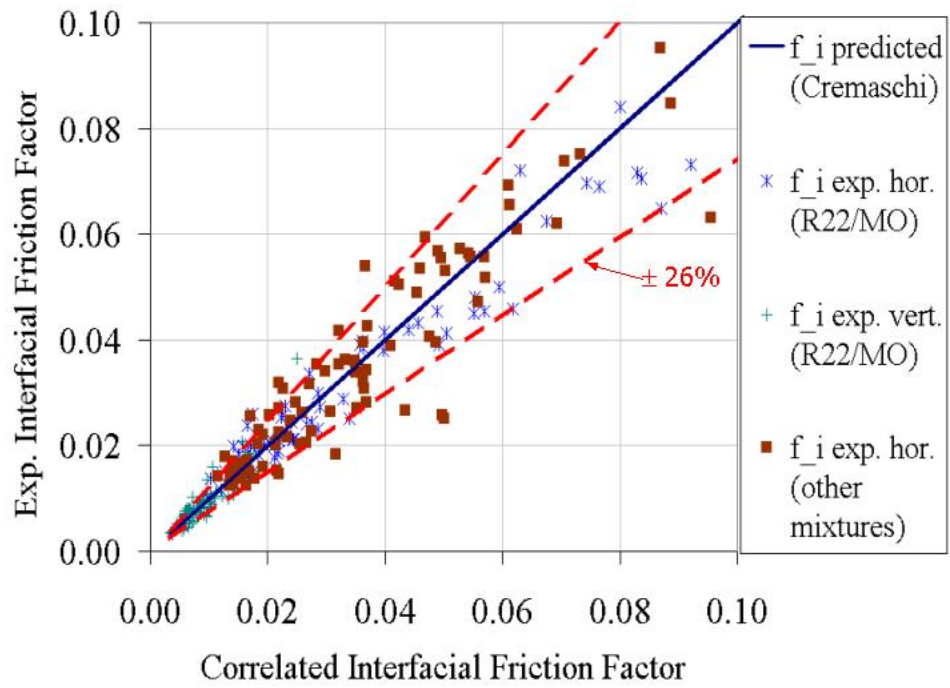
Figure 7.8: Experimental versus Correlated Interfacial Friction Factor in the Suction Line

$$f_i = 4.686 \times 10^{-2} \cdot Re_g^{-0.335} \cdot \left(\frac{\delta}{D}\right)^{-1.056} \cdot We_m^{-0.255}$$
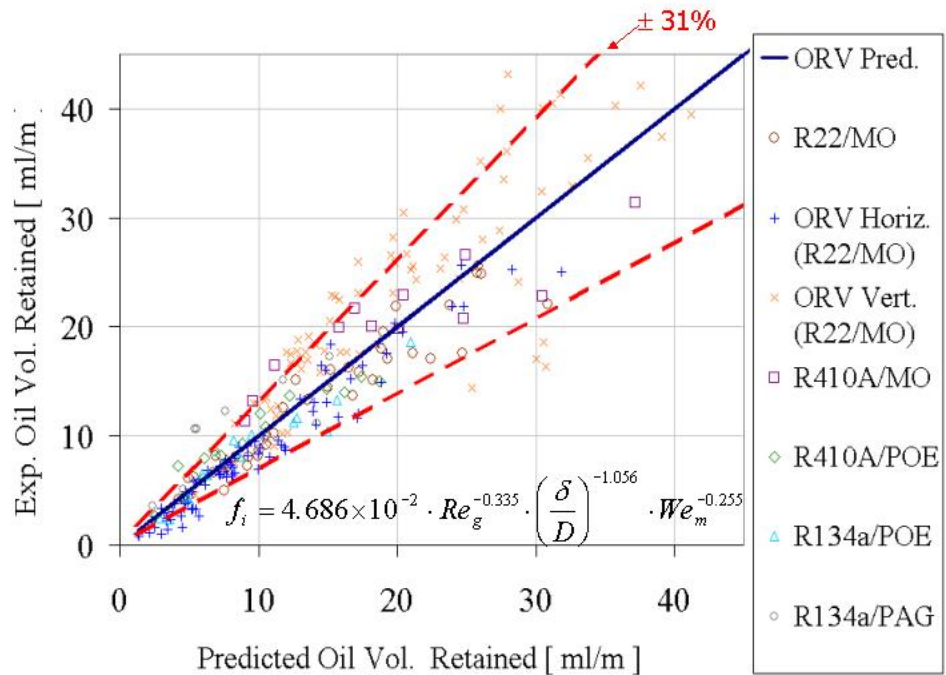
Figure 7.9: Experimental versus Predicted Oil Volume Retained per Unit Length of Suction Line

147

Chapter 8: Modeling of Oil Retention in the Evaporator, Condenser and Liquid Line of a Vapor Compression System

The objective of this section is to analyze the characteristics of the oil retention if phase change processes take place. Significant progress has been made in studies on the influence of lubricants on heat transfer and pressure drop. A critical summary of the influence of oil on refrigerant heat transfer and pressure drop was given recently by Shen and Groll (2003, [98]). They described one possible approach for evaluating the proprieties of liquid refrigerant and oil mixtures, summarized the most common heat transfer correlations used during evaporation and condensation processes, and proposed pressure drop correlations depending on oil mass fraction in the mixture. Their work represents a valuable and systematic literature review about refrigerant and oil mixture characteristics commonly used in air conditioning and refrigeration systems. Thome, who was one of the pioneers in this area, proposed a comprehensive thermodynamic approach to modeling the behavior of refrigerant and oil mixtures (1995,[110]). His theoretical and experimental investigations provided useful insights about the physics involved in the evaporation of a mixture. In the current research work, the model proposed by Thome and various semi-empirical correlations suggested by Shen and Groll were integrated in a software engineering tool (CoilDesigner) usually used for designing heat exchangers. For this thesis the software was updated by including the effects of the oil on the heat transfer and pressure drop in the heat exchanger, and oil retention was estimated. The simulation results were verified with the experimental data of the current work. The design tool was

148

originally developed by Jiang (2003, [57]) and the graphic interface is shown in Figure 8.1. The evaporator consisted of 5 parallel passes with a total of 72 tubes. The length of each tube was about 0.5 m and the inner diameter was 7.8 mm. The fin geometry and refrigerant circuitry of the evaporator were given as input to the software so the local proprieties could be computed accordingly. In the Figure 8.1, the first two refrigerant passes in the top part of the evaporator are shown. They consist of a certain number of tubes connected in series, which varies from one pass to the other. The air flow is from the left to the right. The number of segments for each tube was 10.

The presence of oil during the phase change process changed the thermodynamics of the evaporation and condensation. Refrigerant and oil is a binary mixture that obeys the rules of phase equilibrium. It can be considered as a zeotropric binary mixture where one component is the refrigerant and the second component is the oil, over the range that these fluids are miscible. During the evaporation process, the temperature moves along the bubble point line while condensing processes move along the mixture dew point line. The temperature-concentration phase diagram is the main reference if the enthalpy, temperature, and oil mass fraction of the binary mixture need to be calculated. This approach is extensively described in the Thome's work (1995,[110]) and is summarized next. At the same time, the pressure drop correlations and heat transfer correlations were modified according to the recommendations that Shen and Groll proposed. Their work analyzes the feasibility of these correlations and suggested different void fraction models that can be employed for computing the oil retention.

By using Jian's software, called "CoilDesigner," the actual evaporator used during the experiments was modeled and verified. The model in CoilDesigner was first verified without taking into account oil influence. Simulation results and experimental data obtained in oil-free operating conditions were in agreement for all refrigerants tested, i.e., R22, R410A, and R134a. The geometry of the evaporator, the circuitry of the heat exchanger, and the air inlet conditions were the input of the model. The program can run in two modes: fast solver and general solver. In the fast solver mode, the inlet pressure, inlet refrigerant quality and the mass flow rate of each pass needs to be specified while, in the general solver mode, the program required inlet conditions and outlet pressure. The outputs of the CoilDesigner software were cooling capacity, air and refrigerant outlet conditions, and the pressure drops across the heat exchanger in fast solver mode or mass flow rate in each pass of the heat exchanger in general solver mode. The average relative error between simulation and experimental data were calculated as

$$\varepsilon \ [\%] = \frac{1}{N} \sum \frac{\left|Calculated \ Value - Measured \ Value\right|}{Measured \ Value} \cdot 100$$

where $N=14$, which is the number of samples that have been tested in oil-free conditions. The relative error for the cooling load was about 9% and simulations predicted air and refrigerant outlet temperatures within 2 K. Refrigerant pressure drop across the heat exchanger was estimated within 22% relative error with respect to the experimental data. By using the software in general solving mode, it was possible to estimate the mal-distribution of the refrigerant flow rate between the passes of the evaporator due to varying circuitry at each pass. Refrigerant flow rate in each pass changed less than 2% with respect to the average flow rate. Consequently, the refrigerant flow rate in each pass

was assumed to be the average flow rate of the evaporator divided by 5 (which is the number of the passes), and the software was used in the fast solver mode.

Once the model was verified at oil-free operating conditions, i.e. at OMF= 0 wt.%, then the model that accounts for oil effects on the heat transfer coefficient and pressure drops was implemented in the software. During this step, the cooperation mainly through private communication with Robert Andrew Schwentker, who works as research assistant in the software development division of CEEE at the University of Maryland, was useful and essential for achieving the new program (Jiang, 2002 [58]). The model that describes oil retention characteristics in the evaporator is summarized in the next section.

8.1 Oil Retention in the Evaporator of a Vapor Compression System

The thermodynamic approach is used to describe the behavior of refrigerant and oil mixtures in the evaporator. This method considers the effects of oil on the boiling temperature, specific heat, enthalpies, and pressure drop; it will be described next in the same order that it was implemented in the CoilDesigner software.

8.1.1 Local Oil mass fraction and Mixture Quality

From a design point of view, pressure and temperature at the expansion valve inlet determined the inlet conditions for the evaporator. The liquid phase concentration of oil circulating in a refrigeration system is a function of its location in the system. Thus, to

unequivocally define this concentration, a point is chosen where all the circulating fluid is in the liquid phase, which occurs in the refrigerant line between the condenser and the expansion device. The oil mass fraction at this location is defined as the absolute oil mass fraction ω_0 :

$$\omega_0 [\,wt.] = \frac{\dot{m}_{oil}}{\dot{m}_{oil} + \dot{m}_{ref}} = \frac{OMF\,[\,wt.\%]}{100} \tag{8.1}$$

After the expansion device, the local vapor quality will range from 0.10 to 0.30 and oil mass fraction in the liquid phase will have increased. Along the evaporator, oil mass fraction continues to rise as the refrigerant evaporates into the vapor phase. The local mixture quality (x_{mix}) is defined by the mass of refrigerant vapor divided by the total mass of fluid:

$$x_{mix} = \frac{\dot{m}_{ref,gas}}{\dot{m}_{ref,gas} + \dot{m}_{ref,liq} + \dot{m}_{oil}} \tag{8.2}$$

where $\dot{m}_{ref,gas}$ = mass flow rate of refrigerant vapor;

$\qquad \dot{m}_{ref,liq}$ = mass flow rate of liquid refrigerant;

$\qquad \dot{m}_{oil}$ = mass flow rate of pure oil.

The vapor pressure of oil is negligible in comparison to that of refrigerants. Consequently, the lubricants can be assumed to have no effects on the mixture vapor pressure (Shen and Groll, 2003 [98]). From the conservation of mass of the two components, and assuming no oil enters the vapor phase, the following expression relates local oil mass fraction ω_{local} to local vapor quality x_{mix} and inlet oil mass fraction ω_0:

$$\omega_{local} = \frac{\omega_0}{1 - x_{mix}} \qquad (8.3)$$

Equation (8.3) is based on steady state flow of the mixture through the system, i.e., no local oil holdup in the heat-transfer tubes. Since the oil is assumed non-volatile, the maximum exit vapor quality that can be achieved in the evaporator is

$$x_{mix,max} = \frac{\dot{m}_{ref,gas}}{\dot{m}_{ref,gas} + \dot{m}_{oil}} = 1 - \omega_0 \le 1.$$

If the refrigerant and oil mixture reached $x_{mix,max}$ then the heating fluid can increase the mixture temperature without increasing the mixture quality, as occurs in single phase heat transfer processes. Even though the mixture quality is less than 1, this situation is referred to as superheating of refrigerant because all liquid refrigerant has been evaporated and superheated. Moreover, according the exit pressures and temperatures, a minimum amount of refrigerant remains dissolved in the oil and does not participate in the evaporation process.

8.1.2 Oil and Liquid Refrigerant Proprieties Estimation

An important step in modeling the evaporation process in air conditioning systems is to determine the proprieties of oil and liquid refrigerant mixtures. An entire research area in air conditioning and refrigeration industry focused on mixture proprieties estimation and abundant literature can be found. In the current research work, proprieties of pure oil were obtained from manufacturer data. The liquid mixture proprieties were computed

according to the general thermodynamic approach proposed by Shen and Groll (2003, [98]) and are summarized next.

Liquid mixture density ρ_{mi}.

The mixture density is given by Jensen and Jackman (1984, [56]):

$$\frac{1}{\rho_{mix}} = \frac{\omega_{local}}{\rho_{oil}} + \frac{1-\omega_0}{\rho_{ref,liq}} \quad [\text{kg/m}^3] \tag{8.4}$$

Liquid mixture dynamic viscosity μ_{mi}.

The mixture viscosity is given by Yokozeki (1994, [119]) as

$$ln\,\mu_{mix} = \xi_{ref}\,ln\,\mu_{ref} + \xi_{oil}\,ln\,\mu_{oil} \quad [\text{Pa s}] \tag{8.5}$$

where the Yokozeki factor $\xi_i = \dfrac{W_i^k \psi_i}{\sum_j W_j^k \psi_j}$ is the modified component mole fraction. ψ_i

and W_i are the mole fraction and molecular mass of the component i, respectively. k is a constant specific to a particular mixture. The authors recommended k=0.58 for universal use. The mole fraction of the lubricant in the liquid phase can be obtained from

$$\psi_{oil} = \frac{\omega_{local}\left(\dfrac{W_{ref}}{W_{oil}}\right)_i}{1-\omega_{local} + \omega_{local}\left(\dfrac{W_{ref}}{W_{oil}}\right)}$$

Liquid mixture Surface Tension σ_{mi}.

The mixture surface tension is given by Jensen and Jackman (1984, [56]):

$$\sigma_{mix} = \sigma_{ref,liq} + (\sigma_{oil} - \sigma_{ref,liq})\sqrt{\omega_0} \qquad [\text{ N/m }] \tag{8.6}$$

Liquid mixture Conductivity factor k_{mi}.

The mixture conductance is given by Flilippov and Novoselova (1955):

$$k_{mix} = k_{ref,liq}(1 - \omega_{local}) + k_{oil}\omega_{local} - 0.72(k_{ref,liq} - k_{oil})(1 - \omega_{local})\omega_{local} \tag{8.7}$$

Liquid specific heats of pure lubricating oil $c_{p,oil}$, and refrigerant-oil mixtures $c_{p,mix}$.

The following equation for lubricating oils were recommended by Thome (1995, [110]) as a function of the specific gravity s_g [N/m³] ($s_g = \rho_{oil}/\rho_{water}$) of the oil at 15.6 ºC:

$$c_{p,oil}\left[\frac{kJ}{kg \cdot K}\right] = 4.186 \frac{0.338 + 0.00045 \cdot (1.8 \cdot T[°C] + 32)}{\sqrt{s_g}} \tag{8.8}$$

where equation (8.8) is valid for $-18ºC < T < 204ºC$.

A linear mixing law based on mass fractions of oil gives the liquid specific heats of the mixture as:

$$c_{p,mix} = \omega_{local} c_{p,oil} + (1 - \omega_{local}) c_{p,liq,ref} \tag{8.9}$$

Gas-Phase and Liquid -Phase Reynolds Numbers (Re_g, Re_l).

The Reynolds numbers of the gas-phase and liquid mixture phases are given by

155

$$Re_g = \frac{G_{tot} \cdot x_{mix} \cdot D_h}{\mu_{ref,gas}} \qquad \text{and} \qquad Re_{liq} = \frac{G_{tot} \cdot (1 - x_{mix}) \cdot D_h}{\mu_{mix,liq}} \tag{8.10}$$

Martinelli parameter of the refrigerant-oil mixture(X_{tt}).

The Martinelli parameter of the refrigerant-oil mixture is given by

$$X_{tt} = \left(\frac{1 - x_{mix}}{x_{mix}} \right)^{0.9} \cdot \left(\frac{\rho_{ref,gas}}{\rho_{mix,liq}} \right)^{0.5} \cdot \left(\frac{\mu_{mix,liq}}{\mu_{ref,gas}} \right)^{0.1} \tag{8.11}$$

where x_{mix} is the mixture vapor quality. The definition (8.11) is valid for turbulent two-phase flow in smooth pipes.

8.1.3   Bubble Temperature and Heat Release Enthalpy Curve

An empirical vapor pressure equation for predicting the bubble point temperature for a given saturation pressure and oil mass fraction was first presented by Takaishi and Oguchi (1987) and later verified by Thome (1995, [110]) for different refrigerant and oil pairs. If P_{sat} is the saturation pressure in MPa, and T_{bub} is the bubble point temperature in K, the relation is given by (8.12):

$$T_{bub} = \frac{A(\omega_{local})}{\ln P_{local} - B(\omega_{local})} \tag{8.12}$$

where ω_{local} is the local oil mass fraction in the liquid, P_{local} is the local pressure in each segment of the tube, and $A(\omega_{local})$ and $B(\omega_{local})$ are given by the following expressions:

$$A(\omega_{local}) = a_0 + a_1 \omega_{local} + a_2 \omega_{local}^3 + a_3 \omega_{local}^5 + a_4 \omega_{local}^7$$

$$B(\omega_{local}) = b_0 + b_1\omega_{local} + b_2\omega_{local}^3 + b_3\omega_{local}^5 + b_4\omega_{local}^7.$$

Because the vapor pressure of the lubricant is negligible, there is no big difference in the lubricant partial pressure from different refrigerant-lubricant pairs. Consequently, Thome recommended correlating a_0 and b_0 with the specific pure refrigerant while keeping other constants unchanged. The values of the other empirical constants are:

$a_1 = 182.52$; $a_2 = -724.21$; $a_3 = 3868.0$; $a_4 = -5268.9$;

$b_1 = -0.72212$; $b_2 = 2.3914$; $b_3 = -13.779$; $b_4 = 17.066$;

The constants a_0 and b_0 depend on the specific refrigerant and saturation pressure. They were computed as follows:

- the inlet pressure of each segment of the evaporator was set at P_{local}.

- two saturation temperatures just above and below P_{local} were determined using an accurate equation-of-state relation for the pure refrigerant vapor pressure curve.

- The two sets of values for T_{bub} and P_{local} were set in the equation (8.12) with ω_{local} set to zero.

- The system of two equations in two unknowns (a_0 and b_0) was solved. All other values of a_1 and a_4 and b_1 and b_4 remain the same as in the original correlation since they only refer to the effect of oil on T_{bub} (Thome, 1995).

The local change in enthalpy dh of a mixture during the evaporation consists of three contributions as quoted by Thome:

1. Latent heat to the fraction of the liquid vaporized (dx_{mix});

2. Sensible heat to the fraction of fluid in the liquid phase ($1-x_{mix}$) heated to a higher bubble point temperature;

3. Sensible heat to the fraction of fluid in the vapor phase (x_{mix}) heated to a higher

    bubble point temperature.

Thus, *dh* can be written as follows:

$$dh = h_{LV} \cdot dx_{mix} + (1 - x_{mix}) \cdot c_{p,mix} \cdot dT_{bub} + x_{mix} \cdot c_{p,ref,vapor} \cdot dT_{bub} \qquad (8.13)$$

where h_{LV} = latent heat of vaporization of the refrigerant;

$c_{p,mix}$ = specific heat of the liquid refrigerant-oil mixture;

$c_{p,ref,vapor}$ = specific heat of the pure refrigerant vapor;

dT_{bub} = increase of bubble temperature of the refrigerant-oil mixture;

The values of $c_{p,mix}$ and $c_{p,ref,vapor}$ are functions of the local oil mass fraction and bubble

point temperature while h_{LV} is a function of local pressure. The equation (8.13) neglects

the mixing heats, which are normally small and typically not available for refrigerant-oil

mixtures. The above equation is called heat release enthalpy curve and it reduces to the

latent heat of vaporization for a pure refrigerant.

8.1.4   Heat Transfer Correlation for Refrigerant-Oil Mixture Flow Boiling

Each tube of the heat exchanger was divided into a certain number of segments and

local heat-transfer coefficients were determined for each segment individually. In each

segment, a mean overall heat-transfer coefficient was determined for the evaporating

fluid and the heat source fluid. In the software tool developed by Jiang, the overall heat

transfer coefficient in each segment is given by the equation (8.14):

$$\frac{1}{UA} = \frac{1}{h_{ref} A_{t,in}} + \frac{(D_{out} - D_{in})}{k(A_{t,in} + A_{t,out})} + \frac{R_c}{A_{t,out}} + \frac{R_f}{A_{t,out}} + \frac{1}{h_{air} A_{t,total} \eta_0} \tag{8.14}$$

where U = overall heat transfer coefficient

A = whole segment area

h_{ref} = convective heat transfer coefficients of the refrigerant side

h_{air} = convective heat transfer coefficient of the air side

$A_{t,in}$ = Inner area of the tube ; D_{in} = inner diameter of the tube;

$A_{t,out}$ = Outer area of the tube; D_{out} = outer diameter of the tube;

R_c = Contact resistance of the tube and fin heat exchanger

R_f = Fouling resistance

η_0 = Fins Heat Transfer Efficiency

By setting the heat exchanger dimensions, materials, and air side conditions, the software tool computed the local air side heat transfer coefficient, contact and fouling resistance, and conduction resistance. One of the advantages of using Jiang's software tool was represented by the built-in correlations for fin-and-tube heat exchangers, which allowed achieving a more accurate solution. The only term that was modified in equation (8.14) was the local heat transfer coefficient of the refrigerant side. Since two-phase heat transfer and pressure drop correlations are a function of vapor quality in each zone, the local heat transfer for the refrigerant-oil mixture was computed according to equation (8.15):

$$\frac{h_{TP,mix}}{h_L} = c \left[\frac{1}{X} \right]^n \tag{8.15}$$

159

where X is the Lockhart-Martinelli parameter of the refrigerant-oil mixture. h_l is the liquid-phase heat transfer coefficient based on Equation (8.16) using the mixture viscosity:

$$h_L = 0.023 \cdot \left(\frac{k_{ref,liq}}{D_h} \right) \cdot \left[\frac{G_{tot} \cdot (1 - x_{mix}) \cdot D_h}{\mu_{mix,liq}} \right]^{0.8} \cdot \left(\frac{c_{p,ref,liq} \cdot \mu_{mix,liq}}{k_{ref,liq}} \right)^{0.4} \qquad (8.16)$$

where D_h is the inner hydraulic tube diameter, G_{tot} is the total mass flux of the refrigerant-oil mixture, and $k_{ref,liq}$ and $c_{p,ref,liq}$ are the pure refrigerant liquid thermal conductance and specific heat, respectively. The semi-empirical constants c and n are specific to the oil mass fraction as indicated in Table 8.1.

The relation (8.15) was presented by Chaddock and Murther (1980) and it was developed for flow boiling of R22/Suniso 3 GS oil inside a smooth tube. They indicated that this correlation was only applicable when convective heat transfer dominated flow boiling. In their tests, mass flux ranged from 149 to 908.5 kg/(m²s), heat flux ranged from 7.73 to 40.54 kW/m², and vapor quality ranged from 0.0 to 1.0. The heat exchanger had smooth tubes with an inside diameter of 8.8 mm. Shen and Groll (2003, [98]) recommended using the equation (8.15) as a more general heat transfer correlation for refrigerant and oil mixtures instead of using semi-empirical correlations based on pure refrigerant proprieties. Since a well-accepted theory for refrigerant-oil flow boiling has not been obtained, the correlations (8.15) and (8.16) have been applied in the current research work to investigate their accuracy and applicability to different refrigerant-oil pairs. Furthermore, the heat exchanger tubes had integral helical ridges on the inside surface that enhanced the inside heat transfer coefficient due to increased heat transfer surface

area and induced turbulation. The heat transfer surface area was increased according the actual inside geometry and internal hydraulic diameter defined as

$$D_h = 4 \cdot \frac{A_{cross,actual}}{P_{wet}}$$ (8.17)

was used, where $A_{cross,actual}$ is the actual cross section area and P_{wet} is the wetted perimeter. A triangular profile was used to approximate the actual internal ridges profile and the number of internal ridges per millimeter of circumference was approximately 2.1.

8.1.5 Pressure Drop Correlation for Refrigerant-Oil Mixtures during Evaporation Process

The pressure drop in each segment of the tube was computed using the Lockhart-Martinelli (1949,[71]) pressure drop correlation. Shen and Groll (2003,[98]) recommended this correlation in their investigation of lubricant effects on pressure drop in the evaporating and condensing processes. The Lockhart-Marinelli approach is a semi-empirical model that is easy to use in software tools. It does not provide detailed information about two-phase flow inside the pipe but, as long as it is applied to situations similar to those that were used to obtain the original data, it `can be quite satisfactory. The Lockhart-Martinelli model is summarized as follows:

-   Compute the gas-phase frictional pressure drop as $\Delta p_{ref,vap} = \dfrac{f_{ref,vap}}{2} \dfrac{L_{segm}}{D_h} \dfrac{G^2 x_{mix}^2}{\rho_{ref,vap}}$.

- Compute the liquid-phase frictional pressure drop as

$$\Delta p_{mix,liq} = \frac{f_{mix,liq}}{2} \frac{L_{segm}}{D_h} \frac{G^2(1-x_{mix})^2}{\rho_{mix.liq}}.$$

where the single phase frictional factor is determined by the characteristic pressure drop coefficients of the grooved heat exchanger tube:

$$f_k = C_1 \cdot Re^{D_1} \tag{8.18}$$

The above relation can be applied for a wide range of Reynolds numbers (both gas and liquid Re inside the heat exchanger tubes). Since the integral helical ridges induced turbulence, it is assumed that equation (8.18) be valid for low Reynolds numbers. This is a reasonable approximation for $Re \geq 50$, while at $Re<50$ the difference in the friction factor f_k given by equation (8.18) and the laminar friction factor ($f_{laminar}=64/Re$) is more than 50%. This error increased as Re tended to 0.1. Depending on the nominal inner diameter, ridges height and number of ridges per unit length, the coefficients C_1 and D_1 are chosen from the manufacturer specifications of the coil. These empirical coefficients provide an estimated frictional pressure drop coefficient for all flow regimes in grooved tubes. For the specific evaporator the coefficients of equation (8.18) were $C_1 = 2.450$ and $D_1 = 0.386$.

- The Lockhart-Martinelli parameter X is defined as in equation (8.19):

$$X^2 = (-\Delta p_{mix,liq})/(-\Delta p_{ref,gas}) \tag{8.19}$$

X^2 gives a measure of the degree to which two-phase mixtures behave as liquids rather than as gasses. For turbulent flow during condensation and for smooth tubes, X collapses

to X_{tt} given by equation (8.11). In the next step, the two-phase multiplier for each phase is found using the following equations:

- For the gas phase : $\phi^2_{ref,vap} = 1 + C \cdot X + X^2$

- For the refrigerant-oil liquid phase : $\phi^2_{mix,liq} = 1 + C / X + X^{-2}$.

   where C is the value corresponding to different liquid and gas flow states as listed in Table 8.2.

- Finally, the two-phase frictional pressure drop is determined by equation (8.20):

$$\Delta P_{Frictional} = Max\left((\Delta p_{ref,vap} \cdot \phi^2_{ref,vap}); (\Delta p_{mix,liq} \cdot \phi^2_{mix,liq}) \right) \qquad (8.20)$$

8.1.6   Oil Retention Volume and Void Fraction Models for the Evaporator

When computing oil retention, the most important variable is the refrigerant vapor over the total mixture void fraction α in each segment of the heat exchanger tube. The void fraction α at a given cross section is defined as the ratio of the area occupied by the vapor phase $A_{ref,vapor}$ to the total area available to the mixture. The latter can be the nominal inner cross section area $A_{cross,nominal}$ for smooth tubes, or the actual cross section area $A_{cross,actual}$ for tube with internal ridges. Thus, the definition of α is

$$\alpha = \frac{A_{ref,vapor}}{A_{cross,actual}}$$

and, for the specific evaporator, the estimated geometric ratio of the actual over the nominal inner cross section area was

$$\alpha_{actual} = \frac{A_{cross,actual}}{A_{cross,no\,min\,al}} \cong 0.95$$

Since the liquid fraction in each segment is simply obtained by (1-α), the oil retention

mass in each segment can be computed according equation (8.21):

$$ORM_{segment}\,[\,kg\,] = \omega_{local} \cdot V_{segment} \cdot (1-\alpha) \cdot \rho_{mix,liq} \qquad (8.21)$$

where $V_{segment}$ is the actual internal volume of each segment. Because mass is conserved,

the oil retention mass in the whole evaporator is simply the summation of oil retention in

each segment of the heat exchanger:

$$ORM_{tot}\,[\,kg\,] = \sum_{tube} \left(\sum_{segment} (ORM_{segment}) \right) \qquad (8.22)$$

The oil retention volume (OR) in the entire heat exchanger was obtained by dividing the

ORM_{tot} by the average oil density in the evaporator.

Empirical models for the void fraction can be found in the literature. In the current work,

four methods have been used and compared with the experimental data: Martinelli's void

fraction model for smooth tubes, Lockhart-Martinelli's correlated model (1949,[71]), the

void fraction model of Premoli *et. al* (1971,[90]), and Chisholm's (1972,[25]) void

fraction model. These correlations were recommended by several authors in the most

recent literature as the best methods for computing the void fraction during evaporation

and condensation processes (Lee, 2003, and Shen and Groll, 2003).

Martinelli's Parameter Correlated Void Fraction Model for Smooth Tubes

Martinelli's empirical void fraction $\alpha_{Martinelli}$ is a function of the Martinelli parameter defined by the equation (8.11). It is the simplest possible model for separate two-phase flow but it only applied to turbulent flow during condensation in smooth tubes. It is reported here only for comparison with other more sophisticated models, which will be described below. When comparing with experimental results, the Martinelli parameter (8.11) led to an inaccurate refrigerant vapor void fraction and oil retention was lower than the experimental one. This was due to the presence of internal grooves in the heat exchanger tubes. Furthermore, it does not account for the effect of the oil surface tension on liquid film thickness or the reduction of oil retention due to refrigerant mass flux increase.

Lockhart-Martinelli Parameter Correlated Void Fraction Model

Lockhart-Martinelli's empirical void fraction $\alpha_{Lock\text{-}Mart}$ is a function of the Lockhart-Martinelli parameter according the equation (8.23)

$$\alpha_{Lock-Mart} = \left(1 + X^{0.8}\right)^{-0.378} \tag{8.23}$$

where X is the parameter given by equation (8.19). This model is quite general and oil and liquid refrigerant mixture properties are used instead of pure liquid refrigerant's ones to describe the liquid phase (Shen and Groll, 2003 [98]). To accurately estimate the Lockhart-Martinelli parameter X for grooved tubes, the frictional pressure drop coefficients C_l and D_l in equation (8.18) must properly describe the pressure drop characteristics of the actual geometry of the tube.

Premoli's Correlated Void Fraction Model

Premoli *et. al* (1971) developed an empirical correlation for the void fraction in two-phase vapor and liquid refrigerant flow. When considering refrigerant and oil, mixture proprieties are used in Premoli's model to describe the liquid phase, while refrigerant vapor proprieties are used for the gas phase. The revised Premoli void fraction model calculates the void fraction $\alpha_{Premoli}$ from the slip ratio S of the refrigerant-oil mixture, which is defined by the equation (8.24):

$$S = \frac{\mathrm{v}_{ref,vapor}}{\mathrm{v}_{mix,liq}} = \left(\frac{\rho_{mix,liq} \cdot x_{mix} \cdot (1 - \alpha_{Pr\,emoli})}{\rho_{ref,gas} \cdot (1 - x_{mix}) \cdot \alpha_{Pr\,emoli}} \right) \tag{8.24}$$

The correlation of Premoli et al. (1970), usually know as the CISE correlation, covers a reasonably wide range of data and takes account of the mass flux effects (Hetsroni, 1982 [45]). The main steps of the Premoli empirical correlations are described next.

- Compute the mixture Reynolds and Weber numbers as

$$Re_{mix} = \frac{G_{tot} \cdot D_h}{\mu_{mix,liq}} \quad \text{and} \quad We_{mix} = \frac{G_{tot}^2 \cdot D_h}{\sigma_{mix,liq} \cdot \rho_{mix,liq}} .$$

- Calculate the empirical parameters B_1 and B_2 as

$$B_1 = 1.578 \cdot Re_{mix}^{-0.19} \cdot \left(\frac{\rho_{mix,liq}}{\rho_{ref,vap}} \right)^{0.22} \quad \text{and} \quad B_2 = 0.0273 \cdot We_{mix} \cdot Re_{mix}^{-0.51} \cdot \left(\frac{\rho_{mix,liq}}{\rho_{ref,vap}} \right)^{-0.08} .$$

- Define the vapor to the total volume flow ratio β, which is given by

$$\beta = \frac{\dot{Q}_G}{\dot{Q}_L + \dot{Q}_G} = \frac{\rho_{mix,liq} \cdot x_{mix}}{\rho_{mix,liq} \cdot x_{mix} + (1 - x_{mix}) \cdot \rho_{ref,vap}} .$$

- Obtain the vapor over the liquid volume flow ratio y, which is given by

$$y = \frac{\beta}{1-\beta} .$$

- Finally the refrigerant vapor to the liquid mixture slip ratio S can be correlated according the following expression:

$$S = 1 + B_1 \left[\frac{y}{1+yB_2} - yB_2 \right]^{\frac{1}{2}} .$$

The revised Premoli void fraction model includes the mixture viscosity and surface tension effects on the gas core void fraction. As long as it is applied to situations similar to those that were used to obtain the original data, it can provide very accurate results. It was verified in previous research works for only completely miscible mixtures and for phase-change processes in smooth tubes. For immiscible refrigerant-oil pair, such as R410A/MO, the local viscosity and surface tension near the wall are higher than the bulk average values in the film. Thus, in case of R410A/MO, taking the values for pure oil in the definition of Re_{mix} and We_{mix}, augmented the liquid film viscosity and surface tension and yielded to lower void fraction. This correction caused an improvement of the simulation accuracy for R410A/MO mixture.

Finally, if the slip ratio is known, the void fraction α can be computed according equation (8.25):

$$\alpha = \left[1 + S \cdot \frac{(1-x_{mix})}{x_{mix}} \cdot \frac{\rho_{ref,vap}}{\rho_{mix,liq}} \right]^{-1} \tag{8.25}$$

Chisholm's Correlated Void Fraction Model

Chisholm (1972) suggested a different semi-empirical correlation for the slip ratio S based on mixture quality and density ratio:

$$S = \left[1 - x_{mix} \cdot \left(1 - \frac{\rho_{mix,liq}}{\rho_{ref,vap}} \right) \right]^{\frac{1}{2}} \tag{8.26}$$

He used this correlation to describe two-phase flow during evaporation and condensation. In his work, the Lockhart-Martinelli approach was employed and then the model was corrected by using the slip ratio correlation. From this point of view, Chisholm's void fraction model can be interpreted as a revised Lockhart-Martinelli void fraction model. The Chisholm void fraction $\alpha_{Chisholm}$ was also computed according to the equation (8.25).

Turner and Wallis Correlated Void Fraction Model

Turner and Wallis (1965) have suggested a correlated void fraction model using a modification of the Armand type relationship to take account of entrainment. In this correlation, the single-phase pressure drop for the total liquid flow is replaced by the single-phase pressured drop for that part of the liquid flow which is in the liquid film:

$$\phi^2_{mix,liq} = \frac{(dp/dz)}{(dp/dz)_{mix,liq}} = \frac{1}{(1-\alpha)^2_{mix,liq}} \tag{8.27}$$

where $\phi^2_{mix,liq}$ is the liquid phase multiplier defined in the previous section about pressure drop correlation. The correlation (8.27) was recommended by Hewitt and Hall-Taylor (1970, [46]) and they concluded that moderately good agreement was observed when they compared the predicted film thickness with experimental data.

8.1.7   Flow Patterns in the Evaporator

Flow patterns in the evaporator are quite different from those observed in the suction line. Based on liquid and vapor thermodynamic proprieties, mixture vapor quality and local oil mass fraction, the flow pattern inside each tube of the evaporator can be stratified, wavy-stratified, or annular. At low qualities, flow patterns are generally stratified ($x<0.2$) but when vapor quality is higher than 0.5, flow patterns are annular. Manwell and Bergles (1990,[76]) developed flow pattern maps for refrigerant-oil mixtures. The tested refrigerant was R12 while the oil was 300 SUS naphthenic mineral oil. Mass flux ranged from 45 to 430 kg/(m^{2}s) and oil mass fraction varied from 0 to 10 wt.%. Shen and Groll (2003,[98]) studied the effect of lubricants on flow pattern transition. They concluded that the presence of oil in the refrigerant promoted the early formation of annular flow. Oil increases the volume and surface tension of the liquid mixture inside the segment and raises the wetted surface, as schematically shown in Figure 8.2. The onset of dryout depends on the internal geometry of the pipe. For micro-fin tubes, the swirling effect of micro-fins hindered the onset of dryout with respect to the smooth tubes. They also studied the potential enhancement of heat transfer at low oil mass fractions due to foaming, increased wetted surface, and enhanced nucleate boiling. In this research work, some experimental observations of the flow patterns inside the evaporator tubes were made in order to confirm the flow pattern maps presented in the existing literature. The mixture consisted of R22 with mineral oil and the inner tube

diameter was about 8.7 mm. The test section was provided with an electrical heater positioned just before the sight glass, and both the vapor quality and oil mass fraction were varied. Figure 8.3 shows the flow patterns when the refrigerant vapor quality varied from 0.15 to 0.21. If the OMF=0 wt.%, the flow was stratified with some sporadic waves moving along the vapor-liquid interface. The oil mass fraction was increased from 1 wt.% to 5 wt.%. The difference in the observed flow pattern was appreciable only if the OMF was equal to or greater than 5 wt.%. By increasing the OMF, the liquid mixture flow became more and more wavy. At qualities between 0.3 and 0.4, the flow type is in the transition region from stratified-wavy to annular as shown in Figure 8.4. Indeed, oil promoted annular flow and the observations from the current work verified Shell's conclusions. At qualities greater than 0.5, the flow type was annular and the oil increased the liquid film thickness. This effect was observed qualitatively by an increase in the intensity of the reflecting light during flow visualization tests. However, quantitative measurements of liquid film thickness and wetted surface angle were not performed. Values for refrigerant mass flux, heat mass flux, geometry, and oil mass fractions were similar to those of the work presented by Shen and Groll. Thus, their correlations and flow maps were applied to the models of the current work. Further verifications of their results are recommended in future developments of this research work.

8.1.8 Simulation Results for the Evaporator

Figure 8.5 shows oil retention modeling at each segment in the evaporator. From the inlet conditions, the local oil mass fraction ω_{local} is computed first. Thus, the local properties of the mixture, the Lockhart-Martinelli parameter X, the local two-phase heat transfer coefficient of the mixture $h_{TP,mix}$, and the void fraction of the mixture α in each segment were calculated according to the correlations described in the previous sections. The software estimated the local heat transfer coefficient of the air side $h_{air,side}$ so the overall heat transfer coefficient UA of the segment was calculated. The ε-NTU methods predicted the enthalpy difference across the segment while the refrigerant pressure drop was computed using refrigerant-oil correlations. The relation among enthalpy $h_{mix,out}$, quality $x_{mix,out}$, and bubble temperature $T_{bub,out}$ of the mixture is determined by the heat release enthalpy curve defined by Equation (8.13), and oil retention in the segment $ORM_{segment}$ was estimated using various void fraction models. Figure 8.6 shows an example of the calculated air temperature and mixture bubble temperature profiles versus dimensionless length of the heat exchanger. The temperature is given on the y-axis while the x-axis gives the evaporator dimensionless length. The refrigerant/oil mixture was R134a/PAG and the inlet saturated pressure of the evaporator was about 465 kPa. The inlet refrigerant quality was $x_{ref} = 0.06$ while the OMF was about 2.4 wt.%. Thus, the inlet mixture vapor quality was slightly less than x_{ref}. In Figure 8.6, vapor quality ranges from $0 < x_{mix} < 0.96$ while the maximum possible quality is $x_{mix,max} = 0.976$ (=1 - OMF). The actual effectiveness of the heat exchanger and the approach temperature were computed by the ε-NTU method existing in the simulation tool. For this specific

171

example, the effectiveness of the heat exchanger was about 95% and the approach temperature was 3 K. The figure shows that the rise in the bubble point temperature limits the fraction of the refrigerant that can actually be evaporated. The pressure drop across the heat exchanger was about 14 kPa and the predicted mixture outlet temperature was about 16ºC. It should be noted that, if the pressure is assumed constant, the bubble temperature increases with the vapor quality as shown by the bubble temperature line during evaporation without pressure drop in the Figure 8.6. However, if the pressure drop is included in the model the actual evaporation curve is drawn in figure and the bubble temperature first decreases due to lower saturation pressure and it increases at the end of the evaporator. In the specific example, the number of tubes was 14 and the number of segments for each tube was 16. Thus, the total number of segments along the curve was 224. If the number of segments per tube increased up to 30, the bubble temperature profile changed by less than 0.1 K, and computational time doubled. Consequently, a number of segments between 12 and 20 for each tube represented a good agreement between solution accuracy and computational cost. For a number of segments per tube higher than 12, the sensitivity of the bubble point temperature was equal or less than 0.1 K, the variation of oil retention was less than 0.01 ml/m and the predicted pressure drops across the evaporator did not change.

Figure 8.7 shows the distribution of oil retention and vapor quality with respect to the dimensionless length of the evaporator. The calculated values are for the specific example discussed previously with R134a/PAG at OMF=2.4 wt.%. The oil retention is given on the primary y-axis in dimensionless form, that is, as a ratio between the local oil

retention volume over the maximum oil retention volume in the circuitry (Max OR$_{segm}$≅0.07 ml). The mixture quality is given in the secondary y-axis and the length of the circuitry is measured along the x-axis in dimensionless form. The dimensionless oil retention was about 0.6 at the inlet mixture quality of about x_{mix}=0.06, so almost all the refrigerant was in the liquid phase. Along the heat exchanger the liquid refrigerant started to evaporate, leaving higher percentage of pure oil in the liquid solution. As the local oil mass fraction started to rise, the dimensionless oil retention increased rapidly from 0.4 to 0.8 and reached the maximum value at the evaporator outlet (the dimensionless oil retention at the evaporator outlet is equal to 1). Thus, most of the oil was retained at the end part of the evaporator, where the liquid film viscosity was 2.8 cSt, the highest value in the evaporator. In the graph of Figure 8.7, it should be noted that the local air temperature affected the rate of increase of the mixture quality. The two kinks occurred exactly at the transition between one column and the other in the circuitry, due to a decrease of the air temperature. Moreover, in counter flow configurations, the warmest air entering the heat exchanger increased the mixture quality rate of change in the last tube bank of the refrigerant circuitry.

The oil retention simulation results for the evaporator are showed in Figure 8.8 for all tests conducted. The x-axis gives the predicted oil retention volume from the simulations while the measured oil retention volumes are plotted on the y-axis The continuous curve represents the predicted oil retention volume according Premoli's void fraction model while the data points are the corresponding measured oil retention volumes for all refrigerant-oil mixtures tested. The best model that fit the experimental

data was Premoli's void fraction model. It predicted the oil retention for all refrigerant-oil mixtures quite successfully. The average deviation and standard deviation were computed according to the following equations:

$$\sigma_{avg} = \frac{1}{N} \sum \left(\frac{|OR_{measured} - OR_{calculated}|}{OR_{calculated}} \cdot 100 \right)$$ (8.28)

and

$$\sigma_{s\,tan\,dard} = \left[\frac{n \sum \sigma_{avg}^2 - \left(\sum \sigma_{avg} \right)^2}{n \cdot (n-1)} \right]^{0.5}$$ (8.29)

The average deviation provides the error in the oil retention predicted by CoilDesigner, while the standard deviation is a measure of how widely values are dispersed from the mean value. The approach according to Premoli's void fraction model seems to provide promising results as shown in Figure 8.8. The average deviation was about 21% and the standard deviation was 15%. Moreover, the majority (72%) of the experimental oil retention volumes were predicted within 29% relative error by the model in CoilDesing software. For the highest oil retention volumes, associated with the R410A/MO mixture, if the average bulk liquid film viscosity and surface tension are employed in the model then the simulations always underestimated the measured oil retention volume by more than 50%. When immiscibility occurs, two liquid phases coexist: one is an oil-rich phase, and the other is a refrigerant-rich phase. In this case, cloudiness and/or particles may disperse throughout the liquid mixture. In totally immiscible refrigerant-oil mixtures, the lubricant and the refrigerant can be treated separately. Shen and Groll (2003,[98]) stated that the immiscibility is likely to occur in the evaporator, which leads to the fact that

174

more oil is trapped in the evaporator than in the condenser. In a partially miscible mixture, when the temperature is higher than the critical solution temperature, the refrigerant is totally miscible with the lubricant. When the temperature is lower than the critical solution temperature, the miscibility is dependent on concentration at given pressure. With respect to some new refrigerant-oil paris, such as R410A/POE, immiscibility may occur at both high and low temperatures. Premoli's model should not be employed for immiscible refrigerant-oil pairs because it accounts for average liquid film proprieties. As first approximation Premoli's void fraction model was used for R410A/MO mixtures by substituting the average liquid film viscosity and surface tension with the oil viscosity and surface tension, respectively. When local properties of pure oil are used in the correlations instead of bulk film proprieties, the accuracy improvement of the predicted oil retention volumes for R410A/MO mixture was more than 50%. Overall, 72% of the experimental oil retention volumes were predicted within ±29% relative error for all refrigerant-oil mixtures tested. R134a/PAG and R410A/POE are partially miscible mixtures and the liquid film viscosity and surface tension were increased slightly to account for local behavior. The local liquid film viscosity and surface tension were computed according the following equations:

$$\mu_{local} = \gamma_{misc} \cdot \mu_{oil} + (1 - \gamma_{misc}) \cdot \mu_{liq,film,average} \tag{8.30}$$

$$\sigma_{local} = \gamma_{misc} \cdot \sigma_{oil} + (1 - \gamma_{misc}) \cdot \sigma_{liq,film,average} \tag{8.31}$$

where γ_{misc} is an empirical coefficient ranging from $0 < \gamma_{misc} \leq 1$, and it depends on the degree of miscibility between refrigerant and oil pairs. For the evaporator, γ_{misc} is given in Table 8.3 for all refrigerant-oil mixture tested.

175

At oil retention volumes less than 25 ml, the relative error between the Premoli's oil retention model and the measured one was about 50%. This is due to the internal grooves in the heat exchanger tubes, whose estimated overall volume was about 20 ml. The internal geometry of the heat exchanger was modeled as a smoothed tube with a defined hydraulic diameter. The flow characteristics and the change in the vapor void fraction for tubes with internal ridges are different from those in smooth tubes. By considering an actual cross section area and using a hydraulic diameter, it was possible to improve the predicted oil retention and improve the accuracy of the simulations. However, a more accurate void fraction model that accounts for grooves in heat exchanger tubes, should be studied in future development of this research work.

8.2 Oil Retention in the Condenser of a Vapor Compression System

This section summarizes the simulation results of the oil retention volume in the condenser and the convective condensation heat transfer, pressure drops, and void fraction model in the condenser are discussed next.

The thermodynamic proprieties of the oil and liquid refrigerant mixtures in the condenser were evaluated with the same approach used for the evaporator. The sub-cooled region was separated from the two-phase region. As a first approximation, the liquid refrigerant and the lubricating oil were considered completely miscible and uniformly mixed in the condenser sub-cooled region. Thus, oil retention in this portion of

the condenser, was estimated with the same method adopted for the liquid line described in the next section. In the two-phase region, the frictional pressure drop was computed following the same approach described for the evaporator. The Lockhart-Martinelli's parameter and the void fractions were computed at each segment of the tube. Consequently, frictional pressure drops and oil retention were estimated by adding the contribution of each segment. The heat transfer correlations for the condensation process were different than those described for the evaporator. Shen and Groll (2003, [98]) compared different heat transfer correlations that can be used in condensation processes of refrigerant and oil mixtures. When a lubricant impacts both evaporation and condensation adversely, the lubricant tends to have less influence on convective condensation. Shen and Groll used the concept of the oil excess layer to explain the difference in oil influence between the evaporation and condensation heat transfer in a horizontal tube. The oil excess layer forms where the phase change occurs. The oil excess layer has a very large viscosity and insulation effect, and thus reduces the heat transfer. During evaporation, the oil excess layer exists at both the solid-liquid interface and liquid-vapor interface. However, during condensation, the oil excess layer can only exist at the solid-liquid interface since the lubricant is continuously dissolved by the condensing refrigerant. Shen and Groll concluded that the oil excess layer is removed by the liquid refrigerant at the top of horizontal tube and the top of the tube maintains a high heat transfer performance. Based on a critical literature review of other research works in the same area, they reported that the influence of oil on heat transfer degradation during condensation increases with oil mass fraction and that the lubricant reduces the mean

177

convective condensation regardless of oil mass fraction, mass flux, and tube geometry. In their critical literature review, Shen and Groll did not recommend any particular "best correlation" for the condensation process. Since the presence of the lubricant does not alter the condensation mechanisms significantly, they suggested that it is feasible to use a correlation for pure refrigerant to predict the heat transfer coefficient of the refrigerant-oil mixture by replacing pure refrigerant proprieties with the mixture proprieties. In that case, they recommended using mixture dew point temperature as the reference temperature. During condensation processes the liquid mixture temperature is still the bubble point temperature of the mixture. It has been computed according the same correlation used for the evaporation processes. The enthalpy release curve, described in the previous section, was assumed to be still valid for condensation. Thus, pressure, temperature, local mixture vapor quality, and mixture enthalpy were computed at each segment.

8.2.1   Heat Transfer Correlation for Refrigerant-Oil Mixture during Condensation Process

Heat transfer correlations for pure refrigerant condensation processes already existed in the software tool developed by Jiang (2002, [58]). The heat transfer correlations used in the software were the Dittus-Bolter correlation and the Gnielinski correlation for single-phase flow. For the two-phase flow region during condensation, the implemented correlations were Dobson's, Shah's, and Travis'. These correlations will not be described here, but they can be found in Jiang's thesis (2003, [57], [58]). For the model used in the

current work, the same heat transfer correlations were adopted by replacing pure refrigerant proprieties with mixture proprieties. One more correlation was added to the condenser model to verify its feasibility on the current experimental data. This correlation was suggested by Shen and Groll (2003, [98]), who summarized its feasibility based on experimental works from several researchers. The following heat transfer correlation for convective condensing processes applies:

if $Re_{ref,vap} < 24000$

$$Nu = 15.9 \cdot Pr_{mix,liq}^{\frac{1}{3}} \cdot \left[\frac{h_{fg}}{c_{p,mix}(T_s - T_W)} \right]^{\frac{1}{6}} \cdot Re_{ref,vap}^{0.15} \cdot exp(-5.0\omega_0) \tag{8.32}$$

if $Re_{ref,vap} > 24000$

$$Nu = 0.084 \cdot Pr_{mix,liq}^{\frac{1}{3}} \cdot \left[\frac{h_{fg}}{c_{p,mix}(T_s - T_W)} \right]^{\frac{1}{6}} \cdot Re_{ref,vap}^{0.67} \cdot exp(-5.0\omega_0) \tag{8.33}$$

The correlations (8.32) and (8.33) were originally developed for R134a/POE mixtures and the test section had a smooth tube with an inner diameter of 6 mm. The mass flux varied from 120 to 260 kg/(m^{2}s) while the heat flux varied from 3.2 to 7.6 kW/m^2. The oil mass fraction varied from 0 to 5.1 wt.% and vapor quality ranged from 100% to 0%. The authors indicated that these correlations were quite successful in comparison to their measured condensing coefficients based on the pure refrigerant saturation temperature. Nonetheless, Shen and Groll reported that they did not compare their predicted results with the experimental data from other sources available in literature. In the current work the temperature T_s was set to $T_{bubble,\ mixture}$ since T_w can be higher than the saturation

temperature in the first segments of the condenser. This would cause Nusselt number be negative, and the refrigerant side heat transfer coefficient would be meaningless.

8.2.2   Simulation Results for the Condenser

In a manner similar to the evaporator, various void fraction models were used to calculate oil retention in the condenser and the simulation results were compared with the experiments. One important difference as compared to the evaporator is the oil retention profile. In the first segments the mixture quality is $x_{max,mix} = 1-OMF$, and it is almost 1. The maximum bubble point temperature $T_{max,bubble}$ is calculated according equation (8.12) with $x=x_{max,mix}$. If the local temperature is higher than $T_{max,bubble}$, then the mixture behaves as single phase, i.e., it cools down without any refrigerant condensation. Two-phase oil-refrigerant mixture heat transfer and pressured drop correlations were used with the film consisting entirely of pure oil. When the mixture reached $T_{max,bubble}$, then the vapor refrigerant started to condensate and the mixture quality decreased. If x_{mix} reached the liquid phase, single phase heat transfer and pressure drop correlations apply. Figure 8.9 shows an example of the calculated oil retention, vapor quality, and local oil mass fraction in one circuitry of the condenser. The refrigerant pass consists of 8 in-line tubes with refrigerant flowing from the top to the bottom. Oil retention volume in each segment was computed and divided by the maximum oil retention volume of the circuitry, which was about 0.1 ml. The dimensionless oil retention is given on the primary y-axis while the dimensionless length of the circuitry is given on the x-axis. The mixture quality is

also plotted in the secondary y-axis of Figure 8.9. The refrigerant-oil mixture is R134a/POE and the OMF was about 2.6 wt.%. The air inlet and outlet temperatures were 20.4ºC and 26.7 ºC, respectively, while the refrigerant temperatures were 48ºC at the condenser inlet and 23ºC at the condenser outlet. With a total mass flow rate of 46 g/s, the predicted pressure drop was about 36 kPa, while the measured pressure drop was only 23 kPa. At the condenser inlet, the local oil mass fraction was one but the oil had temperature of about 60ºC. Thus, the temperature influence on liquid film viscosity seemed to be the predominant effect in the first segments of the condenser. As the temperature decreases, the oil retention increases because of higher liquid film viscosity. However, the influence of local oil mass fraction on the liquid film viscosity became more significant. A local maximum of oil retention in the entrance region of the condenser is determined by the influence between temperature and local oil mass fraction effects on liquid film viscosity.

For all simulations of the condenser, the heat transfer correlations used where Gnielinski's correlation in the liquid phase and Shah's correlation in two-phase flow and in the superheated region. The Lockhart-Martinelli pressure drop correlation for refrigerant-oil mixtures was employed to estimate the pressure drop in two-phase region as well as in the superheated region of the condenser. Churchill's single-phase correlation was used to predict the liquid pressure drop in the sub-cooled region of the condenser. In all correlations, liquid refrigerant properties were replaced by oil-refrigerant mixture properties, and actual cross section area and hydraulic diameter were computed according the inside geometry of the heat exchanger tubes. Figure 8.10 shows the comparison

181

between measured and predicted oil retention volumes for all refrigerant-oil mixtures tested. The x-axis gives the predicted oil retention volumes from the simulations while the measured oil retention volumes are plotted on the y-axis The continuous curve represents the predicted oil retention volume according Premoli's void fraction model while the data points are the corresponding measured oil retention volumes for all refrigerant-oil mixtures tested. Premoli's void fraction model is the one that agreed closest with the experimental results. A reasonable agreement was observed for all data points and the average deviation was ±23%. During the condensation processes, the equations (8.30) and (8.31) where used to estimated the local liquid film viscosity and surface tension in Premoli's void fraction correlation. However, the parameter γ_{misc} was set to γ_{misc}=0.1 for R410A/MO mixture while was kept constant to γ_{misc}=1.0 for all other refrigerant-oil mixtures. The correction used for the immiscible refrigerant-oil mixture improved the simulation accuracy of R410A/MO by more than 30%. Overall, about 70% of the experimental oil retention volumes were predicted within 30% relative error for all refrigerant-oil mixtures tested as shown in Figure 8.10.

8.3 Oil Retention in the Liquid Line of a Vapor Compression System

The homogenous model can be applied in the liquid line because the refrigerant is in the liquid phase. Thus, if the OMF is known, oil retention is simply obtained by equation (8.34):

$$OR\ [ml\ ] = \omega_0 \cdot \left(A_{tube} \cdot L_{tube}\right) \cdot \frac{\rho_{mix}}{\rho_{oil}} \cdot 10^6 \qquad\qquad (8.34)$$

where ω_0 is the absolute oil mass fraction in the liquid line, ρ_{mix} is the mixture density, and ρ_{oil} is the pure oil density evaluated at the average temperature of the liquid line.

Figure 8.11 shows the accuracy of predicted oil retention volume in the liquid line with respect to measured oil retention volume. The mixture proprieties were assumed constant along the entire tube since temperature and pressure at the inlet and outlet of the liquid line were very similar. For all refrigerant-oil mixtures, the average relative error was within ±25%. The error is due to the measurement accuracy of OMF, of oil retention, and the estimation of the mixture density. Moreover the accuracy of the internal volume of the liquid line section affected the accuracy of the calculated oil retention values, too. The liquid line included several meters of tubes (~19 m) with about 8 mm inside diameter. The refrigerant mass flow meter internal volume was estimated and it was taken into account, too. However it represented less than 2% of the total internal volume of the liquid line.

8.4   Summary: Oil Retention Simulation Results

Oil retention was predicted in the evaporator, condenser, and liquid line. The liquid line was quite simple to model and oil retention could be easily computed once the oil mass fraction in the mixture was known. In the liquid line the model assumed homogeneous mixture with average bulk properties uniformly in the entire tube. The problem of

measuring the oil retention in the evaporator and condenser was not trivial. The mechanisms of evaporation and condensation of refrigerant-oil mixtures is quite different from that of pure refrigerants. Several heat transfer correlations as well as pressure drop correlations have been used in the simulation and compared with the experimental data. Pure liquid refrigerant proprieties were substituted by oil and liquid refrigerant mixture proprieties. Since oil's vapor pressure is negligible compared to refrigerant's, lubricants can be assumed to have no effect on the mixture vapor proprieties and thus computed as pure refrigerant vapor proprieties.

Next is a summary of conclusions drawn from simulating the processes within evaporator, condenser, and liquid line.

☐ A general comprehensive model that accounts for the oil effects on the heat transfer coefficient and pressure drop during the evaporation and condensation processes was developed and integrated in a simulation model available at CEEE, University of Maryland. The simulation tool was updated so that the oil influence on component performance could be estimated under realistic operating conditions.

☐ In the evaporator, Premoli's void fraction models predicted oil retention volume within 21% average relative error. If local liquid film viscosity and surface tension are used in the Premoli's void fraction model, the simulation follows the same trend as the experimental data and 72% of the data points were predicted within 29% relative error.

184

☐ Existing heat transfer correlations for the evaporation of a refrigerant and oil mixture were verified with the current experimental data. Simulations predicted the cooing load of the heat exchanger as well as the outlet conditions. The relative error was within 16% for the cooling capacity. The refrigerant-oil mixture outlet temperature was predicted with an average relative error of 4K while the temperature of the air leaving the evaporator was predicted within 2K for all the refrigerant-oil mixture tested.

☐ Existing pressure drop correlations for the evaporation of refrigerant and oil mixtures were verified with the current experimental data. Simulations used Lockhart-Martinelli semi-empirical pressure drop correlations for two-phase flow in which liquid refrigerant proprieties were replaced by oil and liquid refrigerant mixture proprieties.

☐ Similar results were obtained for the condenser; Premoli's void fraction model is the model that agreed closest with the experimental results. A reasonable agreement was observed for all data points and the average deviation was ±23%. If local liquid film viscosity and surface tension are used in the Premoli's void fraction model, the simulations behave similarly to the experimental data and about 70% of the data points were predicted within 30% relative error.

☐ In the condenser, while Lockhart-Martinelli pressure drop correlation can still be used to predict the pressure drop, the heat transfer correlation during condensation process was different from that used to estimate the heat transfer coefficient in the two-phase region during evaporation. The refrigerant-oil

185

mixture outlet temperature was predicted with average relative error of 3K while the temperature of the air leaving the condenser was predicted within 2K for all the refrigerant-oil mixture tested. The average relative error on the refrigerant pressure was about 43% as compared as the measured pressure drop across the condenser.

☐ Refrigerant-oil mixture temperatures versus vapor quality profiles were generated using newly developed simulation tools. Local oil retention volume was computed in the evaporator and condenser. The calculated oil retention profiles showed that there is always a balance resulting from two opposing effects on the liquid film viscosity and surface tension: increase of temperature and increase of oil local concentration in the mixture. While in the evaporator the maximum oil retained is always at the end part of the heat exchanger, in the condenser a local maximum of oil retention was observed in between inlet and outlet tubes.

☐ In the liquid line, a simple homogeneous model was used to predict oil retention. The simulation results were in agreement with the experiments and the relative error was about ±25% for all refrigerant-oil mixtures tested.

☐ The experimental results generally verified the Premoli's void fraction model, heat transfer and pressure drop correlations available in literature. The simulations behave similarly to the experimental data and the highest error was observed at the lowest oil retention volumes. This is due to the actual internal geometry of the tubes in the heat exchanger. A satisfactory void fraction model

that account for internal grooves in heat exchanger tubes has not been developed, yet. More research needs to be done to investigate the void fraction model of binary refrigerant-oil mixtures during evaporation and condensation processes in enhanced heat exchanger tubes.

Table 8.1: Coefficient *c* and *n* as a Function of the Oil Mass Fraction in the Refrigerant-Oil Mixture Heat Transfer Correlation presented by Chaddock and Murther (1980)

Oil Mass Fraction [wt.%]	Constant *c*	Constant *n*
0.0	3.90	0.62
1.0	4.72	0.59
2.9	4.36	0.60
5.7	4.97	0.59

Table 8.2: Constant *C* of the Lockhart-Martinelli Pressure Drop Correlation Martinelli (Lockhart-Martinelli, 1949)

Liquid	Gas	Constant *C*
Turbulent	Turbulent	20
Laminar	Turbulent	12
Turbulent	Laminar	10
Laminar	Laminar	5

Table 8.3: Empirical Constant γ_{misc} **to Account for Immiscibility Effects in the Premoli's Void Fraction Model during Refrigerant-Oil Mixture Evaporation**

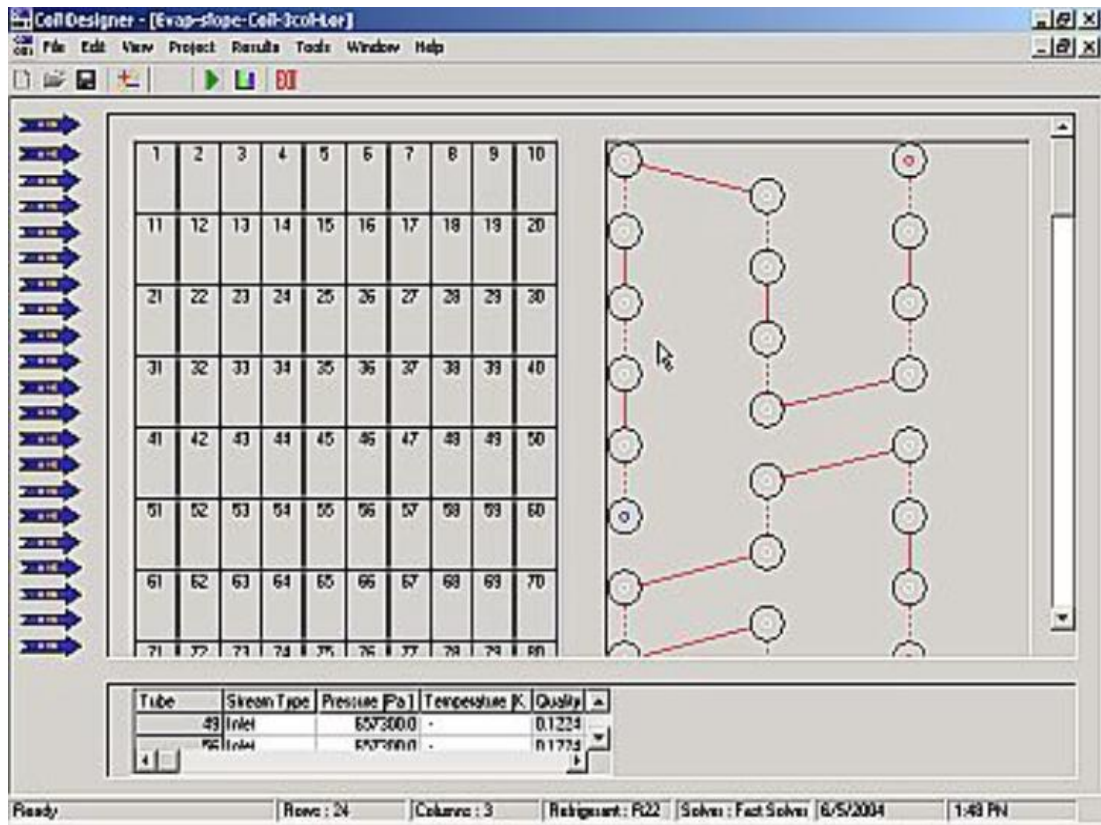| Refrigerant-Oil Mixture	Degree of Miscibility	γ_{misc}
R22-M0, R134a-POE	Completely Miscible	1.0
R410A-POE	Partially miscible	0.9
R134a-PAG	Partially Miscible	0.85
R410A-MO	Almost Immiscible	0.1

Figure 8.1: Evaporator Model in CoilDesigner Sofwtare Simulation Tool.

Liquid Refrigerant
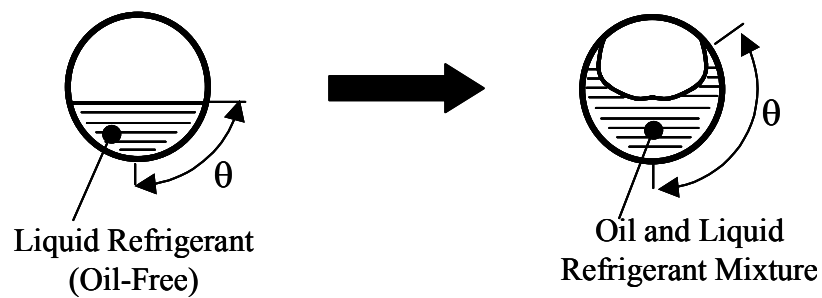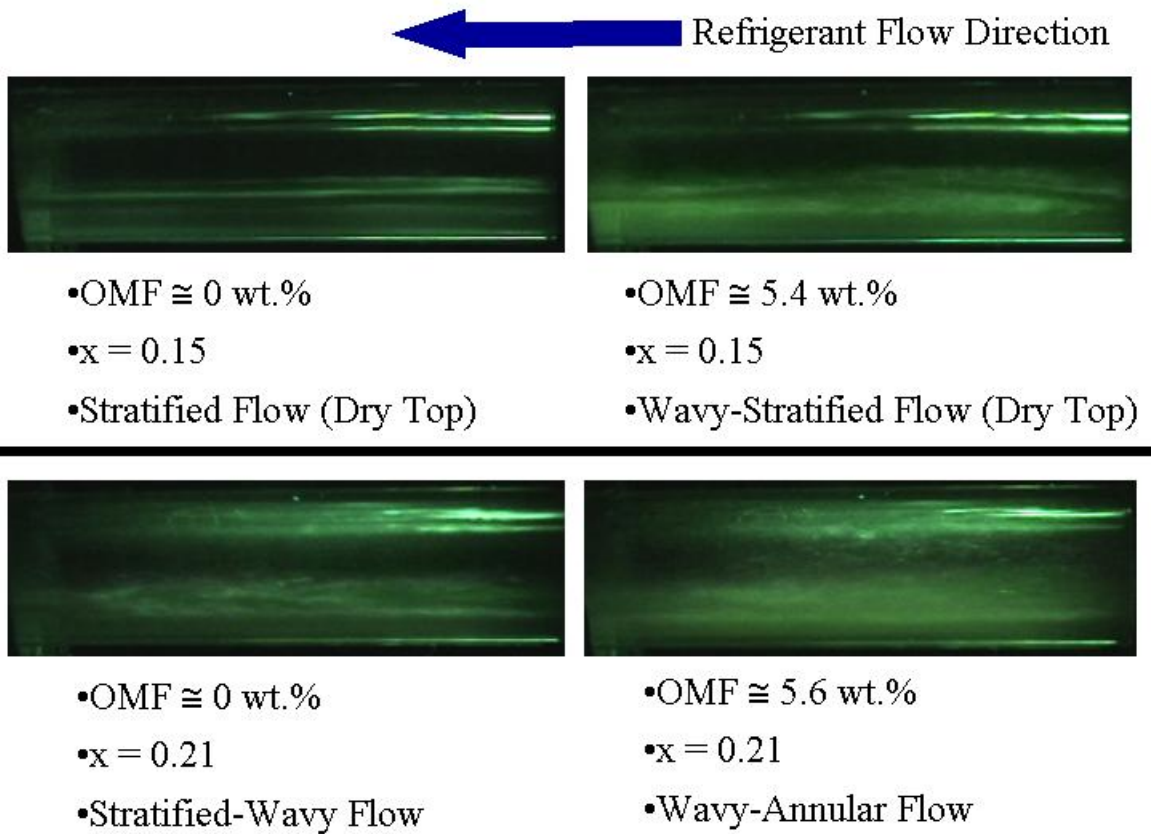(Oil-Free)

Oil and Liquid
Refrigerant Mixture

Figure 8.2: Schematic Representation of the Effects of the Lubricating Oil on

the Wetted Surface Angle (θ) inside the Heat Exchanger Pipes

Figure 8.3: Comparison between Mixture Flow Patterns at Low Quality (x) with and without Oil inside the Evaporator for R22/MO (Refrigerant Mass Flux G = 120 kg/(m^{2}s) and Pipe Diameter D = 8.7mm).

Refrigerant Flow Direction

•OMF ≅ 0 wt.%

•x = 0.38

•Wavy-Annular Flow

•OMF ≅ 8.2 wt.%

•x = 0.38

•Wavy-Annular Flow

•OMF ≅ 0 wt.%

•x = 0.50

•Annular Flow

•OMF ≅ 3.9 wt.%

•x = 0.50

•Annular Flow
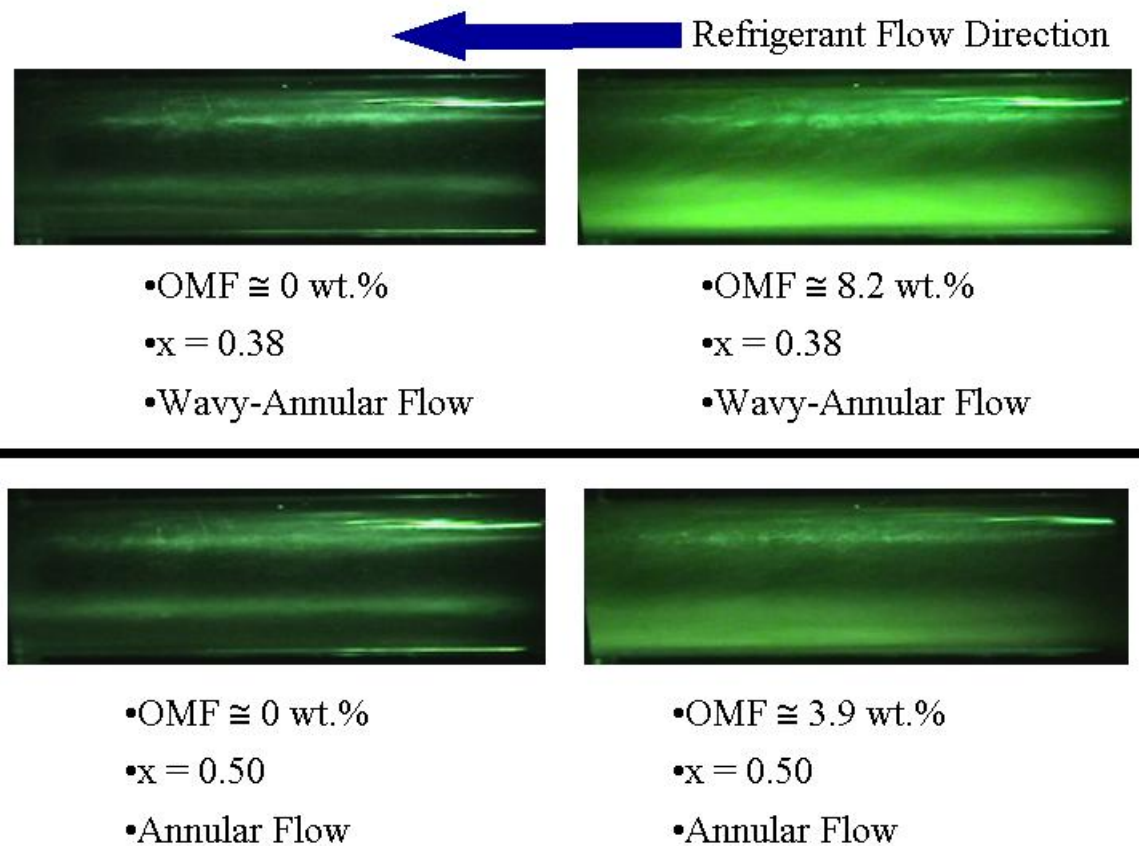
Figure 8.4: Comparison between Mixture Flow Patterns at Medium Quality (x) with and without Oil inside the Evaporator for R22/MO (Refrigerant Mass Flux G = 120 kg/(m^{2}s) and Pipe Diameter D = 8.7mm).
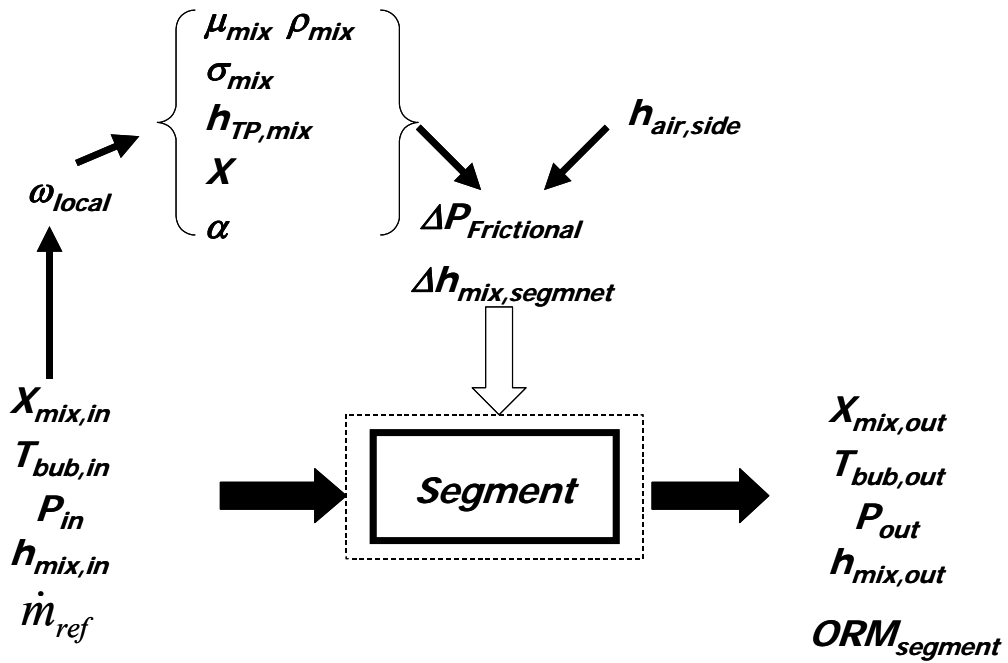
Figure 8.5: Modeling of Oil Retention in the Heat Exchanger Tubes
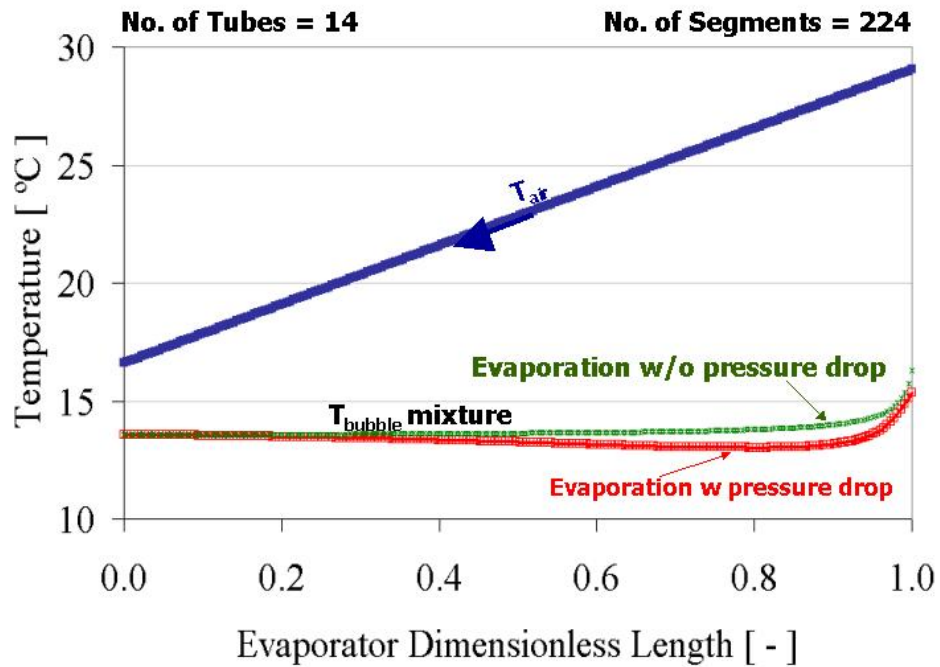
Figure 8.6: Calculated Air and Bubble Temperature in the Evaporator from the Simulation Results of R134a/PAG at OMF = 2.4 wt.%.
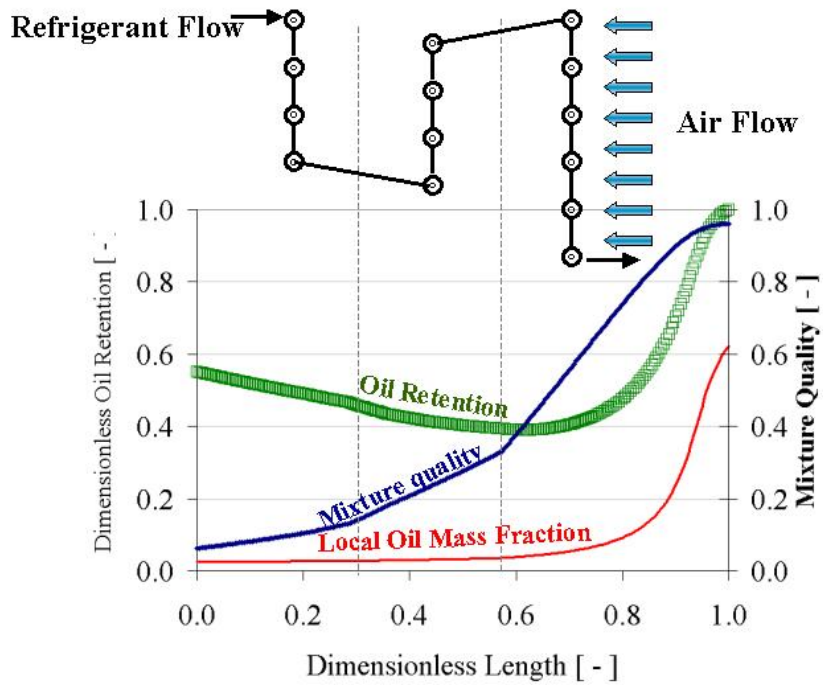
Figure 8.7: Calculated Oil Retention, Vapor Quality, and Local Oil Mass Fraction in the Evaporator (R134a/PAG at OMF = 2.4 wt.%.)
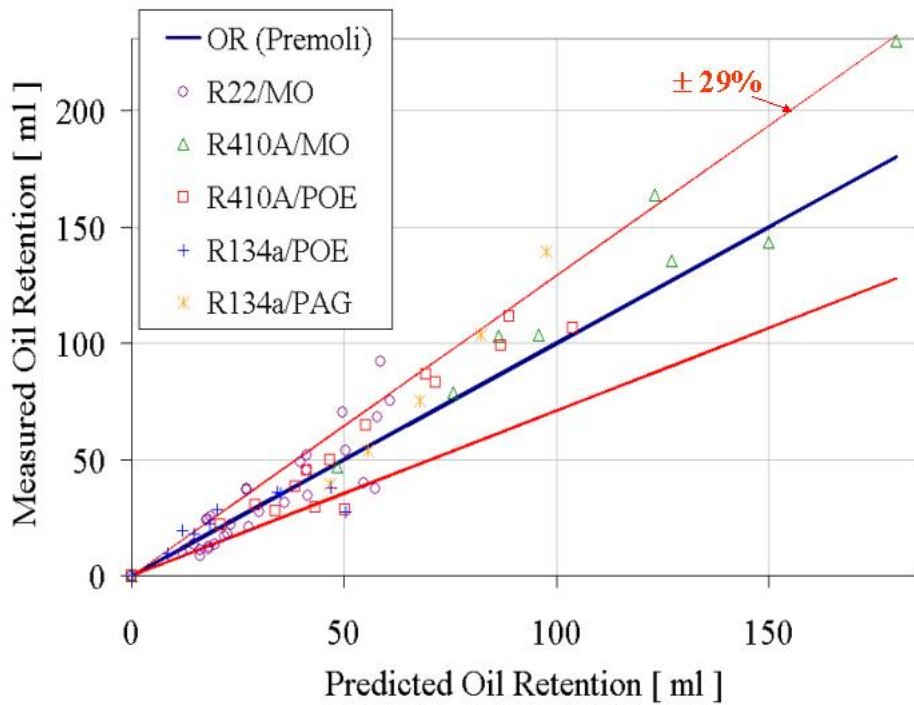
Figure 8.8: Experimental versus Predicted Oil Retention Volume in the Evaporator
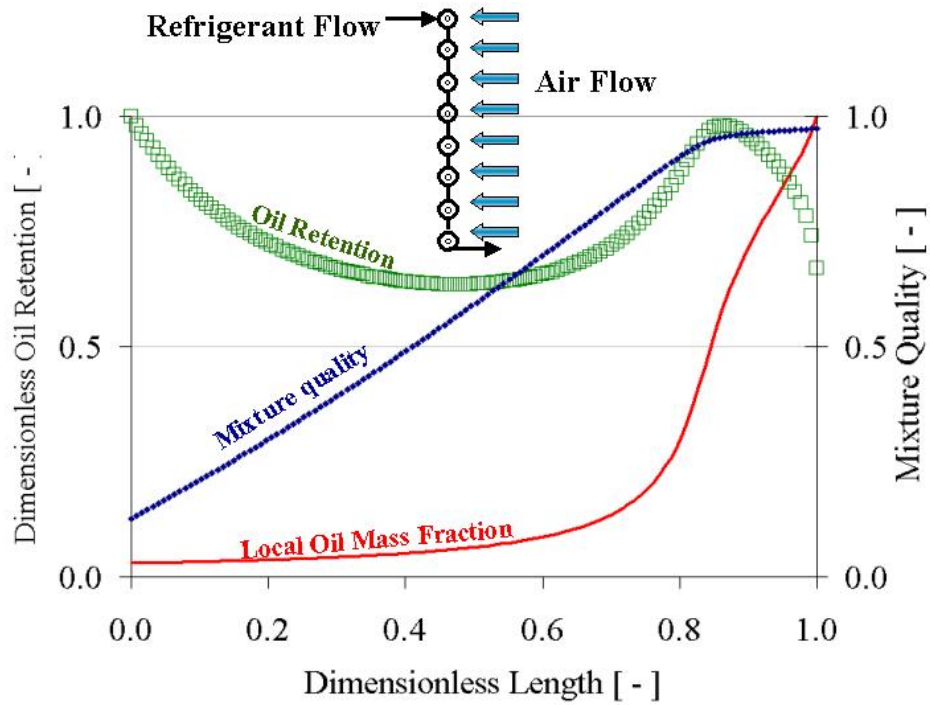
Figure 8.9: Calculated Oil Retention, Vapor Quality, and Local Oil Mass Fraction in the Condenser (R134a/PAG at OMF = 2.6 wt.%)
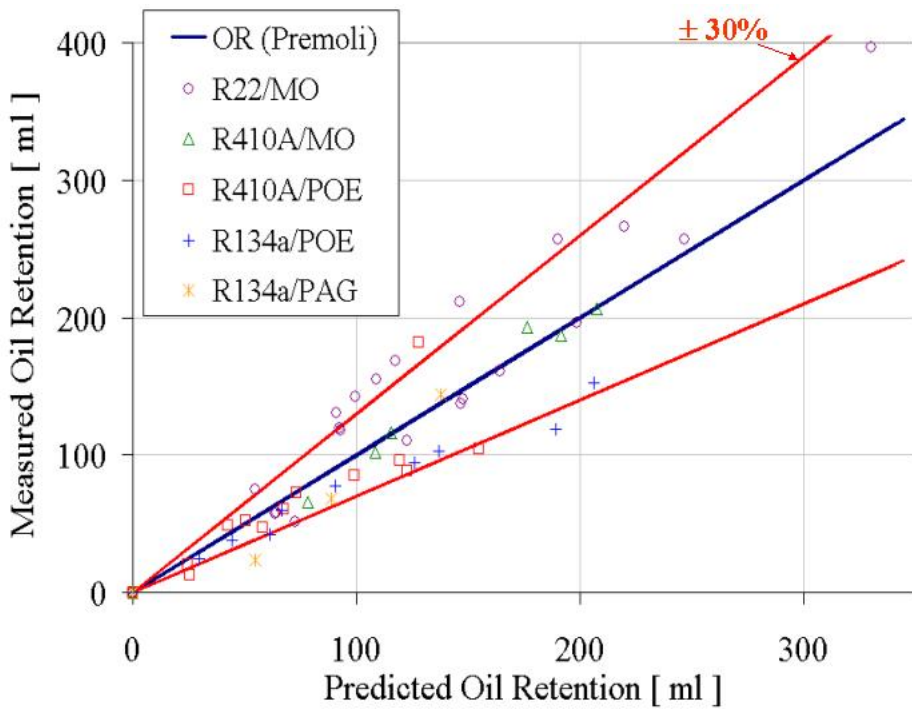
Figure 8.10: Experimental versus Predicted Oil Retention Volume in the Condenser
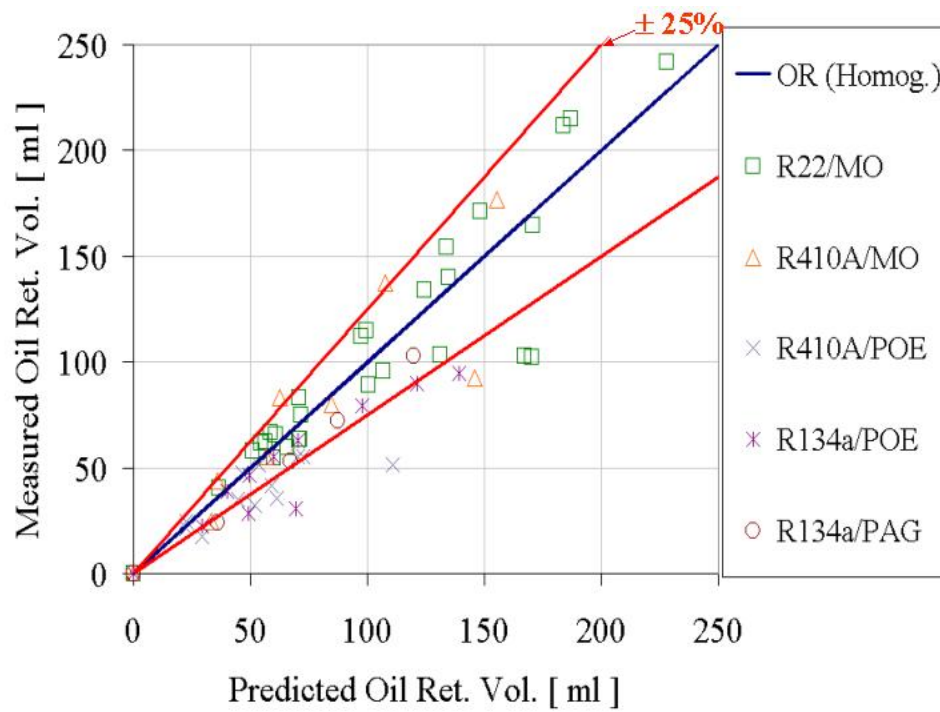
Figure 8.11: Experimental versus Predicted Oil Volume Retained in the Liquid Line

Chapter 9: Conclusion and Recommendations

The objective of this dissertation was to investigate experimentally and theoretically the oil retention characteristics of refrigerant and oil mixtures in vapor compression systems. This was accomplished with extensive experiments and simulations. The conclusions of this dissertation are summarized below in the order in which experimental and simulation work was performed.

9.1   Conclusions from the Experimental Work

The oil injection-extraction method was used to measure oil retention within each component of an air-conditioning system. The experimental studies focused on the oil transport proprieties of a refrigerant-oil mixture. The refrigerant and oil pairs selected for the experiments allowed investigation of oil retention characteristics in the widest possible range of oil film density, viscosity, and surface tension. The refrigerant mass flux varied in the range from 106 to 400 kg/(m^{2}s), which included optimum applications in stationary and automotive air conditioning systems. The conclusions of the experimental work are as follows:

- Oil retention is proportional and very sensitive to the oil mass fraction (OMF) of the refrigerant-oil mixture in each component of the system.

- The suction line is the most critical component for oil retention due to high liquid film viscosity and low inertia force from the vapor refrigerant core, which is the driving force for oil transport.

- Higher refrigerant mass flux reduces the amount of oil retained in the suction line. A reduction of pipe diameter promotes oil transport but also increases the frictional pressure drops along the pipe. Thus, the suction pipe diameter should be a compromising value to minimize the pressure drop and to reduce oil retention. The oil transport needs to be guaranteed even in the most unfavorable operating conditions of the air conditioning system, which usually occur during the system's part load running conditions.

- The gravity effects are important and oil retention can increase up to 50% more in the vertical upward suction line compared to horizontal suction with the same refrigerant mass flux and liquid film viscosity.

- Oil retention is also proportional to the ratio of liquid film over refrigerant vapor viscosity. At constant refrigerant mass flux and OMF, an increase in oil film viscosity leads always to increased oil retention volume.

- A high degree of solubility and miscibility between the refrigerant and the oil reduce liquid film viscosity and thus the oil retained in the system, with respect to mixtures that are poorly soluble and miscible. R410A/MO mixtures fall into the second class and show higher oil retention characteristics.

- Oil retention affects the pressure drops in each component of the system. The most sensitive component is the suction line and the pressure can be up to 40% higher than

in oil-free conditions. In the evaporator, the maximum pressure drop penalty factor was 1.15 but about 1.13 in the condenser. Thus the oil retained in the system components always has a penalizing effect on the pressure drop.

- Refrigerant-oil properties and system geometries need to guarantee proper oil return to the compressor, minimize oil retained in each component, and avoid potential oil accumulations. For annular flow in suction lines, kinetic viscosity ratio versus refrigerant mass flux maps can be developed to qualitatively describe the transport characteristics of refrigerant-oil mixtures. Figure 9.1 shows an example of the suction line oil transport map for the current work and also includes oil retention experimental results of CO_2/PAG mixture obtained from Lee's research work (2002). The x-axis gives the refrigerant mass flux in kg/(m^{2}s), while the liquid film over the vapor refrigerant kinetic viscosity ratios are plotted on the y-axis of Figure 9.1. Refrigerant-oil mixtures that have viscosity ratios higher than 35 and refrigerant vapor mass flux less than 100 kg/(m^{2}s) have poor oil transport characteristics. They are close to the top and left area of the figure, which is characterized by high oil retention ratio. The area at the bottom and right side of the map guarantees good oil transport and minimizes the oil retention in the system components. Consequently, from an oil management point of view, an ideal refrigerant–oil mixture should be close to this area for actual operating conditions of the system.

9.2 Conclusions from the Modeling Work

A numerical semi-empirical model to estimate oil retention was developed. The modeling approach consists of an engineering approach that is both simple and sufficiently accurate to be useful in practical applications. For the suction line, where the flow type is annular flow, interfacial friction factor correlations were developed. In the evaporator and condenser, different void fraction models were compared with the experimental data, and various heat transfer and pressured drop correlations were verified. In the liquid line, the homogeneous model predicted the oil retention quite satisfactorily. The main conclusion of the modeling work of the current research is thusly summarized:

- In the suction line, a semi-empirical model was developed to predict oil film thickness in the pipe. Based on the current experimental data, a more general friction factor correlation was obtained and the predicted oil retention was within ±31% average relative error.

- A comprehensive, semi-empirical model was developed for the evaporator and condenser. The refrigerant and oil heat transfer and pressure drop correlations available in literature were implemented in a simulation tool to design the heat exchangers. These correlations were verified with the current experimental data. Lockhart-Martinelli pressure drop correlation poorly predicted the two-phase frictional pressure drop in the evaporator and the relative error was about 60%. The

cooling capacity of the system was computed within 12% relative error for all refrigerant-oil mixtures tested.

- Oil retention in the evaporator and condenser was estimated using various void fraction models. Among five different choices, Premoli's void fraction model agreed the closest with the experimental data. In the evaporator, oil retention was predicted within 21% average relative error, while the condenser the error was 23%. About 70% of the experimental data was predicted by the simulations within 30% relative error. Further improvements are necessary to account for local mixture properties variation due to miscibility effects. The effect of internal wall surface aspect ratio of the tube and the influence of oil droplets entrainment phenomena on oil retention volume need to be studied in future work.

- In the liquid line, the refrigerant was entirely in liquid phase and a simple homogeneous model, which used bulk average mixture properties, predicted oil retention quite successfully. The relative average error was within ±25% with respect to the experimental data of the current work.

- In the evaporator, oil retention volume reaches a maximum value at the end part of the heat exchanger since the local liquid film viscosity is higher. The liquid viscosity depends on the mixture temperature and local oil mass fraction in the liquid film.

- In the condenser, a local maximum of oil retention occurs at the inlet tubes. As the refrigerant-oil mixture enters the condenser, it cools down and the oil retention increases. The drop of the mixture temperature increases the liquid film viscosity until the local oil mass fraction reaches about 70 wt.%. Then, the dissolved refrigerant

201

decreases the liquid film viscosity and oil retention is reduced. Near the liquid phase region, the void fraction decreases sharply with mixture quality and oil retention increases again. It eventually reaches a maximum value in the sub-cooled region of the condenser.

9.3 Recommendations for Design Guidelines

Based on the research on oil retention in air conditioning systems, recommendations for design guidelines for suction lines and heat exchangers are proposed as follows.

9.3.1 Suction Line

The suction line is the most critical component for oil retention. To minimized the oil retention, reduce potential oil hold up and promote proper oil return the following recommendations are proposed:

- Use refrigerant vapor mass flow rate as higher as possible.
- Tube diameters of the suction line larger than 19 mm are unfavorable for oil transport and it causes an increase of oil retention. The tube diameter should be optimized by minimizing the frictional pressure drops and by promoting the oil transport capability of the tube.
- If possible use short upward vertical suction line and increase the refrigerant mass flux in the upward vertical section of the suction line by reducing the diameter.

- Adopt soluble and miscible refrigerant and oil pairs to decrease the liquid film viscosity in the suction line.

- Minimize the oil mass fraction in the mixtures by adopting oil separators at the compressor discharge line.

- From an engineering perspective, design an air conditioning system and choose a suitable refrigerant-oil mixture such that transport proprieties will tend to the bottom and right side area of the map of Figure 9.1. This is the area with excellent oil transport characteristics due to liquid film over refrigerant vapor viscosity ratio less than 25 and refrigerant vapor mass flux greater than 200 kg/(m^{2}s). In opposition, systems that run close to the region of poor oil transport characteristic need to account for the fact that a significant part of the oil initially charged into the compressor can be eventually retained in the system components and it affect their performances.

9.3.2   Tube-and-Fin Heat Exchangers

The tube-and-fin heat exchanger design should maximize heat transfer capability, minimize pressure drops across the heat exchanger, and avoid any potential oil trap in the circuitry. Recommendations suggested for the heat exchanger are as follows:

- Avoid vertical upward headers or collectors with inner tube diameter larger than 19 mm at the evaporator outlet. A small header is recommended to increase the refrigerant velocity in vertical upward flows. Evaporator outlet headers with large

inner tube diameter may create potential traps for oil accumulations and stagnations. If possible design these collectors such that the refrigerant flow will be downward to minimize oil retention.

- In the evaporator, optimize the circuitry to avoid mal-distribution in the mixture quality. Mal-distribution is an unfavorable effect not only for the evaporator performance but also for oil retention. A circuitry with a higher degree of superheat will suffer high oil retention volume and oil can partially block the local refrigerant flow. Consequently, pressure drop increases and heat transfer capacity reduce, degrading the overall performance of the heat exchanger.

- Reduce the degree of superheat at the minimum limits defined by compressor safety run. Lower degree of superheat decreases oil retention in the end part of the evaporator.

- In the condenser, reduce the inlet condenser temperature as much as possible so that more refrigerant is dissolved into the oil at the condenser inlet tubes. This causes the liquid film viscosity to drop and oil retention to decrease, especially if the distributor has diameter smaller than 19 mm. Reduce also the degree of sub-cooling at the lowest possible value, since the oil retention in the sub-cooled region of the condenser is quite significant.
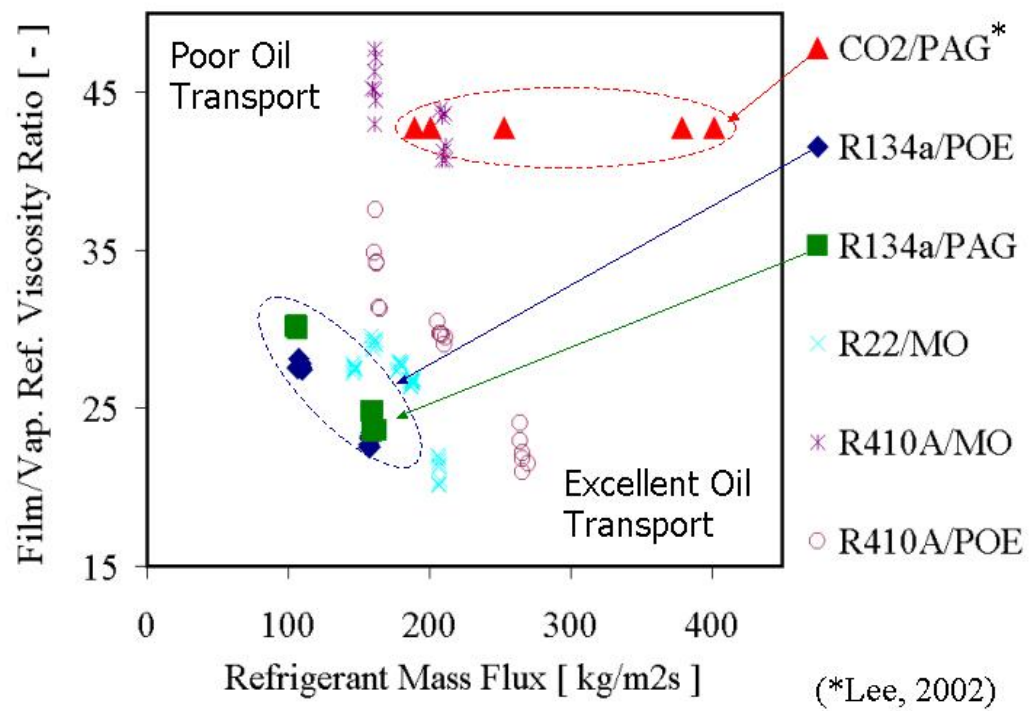
Figure 9.1: Schematic Oil Transport Map in Suction Line of A/C System

Chapter 10:Future Work

This research study has investigated the oil retention of refrigerant-oil mixtures in vapor compression systems. It represents a summary of the state-of-art results in the area of oil management in air conditioning systems used in stationary and automotive applications. The current study offers an engineering approach easily adapted to practical applications without substantially sacrificing accuracy. It does not represent a comprehensive theory for the lubricating oil transport characteristics, and it only covers some aspects of the research area of refrigerant and oil mixture characteristics in vapor compression systems. Further developments are required to understand oil behavior in air conditioning and refrigeration systems; future investigations should address the following:

- Oil retention measurements in fin-and-tube exchangers at oil mass fractions (OMFs) less than 1 wt.%. At OMFs less than 1 wt.% the oil retention cannot be measured accurately with the injection-extraction method used in the current work, so alternative oil retention measurement methodologies need to be developed.

- Conduct oil retention tests with conventional refrigerants (R134a, R410A) in micro channel heat exchangers.

- Study the influence of oil on heat transfer and pressure drops in smooth and grooved tubes, especially at OMFs less than 1 wt.%. The inner wall surface aspect ratio of the tube can affect oil transport characteristics by inducing turbulence on the liquid film and breaking the interfacial surface phase separation between vapor and liquid film.

Void fraction models for binary mixtures in smooth and grooved tubes need to be improved to account for wall surface aspect ratio.

- Oil retention measurements in low temperature applications. Refrigerant mass fluxes less than 100 kg/(m^{2}s) and liquid film viscosities greater than 35 cSt usually characterize refrigeration systems. Oil transport is particularly critical in refrigeration systems, and experimental results are necessary to confirm and extend existing oil retention models.

- Oil retention measurements in transient operating conditions. During the compressor shut off period, a significant amount of oil is mixed with the liquid refrigerant in the compressor crankcase. A stratified level of liquid stands below or above a consistent layer of oil, depending upon the density ratio between the two fluids. Immediately after compressor start up, liquid refrigerant boils and the oil-refrigerant mixture is flung onto the cylinder walls. Then there is a significant rise in the rate at which the oil is pumped from the compressor. Consequently, the amount of oil remaining in the compressor crankcase is reduced during the transient period, leading to potentially dangerous situations for compressor reliable lubrication. Using an electric heater before compressor start up provides only a partial solution to the problem and more research must be done.

- Development of an analytically comprehensive model for oil retention in transient operating conditions; integration with existing models for steady state conditions. Oil behavior theory under transient conditions is still incomplete and unsatisfactory.

- Integration of oil distribution models into vapor compression cycle models for steady state and transient mode conditions.

References

[1]   Alofs, D. J. and M. M. Hassan, 1990, Influence of Oil on Pressure Drop in Refrigerant Compressor Suction Lines, *ASHRAE Transactions*, 96: 249-255.

[2]   ASHRAE Handbook of Air-conditioning and Refrigeration Systems, SI Edition, 1997, Fundamentals, Chapter 2, pp. 2.1 – 2.14.

[3]   ASHRAE Handbook of Refrigeration Systems and Applications SI, 2002, Lubricants in Refrigerants Systems, Chapter 7, pp. 7.1 – 7.26

[4]   ASHRAE Handbook of Refrigeration Systems and Applications, 1994, American Society of Heat, Refrigerating and Air Conditioning Engineers, Atlanta, GA.

[5]   Bai, X., Newell, Ty A., 2002, Investigation of Two-Phase Viscous Liquid Flow, 9th International Refrigeration & Air Conditioning Conf., Purdue, 2002.

[6]   Baker, O., 1954, "Simultaneous Flow of Oil and Gas.", *The Oil and Gas Journal*, July 26, pp.185-195.

[7]   Barao, Teresa, de Castro, Carlos A. Niero, Mardolcar V. Umesh, Okambawa, R., and St-Arnaud, Jean M., Dielectric Constant, Dielectric Virial Coefficients, and Dipole Moments of 1,1,1,2-Tetrafluoroethane, 1995, *Journal of Chemical Engineering,* Vol. 40, pp. 1242-1248.

[8]   Baustian J., J., Pate, M., B., Bergles, A., E., Measuring the Concentration of a Flowing Oil-Refrigerant Mixture with a Vibrating U-Tube Densimeter, *ASHRAE Transaction*, Vol.1, 1988, pp 571-587.

[9]   Baustian J., J., Pate, M., B., Bergles, A., E., Measuring the Concentration of a Flowing Oil-Refrigerant Mixture with a By-Pass Viscometer, *ASHRAE Transaction*, Vol.1, 1988, pp 588-601.

[10]   Baustian J., J., Pate, M., B., Bergles, A., E., Measuring the Concentration of a Flowing Oil-Refrigerant Mixture: Instrument Test Facility and Initial Results, *ASHRAE Transaction*, Vol.2, 1988, pp 167-177.

[11] Baustian J., J., Pate, M., B., Bergles, A., E., Measuring the Concentration of a Flowing Oil-Refrigerant Mixture with an Acoustic Velocity Sensor, *ASHRAE Transaction*, Vol.1, 1988, pp 602-615.

[12] Beckwith, T., R.D. Marangoni, and J.H. Lienhard, 1992, *Mechanical Measurement*, 5th ed, Addison-Wesley Publishing Co., Reading, MA.

[13] Bharathan, D. and G. B. Wallis, 1983, Air-Water Countercurrent Annular Flow, *International Journal of Multiphase Flow*, 9(4): 349-366.

[14] Bharathan, D., Wallis, G., B., 1983, Air-Water Countercurrent Annular Flow, *International Journal of Multiphase Flow,* Vol. 9, No.4, pp 349-366.

[15] Biancardi, F. R., Michels, H., H., Sienel, T., H., and Pandy, D., R., 1996, Study of Lubrication Circulation in HVAC Systems, *The Air-Conditioning and Refrigeration Technology Institute*, ARTI MCLR Project Number 665-53100, DOE/CE/23810-71-Vol 1, UTRC, Connecticut

[16] Bird, R., B., Stewart, W., E., Lightfoot, E., N., 2002, Transport Phenomena, 2nd Edition, J. Wiley& Sons, Inc., New York, ISBN 0-471-41077-2, Chapter 1,2, and 6.

[17] Blankenberger, P. L., A. S. Miller, and T. A. Shedd, 2002, Oil Film Behavior Near the Onset of Flow Reversal in Immiscible Gas/Liquid Vertical Annular Flow, *In Proc. 9th International Refrigeration Conference at Purdue*, R12-3, Purdue University, IN.

[18] Brauner, N., 1991, Two-phase Liquid-Liquid Annular Flow, *International Journal of Multiphase Flow,* Vol. 17, No.1, pp 59-76.

[19] Brauner, N., Ullmann, A., 2002, Modeling of phase inversion phenomena in two-phase pipe flows, *International Journal of Multiphase Flow,* Vol. 28, pp 1177-1204.

[20] Butterworth, D.A., 1975, A Comparison of Some Void Fraction Relationships for Co-Current Gas-Liquid Flow, *International Journal of Multiphase Flow*, 1: 845-850.

[21] Casciaro, S., and J.R. Thome, 2001, Thermal Performance of Flooded Evaporators, Part 2: Review of Void Fraction, Two-Phase Pressure Drop, and Flow Pattern Studies, *ASHRAE Transactions*, 107: 919-930.

[22] Caverstri, R. C., J. Munk and M. Menning, 1994, Solubility, Viscosity, and Density Measurements of Refrigerant-Lubricant Mixtures- Part II: Polyalkylene Glycols with R-134a, *ASHRAE Transactions*, 100(2): 231-238.

[23] Cavestri, R.C. 1993. Measurement of the solubility, viscosity and density of synthetic lubricants with HFC-134a. Final Report for ASHRAE 716-RP.

[24] Cavestri, R.C., and W.R. Schafer. 2000, Measurement of the solubility, viscosity and density of R-41-A refrigerant/lubricant mixture, *ASHRAE Transaction* 106 (1): 277.

[25] Chisholm, D., 1972, A Theoretical Basis for the Lockhart-Martinelli Correlation for Two-Phase Flow, *International Journal of Heat and Mass Transfer,* Vol. 10, pp 1767-78.

[26] Coddington, R., and R. Macian, 2002, A Study of the Performance of Void Fraction Correlations Used in the Context of Drift-Flux Two-Phase Flow Models, *Nuclear Engineering and Design*, 215: 199-216.

[27] Collier, J.G. and J.R. Thome, 1994, *Convective Boiling and Condensation*, 3rd ed, Clarendon Press, Oxford.

[28] Coutris, N., Delhave, J., M., Nakach, R., 1989, Two-Phase Modeling: the closure issue for a two-layer flow, *International Journal of Multiphase Flow,* Vol. 15, No.6, pp 977-983.

[29] Eckels, S. J. and M. B. Pate, 1991, An Experimental Comparison of Evaporation and Condensation Heat Transfer Coefficient for HFC-134a and CFC-12, *International Journal of Refrigeration*, 14: 70-77.

[30] Eckels, S., J., Zoz, S., C., Pate, M., B., Using Solubility Data for HFC-134a and Ester Lubricant Mixtures to Model an In-Tube Evaporator or Condenser, *ASHRAE Transaction*, 1993, pp 383-391.

[31] Feng., F., Klausner, J., F., 1997, A Separated Flow Model for Predicting Two-Phase Pressure Drop and Evaporative Heat Transfer for Vertical Annular Flow, *International Journal of Heat and Fluid Flow*, 18: 541-549.

[32] Fore, L.B., S.G. Beus, and R.C. Bauer, 2000, Interfacial Friction in Gas-Liquid Annular Flow: Analogies to Full and Transition Roughness, *International Journal of Multiphase Flow*, 26: 1755-1769.

[33] Fukano, T. and A. Kariyasaki, 1993, Characteristics of Gas-Liquid Two-Phase Flow in a Capillary Tube, *Nuclear Engineering and Design*, 141: 59-68.

[34] Fukano, T. and T. Furukawa, 1998, Prediction of the Effects of Liquid Viscosity on Interfacial Shear Stress and Frictional Pressure Drop in Vertical Upward Gas-Liquid Annular Flow, *International Journal of Multiphase Flow*, 24: 587-603.

[35] Fukuta, M., T. Yanagisawa, K. Sawai, and Y. Ogi, 2000, Flow Characteristics of Oil Film in Suction Line of Refrigeration Cycle, *In Proc. 8th International Refrigeration Conference at Purdue*, 273-280. Purdue University, IN.

[36] Fung, K. and S. G. Sundaresan, 1994, Study of Oil Return Characteristics in a Display Case Refrigeration System. Comparison of Different Lubricants for a HFC-Blend Refrigerant, *In Proc. 5th International Refrigeration Conference at Purdue*, 121-128, Purdue University, IN.

[37] Gnielinski, V., 1976, New equations for Heat and Mass Transfer in Turbulent Pipe and Channel Flow, *International Journal of Chemical Engineering*, 16: 359-368.

[38] Graebel, W., P., 2001, Engineering Fluid Mechanics, Taylor & Francis Publisher, London, ISBN 1-560-32711-1, Chapter 5, pp 265 – 293.

[39] Grebner, J. J. and R. R. Crawford, 1993, The Effects of Lubricant on Evaporator Capacity for Systems Using Mixtures of R-12/Mineral Oil and R-134a/Symthetic Oil, *ASHRAE Transactions*, 99: 380-386.

[40] Green G. H., 1971, The Effect of Oil on Evaporator Performance, *ASHRAE Symposium Bulletin*, 23-27.

[41] Guy, P., D., Tompsett, G., Dekleva, T., W., Compatibilities of Nonmetallic Material with R-134a and Alternative Lubricants in Refrigeration System, *ASHRAE Transaction*, 1992, pp 804-816.

[42] Hall, A., R., W., Hewitt, G., F., 1993, Application of Two-Fluid Analysis to Laminar Stratified Oil-water Flows, *International Journal of Multiphase Flow*, Vol. 19, No. 4, pp.711-717.

[43] Hashizume, K., Ogiwara, H., and Taniguchi, H., 1985, Flow Pattern, Void Fraction and Pressure Drop of Refrigerant Two-Phase Flow In Horizontal Pipe-II: analysis of Frictional Pressure Drop, *International Journal of Multiphase Flow*, Vol.11, No. 5, pp 643 – 658.

[44] Hauk, A. and E. Weidner, 2000, Thermodynamic and Fluid-Dynamic Properties of Carbon Dioxide with Different Lubricants in Cooling Circuits for Automobile Application, *Industrial & Engineering Chemistry Research*, 39: pp. 4646-4651.

[45] Hetsroni, G., 1982, Handbook of Multiphase Systems, Hemisphere Publishing Corporation, ISBN 0-07-028460-1, pp: 2-44 to 2-94.

[46] Hewitt, G., F., Hall-Taylor, N., S., 1970, Annular Two-Phase Flow, Pergamon Press, Library of Congress Catalog Card No. 70-119854, pp: 50-88.

[47] Hughmark, G.A., 1962, Holdup in Gas-Liquid Flow, *Chemical Engineering Progress*, 58(4): 62-65.

[48] Hurlburt, E. T. and T. A. Newell, 2000, Prediction of the Circumferential Film Thickness Distribution in Horizontal Annular Gas-Liquid Flow, *Transactions of ASME Journal of Fluid Engineering*, 122: 396-402.

[49] Hwang, Y., 1997, Comprehensive Investigation of Carbon Dioxide Refrigeration Cycle, Ph.D. Thesis, University of Maryland, College Park, MD

[50] Hwang, Y., Cremaschi, L., Radermacher, R., Hirata, T., Ozaki, Y., and Hotta, T., 2003, Oil Circulation Ratio in CO2 Climate Control Systems, SAE World Congress, Detroit.

[51] Hwang, Y., Cremaschi, L., Radermacher, R., Hirata, T., Ozaki, Y., and Hotta, T., 2002, Oil Circulation Ratio Measurement in CO2 Cycle, Proceedings of the

2002 International Conference-New Technologies in Commercial Refrigeration, pp. 22-28, University of Illinois, IL.

[52] Hwang, Y., J. P. Lee, R. Radermacher, and R. H. Pereira, 2000, An Experimental Investigation on Flow Characteristics of Refrigerant/Oil mixture in Vertical Upward Flow, *In Proc. 8th International Refrigeration Conference at Purdue*, 265-272. Purdue University, IN.

[53] Issa, R., I., 1988, Prediction of turbulent, stratified, two-phase flow in inclined pipes and channels, *Int Journal of Multiphase Flow*, vol. 14, pp 141-154.

[54] Jacobs, M. L, F. C. Scheideman, S. M. Kazem and N. A. Macken, 1976, Oil Transport by Refrigerant Vapor, *ASHRAE Transactions*, 82: 318-329.

[55] James, P., W., Wilkes, N., S., Conkie, W., Burns, A., 1987, Development in the modeling of horizontal annular two-phase flow, *International Journal of Multiphase Flow,* Vol. 13, No.2, pp 173-198.

[56] Jensen, M., K., Jackman, D., L., 1984, Prediction of Nucleate Pool Boiling Heat Transfer Coefficients of Refrigerant-Oil Mixtures, Trans. of ASME, *Journal of Heat Transfer*, Vol. 106 : 184-190.

[57] Jiang, H., Development of a Simulation and Optimization Tool for Heat Exchanger Design, 2003, Ph.D. Thesis, CEEE, University of Maryland, College Park, MD.

[58] Jiang, H., Aute, V., and Radermacher, R., A User-Friendly Simulation And Optimization Tool for Design of Coils, 2002, *In Proc. 9th International Refrigeration Conference at Purdue*, R5-1, Purdue University, IN

[59] Kakaç, S., 1991, Boilers, Evaporators, and Condensers, John Wiley & Sons, Inc., pp 751-766.

[60] Kattan, N., Thome, J., R., Favrat, D., 1998, Flow Boiling in Horizontal Tubes: Part 1 – Development of a Diabatic Two-Phase Flow Pattern Map, *Journal of Heat Transfer-Transactions of the* ASME, vol 120: 140-147.

[61] Kattan, N., Thome, J., R., Favrat, D., 1998, Flow Boiling in Horizontal Tubes: Part 3 – Development of a New Heat Transfer Model Based on Flow Pattern, *Journal of Heat Transfer-Transactions of the* ASME, vol 120: 156-165.

[62] Kawaguchi, Y., M. Takesue, M. Kaneko, and T. Tazaki, 2000, Performance Study Refrigerating Oil with CO_2, *2000 SAE Automotive Alternative Refrigerant System Symposium*, Scottsdale, AZ.

[63] Kesim, S. C., K. Albayrak and A. Ileri, 2000, Oil Entrainment in Vertical Refrigerant Piping, *International Journal of Refrigeration*, 23: 626-631.

[64] Khor, S. H., M. A. Mendes-Tatis and G. F. Hewitt, 1997, One-Dimensional Modeling of Phase Holdups in Three-Phase Stratified Flow, *International Journal of Multiphase Flow*, 23(5): 885-897.

[65] Kolev, N., I., 2002, Multiphase Flow Dynamics 2 Mechanical and Thermal Interactions, Springer-Verlag Berlin Heidelberg, New York, ISBN 3-540-43017-2, Chapter 2 pp. 48-55, and pp.599-601.

[66] Kramer, D., E., 1999, "CFC to HFC Conversion Issue Why Not Mineral Oil?", Practical Guide Refrigeration, Nov. 1999, pp55 – 61.

[67] Kruse, H. H. and M. Schroeder, 1984. Fundamentals of Lubrication in Refrigerating Systems and Heat Pumps. *ASHRAE Transactions*, 90 Part 2B: 763-783.

[68] Lee, J.P., 2002, Experimental and Theoretical Investigation of Oil Retention In Carbon Dioxide Air-Conditioning System, Ph.D. Thesis, CEEE, University of Maryland, College Park, MD.

[69] Lee, J.P., Y. Hwang, R. Radermacher, and S. S. Mehendale, 2001, Experimental Investigations on Oil Accumulation Characteristics in a Vertical Suction Line, *In Proc. of ASME IMECE 2001, Vol. 3, AES 23607*, New York, NY.

[70] Li, H. and T. E. Rajewski, 2000, Experimental Study of Lubricant Candidates for the CO_2 Refrigeration System, *In Proc. 8th International Refrigeration Conference at Purdue*, 409-416. Purdue University, IN.

[71] Lockhart, R.W., and R.C. Martinelli, 1949, Proposed Correlation of Data for Isothermal Two-Phase, Tow-Component Flow in Pipes, *Chemical Engineering Progress*, 45:39-48.

215

[72] Lorentzen, G. and J. Pettersen, 1993, A New, Efficient and Environmentally Benign System for Car Air-Conditioning, *International Journal of Refrigeration*, 16(1): 4-12.

[73] Luninski, Y., D. Barnea and Y. Taitel, 1983, Film Thickness in Horizontal Annular Flow, *The Canadian Journal of Chemical Engineering*, 61: 621-626.

[74] Macken, N. A., F. C. Scheideman and M. L. Jacobs, 1979, Pressure Loss and Liquid transport of Oil-Refrigerant Mixtures in Suction and Discharges Lines, *ASHRAE Transactions*, 85(2): 77 –92.

[75] Mandhane, J., .M., Gregory, G., A., Aziz, K., 1974, A flow Pattern Map for Gas-Liquid in Horizontal Pipes, *International Journal of Multiphase Flow*. Vol.1: 537-553.

[76] Manwell, S., P., and Bergles, A., S., 1990, Gas-Liquid Flow Patterns in Refrigerant-Oil Mixtures, *ASHRAE Transaction*, Vol. 1: 456-464.

[77] Mehendale, S. S. and R. Radermacher, 2000, Experimental and Theoretical Investigation of Annular Film Flow Reversal in a Vertical Pipe: Application to Oil Return in Refrigeration Systems, *International Journal of HVAC & R Research*. 6(1): 55-74.

[78] Mehendale, S.S., 1998, Experimental and Theoretical Investigation of Annular Film Flow Reversal In a Vertical Pipe, Ph.D. Thesis, CEEE, University of Maryland, College Park, MD.

[79] Moriyama, K. and A. Inoue, 1992, The Thermohydraulic Characteristics of Two-Phase Flow in Extremely Narrow Channels (The Friction Pressure Drop and Heat Transfer of Boiling Two-Phase Flow, Analytical Model), *Heat Transfer- Japanese Research*, 21(8): 838-856.

[80] Newton, C. H., M. Behnia, and J.A., Reizes, 1999, The Effect of Liquid Viscosity on Gas Wall and Interfacial Shear Stress in Horizontal Two-Phase Pipe Flow, *Chemical Engineering Science*, 54:1071-1079.

[81] Nidegger, E., J. R. Thome, and D. Favrat, 1997, Flow Boiling and Pressure Drop Measurements for R-134a/Oil Mixtures Part 1 - Evaporation in a Microfin Tube, *International Journal of HVAC & R Research*, 3(1): 38-53.

216

[82] Nino, V.G., P.S. Hrnjak, and T.A. Newell, 2002, Analysis of Void Fraction in Microchannels, *In Proc. 9th International Refrigeration Conference at Purdue*, R10-3. Purdue University, IN.

[83] Oliemans, R. V. A., B. F. M. Pots, and N. Trompe, 1986, Modeling of Annular Dispersed Two-Phase Flow in Vertical Pipes, *International Journal of Multiphase Flow*, 12(5): 711-732.

[84] Olson, R., M., Wright, S., J., 1990, Essentials of Engineering Fluid Mechanics, 5th Edition Harper & Row, Publishers, New York, Chapter 8, pp. 279 – 309.

[85] Omega Handbook and Encyclopedia of Flow & Level, 2000, Omega Engineering Inc., Stamford, CT.

[86] Omega Operator's Manual LV5000 SERIES, LV5900 Level Transmitters, LV5000, 5100,5200, 5300,5500,5603 Level Sensing Elements, Omega Engineering Inc., Stamford, CT.

[87] Pavel. V., S., Starostin, A., A., Volosnikov, D., V., Zhelezny, V., P., 2003, Comparison of thermophysical properties for oil/refrigerant mixtures by use of the pulse heating method, *International Journal of Refrigeration*, Vol. 26, pp. 721-728.

[88] Peles, Y. P. and S. Haber, 2000, A Steady State, One Dimensional, Model for Boiling Two Phase Flow in Triangular Micro-Channel, *International Journal of Multiphase Flow*, 26: 1095-1115.

[89] Popovic, P., 1999, Investigation and Analysis of Lubricant Effects on the Performance of an HFC-134a Refrigeration System, Ph.D. Thesis, Iowa State University, Ames, IA

[90] Premoli, A., D. Francesco, and A. Prina, 1971, A Dimensionless Correlation for Determining the Density of Two-Phase Mixtures, *La Termotecnica* 25: 17-26.

[91] Reyes-Gavilan, J., G. T. Flak and T. R. Tritcak, 1996, Lubricant Return Comparison of Naphthenic and Polyol Ester Oils in R-134a Household Refrigeration Applications, *ASHRAE Transactions*, 102(2): 180-185.

[92] Rice, C.K., 1987, The Effect of Void Fraction Correlation and Heat Flux Assumption on Refrigerant Charge Inventory Predictions, *ASHRAE Transactions*, 93: 341-367.

[93] Riedle, K. J., N. A. Macken and S. W. Gouse, Jr., 1972, Oil Transport by Refrigerant Vapor: A Literature Survey and Proposed Analytical Model, *ASHRAE Transactions*, 78: 124-133.

[94] Scheideman, F. C. and N. A., Macken, 1975, Pressure Loss of Refrigerant-Oil Mixtures in Horizontal Pipes, *ASHRAE Transactions*, 81: 235 –249.

[95] Schlager, L., M., Pate, M., B., Bergles, A., E., Oil Quantity Measurements in Smooth and Micro-Fin Tubes During Evaporation and Condensation of Refrigerant-Oil Mixtures, *ASHRAE Transaction*, Vol.1, 1990, pp 465-469.

[96] Seeton, C., J. Fahl and D. Henderson, 2000, Solubility, Viscosity, Boundary Lubrication and Miscibility of CO_2 and Synthetic Lubricants. *In Proc. 8th International Refrigeration Conference at Purdue*, 417-424. Purdue University, IN.

[97] Shedd, T., A., Newell, T., A., Automated Optical Liquid Film Thickness Measurement Method, Review of Scientific Instruments, Vol. 69, No. 12, 1998, pp. 4205-4213.

[98] Shen, B., Groll, A., Critical Literature Review of Lubricant Influence on Refrigerant Heat Transfer and Pressure Drop, 2003, Final Report ARTI-21CR/611-20080.

[99] Short, G, and R. Cavestri, 1992, High-Viscosity Ester Lubricants for Alternative Refrigerant, *ASHRAE Transactions*, 98: 785–795.

[100] Skouloudis, A. N. and J. Wijrtz, 1993, Film-Thickness, Pressure-Gradient, and Turbulent Velocity Profiles in Annular Dispersed Flows, *Journal of Fluid Engineering*, 115: 264-269.

[101] Sumida, Y., Nakayame, M., Suzuki, S., and Kawaguchi, S., 1998, Alkylbenzene for Split Air Conditioner with R-410A Part 2: Oil Return Characteristics, *In Proc. 1998 International Compressor Engineering Conference at Purdue*, 471-476, Purdue University, IN.

[102] Sunami, M., K. Takigawa, and S. Suda, 1994, New Immiscible Refrigeration Lubricant for HFCs, *In Proc.5th International Refrigeration Conference at Purdue*, 129-134, Purdue University, IN.

[103] Sunami, M., K. Takigawa, and S. Suda, and U. Sasaki, 1995, New Immiscible Refrigeration Lubricant For HFCs, *ASHRAE Transactions*, 101: 940–946.

[104] Sunami, M., Shimomura, Y., Sawada, K., Fukunaga, Y., and Sasaki, U., 1998, Compressor Durability Tests with AB and HFCs*, In Proc.7th International Refrigeration Conference at Purdue*, 355-360, Purdue University, IN.

[105] Sundaresan, S. G., Radermacher, R., 1996, Oil Return Characteristics of Refrigerant Oils in Split Heat Pump System, ASHRAE Journal, 38(8): pp.57-61.

[106] Taitel, Y., and Dukler, A.E., 1976, A Model for Predicting Flow Regime Transitions in Horizontal and Near Horizontal Gas-Liquid Flow, *AIChE,* 22: 47-55.

[107] Taitel, Y., Barnea, D., 1982, A film Model for the Prediction of Floading and Flow Reversal for Gas-Liquid Flow in Vertical Tubes, *International Journal of Multiphase Flow,* Vol. 8, No.1, pp 1-10.

[108] Taitel, Y., D. Barnea and J. P. Brill, 1995, Stratified Three Phase Flow in Pipes, *International Journal of Multiphase Flow*, 21(1): 53-60.

[109] Tatara, R. A., P. Payvar, 2000, Effects of Oil on Boiling of Replacement Refrigerants Flowing Normal to a Tube Bundle - Part II: R-134a, *ASHRAE Transactions*, 106: 786-791.

[110] Thome, J., R., Comprehensive Thermodynamic Approach to Modeling Refrigerant-Lubricating Oil Mixtures, 1995, HVAC&R Research Vol.1 No. 2 :110-126.

[111] Tomas, R. H. P. and H. T. Pham, 1992, Solubility and Miscibility of Environmentally Safer Refrigerant/Lubricant Mixtures, *ASHRAE Transactions*, 98: 783-788.

[112] Vaughn, R. S., 1971, Refrigeration Compressors, Lubricating Oil, and Refrigerant-An Uneasy Trio, ASHRAE Symposium Bulletin, pp.14-18.

[113] Wallis, G. B., 1969, *One-Dimensional Two-Phase Flow*, McGraw-Hill Book Company, N.Y., NY.

[114] Wallis, G., B., 1970, Annular Two-Phase Flow, Part I: A Simple Theory, *Transactions of ASME Journal of Basic Engineering*, 92: 59-72.

[115] Wallis, G., B., 1970, Annular Two-Phase Flow, Part II: Additional Effects, *Transactions of ASME Journal of Basic Engineering*, 92: 73-82.

[116] Wongwises, S. and W. Kongkiatwanitch, 2001, Interfacial Friction Factor in Vertical Upward Gas-Liquid Annular Two-Phase Flow, *International Communication Heat and Mass Transfer*, 28(3): 323-336.

[117] Yang, C.Y. and C.C. Shieh, 2001, Flow Pattern of Air-Water and Two-Phase R-134a in Small Circular Tubes, *International Journal of Multiphase Flow*, 27: 1163-1177.

[118] Yashar, D.A., M.J. Wilson, H.R. Kopke, D.M. Graham, J.C. Chato, and T.A. Newell, 2001, An Investigation of Refrigerant void Fraction in Horizontal, Microfin Tubes, *International Journal of HVAC & R Research*, 7(1): 67-82.

[119] Yokozeki, A., 1994, Solubility and Viscosity of Refrigerant-Oil Mixtures, *In Proc. 5th International Refrigeration Conference at Purdue*, 335-340, Purdue University, IN.

[120] Yokozeki, A., 2002, Time-Dependent Behavior of Gas Absorption in Lubricant Oil, *Int Journal of Refrigeration* vol. 25, No. 6,2002.

[121] Yokozeki, A., K. Takigawa, and S. I. Sandler, 2000, Solubility and Viscosity of Hydrofluorocarbon/Alkylbenzene Oil Mixtures, *In Proc. 8th International Refrigeration Conference at Purdue*, 241-247. Purdue University, IN.

[122] Zhao, Y., 2001, Flow Boling Characteristics of Carbon Dioxide in Microchannels, Ph.D. Thesis, University of Maryland, College Park, MD.

[123] Zhao, Y., M. Molki, M. M. Ohadi and S. V. Dessiatoun, 2000, Flow Boiling of CO_2 in Microchannels, *ASHRAE Transactions*, 106: 437–445.

[124] Zhao, Y., M. Molki, M. M. Ohadi, F. H. R. Franca, and R. Radermacher, 2002, Flow Boiling of CO_2 with Miscible Oil in Microchannels, ASHRAE Transactions, 108: 4505.

[125] Zurcher, O., J. R. Thome, and D. Favrat, 1998, In-Tube Flow Boiling of R-407C and R-407C/Oil Mixtures. Part II: Plain Tube Results and Predictions, *International Journal of HVAC & R Research*, 4(4): 373-399.